

NUMERICAL ANALYSIS, DESIGN AND TWO PORT EQUIVALENT
CIRCUIT MODELS FOR SPLIT RING RESONATOR ARRAYS

A THESIS SUBMITTED TO
THE GRADUATE SCHOOL OF NATURAL AND APPLIED SCIENCES
OF
MIDDLE EAST TECHNICAL UNIVERSITY

BY

PINAR YAŞAR ÖRTEN

IN PARTIAL FULFILLMENT OF THE REQUIREMENTS
FOR
THE DEGREE OF MASTER OF SCIENCE
IN
ELECTRICAL AND ELECTRONICS ENGINEERING

FEBRUARY 2010

Approval of the thesis:

**NUMERICAL ANALYSIS, DESIGN AND TWO PORT EQUIVALENT
CIRCUIT MODELS FOR SPLIT RING RESONATOR ARRAYS**

submitted by **PINAR YAŞAR ÖRTEN** in partial fulfillment of the requirements
for the degree of **Master of Science in Electrical and Electronics Engineering**
Department, Middle East Technical University by,

Prof. Dr. Canan Özgen _____
Dean, Graduate School of **Natural and Applied Sciences**

Prof. Dr. İsmet Erkmek _____
Head of Department, **Electrical and Electronics Engineering**

Prof. Dr. Gönül Turhan Sayan _____
Supervisor, **Electrical and Electronics Engineering Dept., METU**

Examining Committee Members:

Prof. Dr. Gülbin Dural _____
Electrical and Electronics Engineering Dept., METU

Prof. Dr. Gönül Turhan Sayan _____
Electrical and Electronics Engineering Dept., METU

Prof. Dr. Mustafa Kuzuoğlu _____
Electrical and Electronics Engineering Dept., METU

Prof. Dr. Kemal Leblebicioğlu _____
Electrical and Electronics Engineering Dept., METU

Prof. Dr. Adnan Köksal _____
Electrical and Electronics Engineering Dept., Hacettepe Univ.

Date: _____ 04.02.2010

I hereby declare that all information in this document has been obtained and presented in accordance with academic rules and ethical conduct. I also declare that, as required by these rules and conduct, I have fully cited and referenced all material and results that are not original to this work.

Name, Last name : Pınar YAŞAR ÖRTEN

Signature :

ABSTRACT

NUMERICAL ANALYSIS, DESIGN AND TWO PORT EQUIVALENT CIRCUIT MODELS FOR SPLIT RING RESONATOR ARRAYS

Yaşar Örtten, Pınar

M. Sc., Department of Electrical and Electronics Engineering

Supervisor: Prof. Dr. Gönül Turhan Sayan

February 2010, 95 pages

Split ring resonator (SRR) is a metamaterial structure which displays negative permeability values over a relatively small bandwidth around its magnetic resonance frequency. Unit SRR cells and arrays have been used in various novel applications including the design of miniaturized microwave devices and antennas. When the SRR arrays are combined with the arrays of conducting wires, left handed materials can be constructed with the unusual property of having negative valued effective refractive indices.

In this thesis, unit cells and arrays of single-ring multiple-split type SRR structures are numerically analyzed by using Ansoft's HFSS software that is based on the finite elements method (FEM). Some of these structures are constructed over low-loss dielectric substrates and their complex scattering parameters are measured to verify the numerical simulation results. The major purpose of this study has been to establish equivalent circuit models to estimate the behavior of SRR structures in a simple and computationally efficient manner. For this purpose, individual single ring SRR cells with multiple splits are modeled by appropriate two-port RLC resonant circuits paying special attention to conductor and dielectric loss effects. Results obtained from these models are compared with the results of HFSS

simulations which use either PEC/PMC (perfect electric conductor/perfect magnetic conductor) type or perfectly matched layer (PML) type boundary conditions. Interactions between the elements of SRR arrays such as the mutual inductance and capacitance effects as well as additional dielectric losses are also modeled by proper two-port equivalent circuits to describe the overall array behavior and to compute the associated transmission spectrum by simple MATLAB codes. Results of numerical HFSS simulations, equivalent circuit model computations and measurements are shown to be in good agreement.

Keywords: Split ring resonator (SRR), metamaterials, two-port networks, equivalent circuit modeling, resonance frequency, HFSS simulations.

ÖZ

YARIKLI HALKA REZONATÖR DİZİLERİNİN SAYISAL ANALİZİ, TASARIMI VE İKİ KAPILI EŞDEĞER DEVRE MODELLEMESİ

Yaşar Örten, Pınar

Yüksek Lisans, Elektrik ve Elektronik Mühendisliği Bölümü

Tez Yöneticisi: Prof. Dr. Gönül Turhan Sayan

Şubat 2010, 95 sayfa

Yarıklı halka rezonatörü (YHR) manyetik rezonans frekansı etrafındaki göreceli olarak dar bir bantta etkin negative manyetik geçirgenlik özelliği gösteren bir metamalzeme yapısıdır. YHR birim hücre ve dizileri, küçük boyutlu mikrodalga gereçleri ve antenlerin tasarımını da içeren çeşitli özgün uygulamalarda kullanılmaktadırlar. YHR dizilerinin iletken tel dizileri ile birlikte kullanılmasıyla, olağan dışı bir şekilde, negatif etkin kırılma indisine sahip olma özelliği gösteren sol-elli malzemeler tasarlanabilmektedir.

Bu tezde, çoklu yarıklı tek halkalı YHR birim hücreleri ve dizileri, sonlu elemanlar yöntemine dayalı bir yöntem kullanan Ansoft firmasının HFSS yazılımı ile sayısal olarak analiz edilmiştir. Bu yapıların bazıları düşük kayıplı dielektrik levhalar üzerinde gerçekleştirilmiş ve sayısal benzetim sonuçlarını doğrulamak için kompleks S-parametreleri ölçülmüştür. Bu çalışmanın esas amacı, YHR yapılarının davranışını basit ve etkin bir şekilde tahmin edip hesaplayabilmek için eşdeğer devre modelleri kurmaktır. Bu nedenle, çoklu yarıklı tek halkalı YHR birim hücreleri ve dizileri, iletken ve dielektrik bölgelerden kaynaklanan kayıp etkilerinin de özenle hesaba katıldığı uygun iki kapılı RLC rezonans devreleri ile modellenmiştir. Bu modellerden elde edilen sonuçlar, sınır koşul olarak mükemmel

elektrik iletken/mükemmel manyetik iletken veya mükemmel uyumlu tabaka tipi sınır koşullarının kullanıldığı HFSS benzetim sonuçları ile karşılaştırılmıştır. YHR dizilerinin elemanları arasındaki karşılıklı endüktans, kapasitans etkileri ve ilave dielektrik kayıplar gibi etkileşimler uygun iki kapılı eşdeğer devre yapıları ile modellenerek dizi davranışları tahmin edilmiş ve ilgili dizi yapısının iletim spektrumu yalnız MATLAB kodları ile hesaplanmıştır. Sayısal HFSS benzetimlerinden, eşdeğer devre modellerinin hesaplamalarından ve ölçümlerden elde edilen sonuçların birbirleriyle uyumlu oldukları gösterilmiştir.

Anahtar kelimeler: Yarıkli halka rezonatörü (YHR), metamalzemeler, iki kapılı devreler, eşdeğer devre modellemesi, rezonans frekansı, HFSS simülasyonları.

Canım Aileme

ACKNOWLEDGEMENTS

I would like to express my gratitude to my supervisor Prof. Dr. Gönül Turhan Sayan not only for her invaluable guidance but also for helping me to be optimistic even at the most difficult times of this thesis research. I have learned lots of things from her both about engineering and life.

I would like to thank the members of my thesis committee, Prof Dr. Gülbin Dural, Prof Dr. Mustafa Kuzuoğlu, Prof. Dr. Kemal Leblebicioğlu and Prof. Dr. Adnan Köksal for reading the manuscript and sharing their opinions. I also would like to thank Evren Ekmekçi for his helps especially during the experimental work.

I also would like to thank ASELSAN A.Ş. for the facilities provided during my graduate degree and TÜBİTAK-BİDEB (The Scientific and Technological Research Council of Turkey-The Department of Science Fellowships and Grant Programmes) for its support to scientific research.

Thanks to all of my close friends for their support and encouragement.

Lastly but mostly, I would like to thank my mother, father and sister for giving me a great and special family. Without their support, I would not be able to overcome the difficulties throughout my life. And special thanks to my spouse Hasan who has never given up believing in me and even at the hardest times made me smile to life. I love all of you so much my dear family.

TABLE OF CONTENTS

ABSTRACT.....	iv
ÖZ.....	vi
ACKNOWLEDGEMENTS.....	ix
ACKNOWLEDGEMENTS.....	ix
TABLE OF CONTENTS.....	x
LIST OF TABLES.....	xiii
LIST OF FIGURES.....	xiv
CHAPTER	
1. INTRODUCTION.....	1
2. BASICS OF NUMERICAL SIMULATIONS AND EQUIVALENT CIRCUIT MODELING FOR SRR STRUCTURES.....	6
2.1 Introduction.....	6
2.2 Use of HFSS Simulations to Compute the Transmission Spectra of SRR Structures.....	7
2.2.1 Simulation Problem 1.....	8
2.2.2 Simulation Problem 2.....	12
2.2.3 Simulation Problem 3.....	17
2.3 Basics of SRR Modeling by Equivalent Lumped Circuit Models.....	20
2.3.1 Modeling an SRR Unit Cell by a Proper RLC Circuit.....	21

3. NUMERICAL SIMULATIONS AND TWO PORT EQUIVALENT CIRCUIT MODELING OF SQUARE SHAPED SINGLE LOOP SRR STRUCTURES.....	36
3.1 Introduction.....	36
3.2 Single-Loop Square-Shaped SRR Unit Cell.....	37
3.2.1 Numerical Simulation and Equivalent Circuit Modeling of the Isolated SRR Unit Cell.....	37
3.2.2 Numerical Simulation and Equivalent Circuit Modeling of the Infinite SRR Array along the Electric Field Direction.....	43
3.3 An SRR Array Extending Along the Propagation Direction.....	48
3.3.1 Analysis of the Isolated Two-Element Array of Size $2 \times 1 \times 1$	49
3.3.2 Numerical Simulation and Equivalent Circuit Modeling of Two Layer Infinite SRR Array.....	54
3.4 An SRR Array Extending Along the Electric Field Direction.....	58
3.4.1 Analysis of the Isolated Two-Element Array of Size $1 \times 2 \times 1$	59
3.4.2 Numerical Simulation and Equivalent Circuit Modeling of Infinite SRR Array Along the Electric Field Direction.....	63
3.5 The $2 \times 2 \times 1$ SRR Array.....	64
3.5.1 Analysis of the Isolated Four Element Array of Size $2 \times 2 \times 1$	67
3.5.2 Numerical Simulation and Equivalent Circuit Modeling of Infinite Two Layer SRR Array.....	71
4. NUMERICAL SIMULATIONS, MEASUREMENTS AND TWO PORT EQUIVALENT CIRCUIT MODELING OF SQUARE SHAPED SINGLE LOOP SRR STRUCTURES.....	72
4.1 Introduction.....	72
4.2 Analysis and Measurements of the SRR Unit Cell.....	73
4.2.1 Analysis of the Isolated SRR Unit Cell.....	74
4.2.2 Numerical Simulation, Equivalent Circuit Modeling and Measurement of the SRR Unit Cell within Waveguide.....	76

4.3	Analysis and Measurements of the 4x1x1 SRR Array	80
4.3.1	Analysis of the Isolated 4x1x1 SRR Array.....	81
4.3.2	Measurements and Numerical Simulations for the 4x1x1 SRR Array Placed Within a Waveguide.....	85
5.	CONCLUSIONS AND FUTURE WORK.....	89
	REFERENCES	93

LIST OF TABLES

TABLES

Table 2-1: Comparison of mesh numbers used in HFSS simulations with PML boundary conditions for different number of array elements in electric field direction	19
Table 3-1: Geometrical parameters of the SRR unit cell shown in Figure 3-2.....	39
Table 3-2: Calculated values of circuit parameters for the SRR unit cell	40
Table 3-3: Calculated circuit model parameters of the infinite SRR array extending in the electric field direction	47
Table 3-4: Calculated model parameters for the infinite SRR array in electric field direction	58
Table 4-1: Geometrical parameters of the fabricated SRR unit cell.....	74
Table 4-2: Model parameters of the fabricated SRR unit cell	75
Table 4-3: Calculated model parameters of the infinite SRR array extending along the incident electric field direction	79

LIST OF FIGURES

FIGURES

Figure 1-1: Unit cell geometry for a) Conventional SRR, b) BC-SRR.	2
Figure 2-1: Notation used to identify SRR array topologies.	6
Figure 2-2: Schematic views of SRR unit cell and the HFSS simulation set-up a) Geometry and dimensions of the SRR unit cell, b) Boundary conditions used for HFSS simulations.	9
Figure 2-3: Two dimensional periodic SRR array implemented by the use of PEC and PMC boundary conditions in HFSS simulation a) Array in E field direction, b) Array in H field direction.	10
Figure 2-4: Effect of vacuum length in H field direction on resonance frequency (red curve $D_H=1.75$ mm, blue curve $D_H=3.5$ mm).	12
Figure 2-5: Variation of transmission minimum with substrate length in electric field direction.	13
Figure 2-6: Variation of mutual inductance with cell to cell separation distance along the electric field direction.	14
Figure 2-7: Variation of mutual capacitance with cell to cell separation distance along the electric field direction.	15
Figure 2-8: Rate of change of mutual inductance with d.	16
Figure 2-9: Rate of change of mutual capacitance with d.	16
Figure 2-10: Variation of resonance frequency with d based on calculated circuit parameters.	17
Figure 2-11: Unit cell geometry used for comparison of boundary conditions.	18
Figure 2-12: Comparison of transmission spectrum of different SRR configurations with PEC and PML boundaries using $D_E=1$ mm and $D_H=11.049$ mm.	19
Figure 2-13: Two-port equivalent circuit representation of a single loop SRR cell with either series or parallel LC resonant circuit in the shunt branch.	22

Figure 2-14: Two different representations for the impedance Z a) Series LC circuit, b) Parallel LC circuit.....	25
Figure 2-15: A feasible two-port equivalent circuit representation for SRR unit cell including ohmic loss effects.	27
Figure 2-16: Transmission spectrum curves of the isolated SRR cell, which are obtained by HFSS simulation with PML boundary conditions (with $D_E=1$ mm and $D_H=5$ mm) and by equivalent circuit modeling approach. Geometry and dimensions for the SRR cell are described in Section 2.2.3. Equivalent circuit model is given in Figure 2-15.....	29
Figure 2-17: Alternative two-port equivalent circuit representation of a single loop SRR with either series or parallel LC resonant circuit in the series branch.	30
Figure 2-18: Alternative representations of two-port network consisting of series impedance a) Series LC circuit, b) Parallel LC circuit.	33
Figure 2-19: Improved version of the two-port circuit representation shown in Figure 2-18 (b) with the inclusion of equivalent loss resistances.....	34
Figure 2-20: Transmission spectrum curves of the isolated SRR cell, which are obtained by HFSS simulation with PML boundary conditions (with $D_E=1$ mm and $D_H=5$ mm) and by equivalent circuit modeling approach. Geometry and dimensions for the SRR cell is described in Section 2.2.3. Equivalent circuit model is given in Figure 2-19.....	35
Figure 3-1: Boundary conditions for HFSS simulations: a) PML boundary conditions to examine an isolated SRR unit cell, b) PEC/PMC boundary conditions to examine a two dimensional infinite SRR array.	37
Figure 3-2: a) Unit cell geometry of a single square loop SRR, b) Parameters of the isolated SRR cell, c) Equivalent two-port circuit model of the SRR cell.....	39
Figure 3-3: Estimated transmission spectra of the SRR unit cell using HFSS simulations with PML boundary conditions and $D_H=2$ mm and using the equivalent two-port circuit given in Figure 3-2 (c).	42
Figure 3-4: Estimated transmission spectra of the SRR unit cell using HFSS simulations with PML boundary conditions and $D_H=1$ mm and using the equivalent two-port circuit given in Figure 3-2 (c).	43

Figure 3-5: Equivalent circuit model for the SRR array which effectively extends to infinity in the electric field direction.	45
Figure 3-6: Transmission spectrum of the infinite SRR array as estimated by an HFSS simulation using the PEC/PMC boundary conditions.....	48
Figure 3-7: a) Geometry of 2x1x1 SRR array, b) Elements of 2x1x1 array, c) Two-port representation of 2x1x1 array (First alternative for the coupling two-port connection).....	49
Figure 3-8: Estimated transmission spectrum of 2x1x1 SRR array using HFSS simulations with PML boundary conditions and $D_H=1$ mm and using the equivalent two-port circuit given in Figure 3-7(c).	52
Figure 3-9: Two-port representation of the 2x1x1 array (Second alternative for the coupling two-port connection).	53
Figure 3-10: Estimated transmission spectrum of the 2x1x1 SRR array using HFSS simulations with PML boundary conditions and $D_H=1$ mm. and using the equivalent two-port circuit given in Figure 3-9.....	54
Figure 3-11: An equivalent circuit model for the double layer SRR array ($m \times n \times p$) where $m=2$, $p=1$ (due to sparse array approximation) and n approaches to infinity.	56
Figure 3-12: Simulation of 2x1x1 array with PEC/PMC boundary.	58
Figure 3-13: a) Geometry of the 1x2x1 array, b) Elements of 1x2x1 array, c) Equivalent two-port circuit model for the 1x2x1 array.	60
Figure 3-14: Estimated transmission spectra of the 1x2x1 SRR array using HFSS simulations with PML boundary conditions and $D_H=1.75$ mm and using the equivalent two-port circuit given in Figure 3-13 (c).....	63
Figure 3-15: Transmission spectrum of the 1x2x1 SRR array obtained by HFSS simulation with PEC/PMC boundary conditions.....	64
Figure 3-16: a) Unit cell geometry of 2x2x1 array, b) Parameters of the 2x2x1 SRR array.	66
Figure 3-17: Two-port model for 2x2x1 SRR array.	68

Figure 3-18: Estimated transmission spectra of the 2x2x1 SRR array using HFSS simulations with PML boundary conditions and $D_H=1.75$ mm and using the equivalent circuit model shown in Figure 3-17.	70
Figure 3-19: Transmission spectrum for the 2x2x1 SRR array estimated by HFSS with PEC/PMC boundary conditions.	71
Figure 4-1: Boundary conditions used in HFSS simulations: a) Use of PML conditions to examine the isolated SRR cell, b) Use of PEC boundary conditions to simulate SRR behavior within a metallic waveguide.	73
Figure 4-2: SRR unit cell a) Geometry and excitation, b) Design parameters.	74
Figure 4-3: Equivalent two-port circuit representation of the SRR unit cell.	75
Figure 4-4: Estimated transmission spectra of the SRR unit cell using HFSS simulations with PML boundary conditions and $D_H=5$ mm. and using the equivalent two-port circuit given in Figure 4-3.	76
Figure 4-5: Equivalent circuit model of the effective SRR array formed by placing SRR unit cell within the waveguide in measurements.	78
Figure 4-6: Simulated transmission spectrum of the fabricated SRR unit cell using HFSS with PEC boundary conditions.	79
Figure 4-7: Measured transmission spectrum of the fabricated SRR unit cell when it is placed within a measurement waveguide.	80
Figure 4-8: Four element SRR array of size 4x1x1 a) Geometry and excitation, b) Capacitive coupling effects along the propagation direction.	81
Figure 4-9: Two-port equivalent circuit model suggested for the isolated 4x1x1 SRR array.	83
Figure 4-11: Estimated transmission spectrum of the isolated 4x1x1 SRR array using HFSS with PML boundary conditions and using the equivalent two-port model given in Figure 4-10.	85
Figure 4-12: Transmission spectrum of the 4x1x1 array simulated by HFSS with PEC boundary conditions.	86
Figure 4-13: Measured (within a waveguide) transmission spectrum of the 4x1x1 SRR array.	87

Figure 4-14: Fabricated SRR unit cell and probes used to measure its transmission spectrum.....	87
Figure 4-15: Comparison of the fabricated SRR unit cell and 4x1x1 SRR array....	88
Figure 4-16: A simple experimental set-up used to measure transmission spectrum of SRR structures in air.....	88

CHAPTER 1

INTRODUCTION

Research on metamaterials, which are engineered materials with unusual properties not occurring naturally, has become increasingly important over the last decade. The first and one of the most important contributions to this topic was made in 1968 by V.G. Veselago who showed that materials with both negative permittivity and negative permeability are theoretically possible. Veselago used the term “left-handed medium” for such materials as the \vec{E} , \vec{H} and \vec{k} vectors of plane wave propagation form a left-handed mutually perpendicular vector set instead of a right-handed one. In his paper, it is also indicated that in left-handed media wave vector \vec{k} and the Poynting vector \vec{S} are in opposite directions. Because of the reversed direction of \vec{k} vector, phase velocity is also reversed in these materials. Veselago implied that as a result of these reversals, Doppler Effect, Snell’s Law and Cherenkov radiation will all be reversed in left-handed materials [1]. The next important contribution was made almost 30 years later, in 1999, by Pendry *et al.* They demonstrated experimentally that “Split-Rings” are useful to obtain negative effective permeability μ_{eff} [2]. The following year, in 2000, Smith *et al* experimentally demonstrated that the use of thin wire arrays in addition to SRR (Split Ring Resonator) arrays provided negative effective permittivity, ϵ_{eff} , and negative effective permeability, μ_{eff} , simultaneously over a common frequency band [3].

The conventional split-ring resonator unit cell suggested by Pendry *et al* was composed of two circular coplanar metallic rings each with a split displaced by 180 degrees. These rings were printed on a low-loss dielectric substrate having the same center and separated from each other by a short gap distance as shown in Figure 1-1

(a). Bianisotropic behavior of this SRR unit cell structure was investigated in 2002 by Marques *et al* in [4]. A modified version of SRR (later called as broadside coupled (BC) SRR) was suggested in the same paper to avoid bianisotropy. Next year, in 2003, comparative analysis of the conventional (or edge-coupled) SRR and BC-SRR was given in [5] where metallic rings of the BC-SRR were printed on both sides of the dielectric substrate and aligned in such a way that their splits were displaced by 180 degrees as shown in Figure 1-1 (b). SRR unit cells with multiple rings were suggested and analyzed later by Bilotti *et al* in 2007 [6]. These and many other studies on the theory and analysis of SRRs have appeared in the metamaterial literature so far. In the mean time, SRRs have been used in diverse applications at microwave and optical frequencies extending from superlenses [7, 8] to cloaking [9].

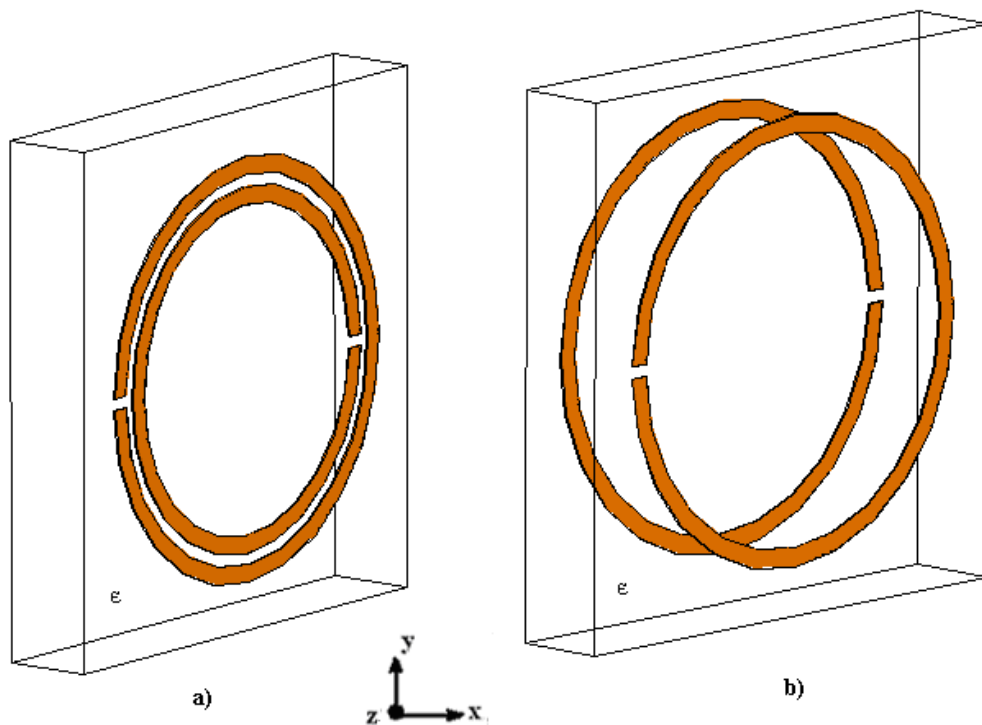


Figure 1-1: Unit cell geometry for a) Conventional SRR, b) BC-SRR.

Most of the investigations on SRRs have involved either measurements or numerical simulations of SRR unit cell or array topologies. Studies for developing equivalent circuit models for SRR structures are still in their crawling phase. The results obtained and reported in literature in this important area are neither complete nor fully consistent yet.

Describing SRR structures by their equivalent circuit models is important for two major reasons: First of all, transmission/reflection spectra obtained by measurements or by highly complex commercial simulation tools do not provide enough insight about the operational mechanism of the SRR topology under investigation. When an equivalent circuit model is available, it is much easier to establish explicit relationships between the physical properties (i.e. electrical parameters, dimensions, etc.) of the SRR structure and its frequency dependent transmission/reflection behavior. Secondly, use of equivalent circuit models makes a computationally efficient optimization approach possible in metamaterial design. Using commercial full-wave electromagnetic solver packages such as Ansoft HFSS or CST Microwave Studio is not feasible in the analysis phase of an optimization process since such solvers would have intolerably long run times at each iteration. Instead, the analysis of a metamaterial structure can be completed in a fraction of a second in each iteration of the optimization process if an equivalent circuit model is available for the metamaterial topology to be designed. Hence, not only the resonance frequency but also the overall S-parameter spectra of an SRR array can be optimally estimated (or simply calculated without optimization) by using sufficiently accurate equivalent circuit models which account for the loss effects also.

In recent years, several researchers have contributed to the area of SRR modeling [5, 6, 10-17]. In 2003, following the work done in [4], Marques *et al* proposed a simple RLC equivalent circuit model for conventional SRRs in the presence of a dielectric substrate [5]. In 2005 Baena *et al* analyzed SRR and complementary SRR (CSRR) structures coupled to planar transmission lines and proposed equivalent

circuit models for the SRR and transmission line combinations. SRR unit cells are represented by simple resonant LC circuits in their work [10]. In 2005, Qun Wu *et al* [11] suggested an equivalent circuit model for a conventional SRR cell based on the quasi-static approach. In 2006, Johnson *et al* analyzed two elements of SRR array with co-planar and parallel plate capacitance approach [12]. In 2007, Bilotti *et al* introduced multiple SRR structures and modeled them using as LC resonance circuits. They also provided total inductance and total capacitance expressions [6]. In 2008, Wang *et al* modeled a modified SRR structure where the resonance frequency of the structure could be changed by rotating the inner ring of the SRR [13].

The main objective of this thesis is to establish useful equivalent circuit models for SRR unit cell and array topologies. Extension of metamaterial applications from microwave frequencies to terahertz (THz) and optical frequencies [18, 19] requires geometrical simplicity as the wavelengths become very small (in the order of submillimeters and microns) in the optical range and the SRR cells must be of subwavelength size. For that reason, single ring SRR topologies are investigated in this thesis. Square shaped single metallic rings with multiple gaps and their array forms are analyzed, designed and modeled by lumped circuit elements. Use of two-port equivalent circuit representations of these elements is suggested in particular to compute the complex S-parameters for SRR arrays. The transmission spectra (i.e. magnitudes of S_{21} spectra) estimated by equivalent circuit models and computed by simple Matlab codes are compared with transmission spectra computed via HFSS simulations. The results are found to be in good agreement in most cases, although the equivalent circuit models can describe the SRR array topologies only approximately. For a selected square ring SRR structure resonating in 10-13 GHz band, experimental results are also obtained. An SRR unit cell and a four-element SRR array, extending in the propagation direction are manufactured and measured within a metallic waveguide environment.

In Chapter 2, basics of numerical HFSS simulations and equivalent circuit modeling for SRR structures are presented. Importance of choosing proper boundary conditions and proper computational volume dimensions to simulate SRR behaviors are discussed and demonstrated by examples. In this context, effect of periodicity parameters on the resonance frequency is investigated. Basics of two-port equivalent circuit modeling for SRR structures are also discussed in Chapter 2.

In Chapter 3, unit cell structure and arrays of single loop square shaped SRRs with four splits are analyzed and modeled. These SRR structures are found to have resonance frequencies around 35 GHz. Using two-port circuit representations and Matlab programming, transmission spectra of these topologies are estimated. Modeling results are compared with HFSS simulation results for validation.

In Chapter 4, a four split single square loop SRR unit cell and a four-element SRR array (named as 4x1x1 array) are designed and fabricated. In addition to examining these structures via HFSS simulations and equivalent circuit modeling, their transmission spectra are also measured over the frequency band from 10 GHz to 13 GHz. All these results are found to be in good agreement.

Finally, conclusions of this thesis work along with possible future work suggestions are given in Chapter 5.

CHAPTER 2

BASICS OF NUMERICAL SIMULATIONS AND EQUIVALENT CIRCUIT MODELING FOR SRR STRUCTURES

2.1 Introduction

In this chapter, basics of numerical simulations and equivalent circuit modeling for SRR structures (unit cells or arrays) will be discussed. First, examples of HFSS simulations will be presented with special emphasis on the choice of boundary conditions and on the dimensions of computational volume. Then, basics of the equivalent circuit modeling for SRR unit cells and arrays will be introduced. The notation used for array forms is shown in Figure 2-1.

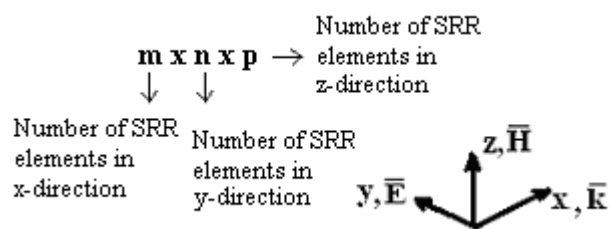


Figure 2-1: Notation used to identify SRR array topologies.

2.2 Use of HFSS Simulations to Compute the Transmission Spectra of SRR Structures

Use of commercial full wave electromagnetic solvers such as Ansoft's HFSS or CST Microwave Studio is very common in the analysis of metamaterial structures. In this thesis HFSS, which is based on finite elements method (FEM), is used for the analysis of SRR structures. Proper use of boundary conditions is very important in HFSS simulations. To simulate the behavior of a single SRR unit cell in isolation, perfectly matched layer (PML) type of boundaries must be implemented. PMLs are frequency dependent structures. While using these layers as boundaries, it is vital to define the minimum reference frequency of the simulation frequency range. The use of perfect electric conductor (PEC) or perfect magnetic conductor (PMC) type boundary conditions around an SRR unit cell, on the other hand, leads to the simulation of infinite SRR array structures due to the formation of images of the SRR unit cell with respect to the PEC and PMC boundaries.

It is well known in metamaterial literature that SRR structures are magnetic resonators providing negative permeability (μ -negative or MNG) regions around their resonance frequencies. As to be discussed in this chapter, a single loop SRR cell can be modeled by a simple RLC resonant circuit. The inductance " L_{self} " refers to the self inductance of the metallic loop and the capacitance " C " is created at the split location as a result of magnetic induction. The incident time-varying magnetic field vector must be perpendicular to the SRR plane to excite the SRR's magnetic resonances. To compute the complex S-parameters of an infinite (in the E-field and H-field directions) SRR array by HFSS under plane wave excitation, PEC and PMC boundary conditions are frequently used in literature.

Location of the PEC and/or PMC boundaries (i.e. the dimensions of the computational volume) is also important as their distance to metallic inclusions determine the parameters of periodicity of the SRR array. Computed transmission/reflection spectra, values of the resonance frequencies (i.e. the

complex S-parameter spectra, in general) change according to the type of boundary conditions and location of the boundaries. Similar concerns regarding the location of PMLs are also important in the simulation of isolated SRR cells. All these issues will be addressed in the following subsections.

2.2.1 Simulation Problem 1

In this subsection, transmission spectrum of the SRR unit cell shown in Figure 2-2 (a) is simulated via HFSS over the frequency range 30-40 GHz by using PEC and PMC boundary conditions. Dimensions of this SRR unit cell are as follows: Side length of SRR (L) is 2.8 mm, gap width (g) and metal strip width (w) are both 0.3 mm, substrate dimensions ($D=D_x=D_y$) along the x and y directions are both 4 mm, and substrate thickness (h) along the z direction is 0.5 mm. Gold is used for metal inclusions and a low loss dielectric material with relative permittivity (ϵ_r) of 4.6 and dielectric loss tangent ($\tan \alpha$) of 0.01 is used as the substrate. The PEC boundary conditions are applied at those surfaces of the computational volume which are perpendicular to the \vec{E} field vector. Similarly, PMC type boundary conditions are applied at those surfaces of the computational volume which are perpendicular to the \vec{H} field vector. The remaining two surfaces are obviously labeled as the input and output planes in Figure 2-2 (b).

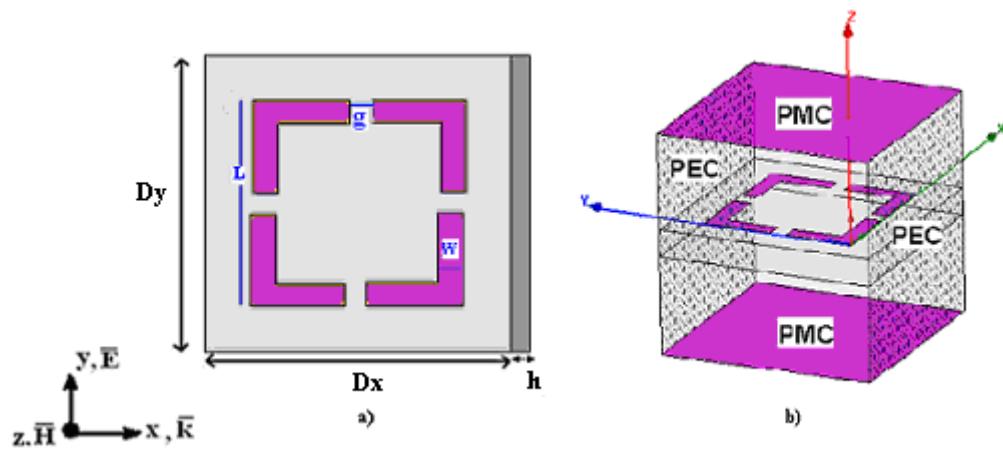


Figure 2-2: Schematic views of SRR unit cell and the HFSS simulation set-up a) Geometry and dimensions of the SRR unit cell, b) Boundary conditions used for HFSS simulations.

Due to the imaging effects of PEC and PMC boundaries, the computed transmission spectrum (i.e. $|S_{21}|$ versus frequency curve) belongs to a two dimensional infinite SRR array as explained in Figure 2-3 which shows periodicity of the array in \bar{E} field and \bar{H} field directions, respectively.

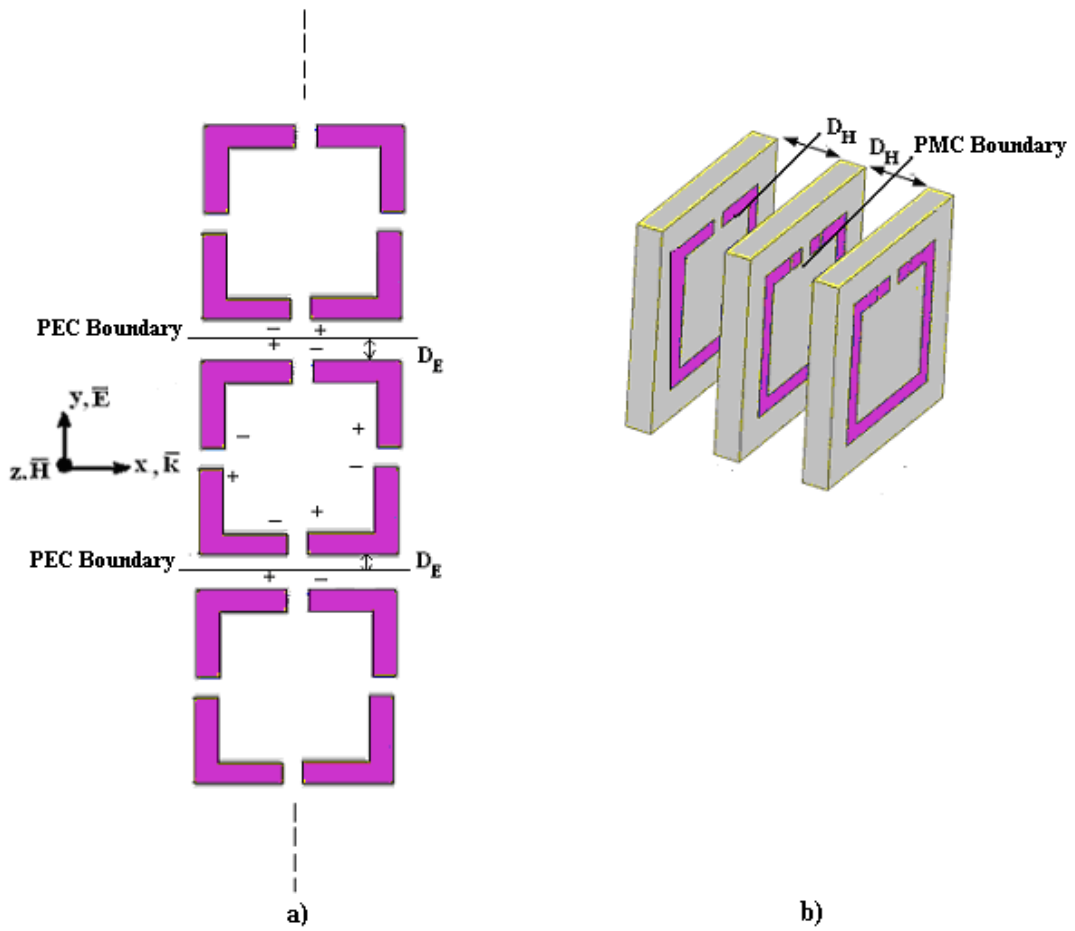


Figure 2-3: Two dimensional periodic SRR array implemented by the use of PEC and PMC boundary conditions in HFSS simulation a) Array in E field direction, b) Array in H field direction.

First, the transmission spectrum of this SRR array is simulated by using the dimension $D_H = 1.75$ mm where D_H is the depth of the vacuum regions over and under the SRR cell within the computation volume in the direction of \bar{H} field as seen in Figure 2-3 (b). The resultant transmission curve is plotted in Figure 2-4 (the red one) with a resonance frequency very close to 34 GHz. Next, the simulation is repeated by keeping all the parameters the same but doubling the value of the parameter D_H this time. The transmission spectrum of the SRR array with $D_H = 3.5$ mm is plotted in Figure 2-4 (the blue curve), indicating a shift of approximately 0.3 GHz in resonance frequency which is now 34.28 GHz. The periodicity distance D_z

in \overline{H} field direction (along the z axis) is given by $D_z = 2D_H + h$ where $h=0.5$ mm is the substrate thickness. The periodicity distance D_z is changed from 4 mm to 7.5 mm in these simulations resulting a negligible shift of only 0.3 GHz, which corresponds to a $(0.3/34) \times 100 = 0.88$ % change, even less than one percent. This is an expected observation as the array in z direction is relatively sparse leading to the result that the inductive coupling effects between array elements are not strong along this dimension of the SRR array. It should be also emphasized that there is no capacitive coupling between the SRR elements stacked along the \overline{H} field direction of the array. Due to the PMC boundary condition, the image of the SRR unit cell is simulated to form an array in \overline{H} field direction but charges accumulated at the split locations of an image cell have exactly the same polarity pattern as that of the original SRR cell.

Next, similar simulations are performed by changing the distance D_E between the PEC boundary and the outer border of the metallic strip, which determines the periodicity distance $D_y = 2D_E + L$ along the \overline{E} field direction. Results will be reported in the next subsection.

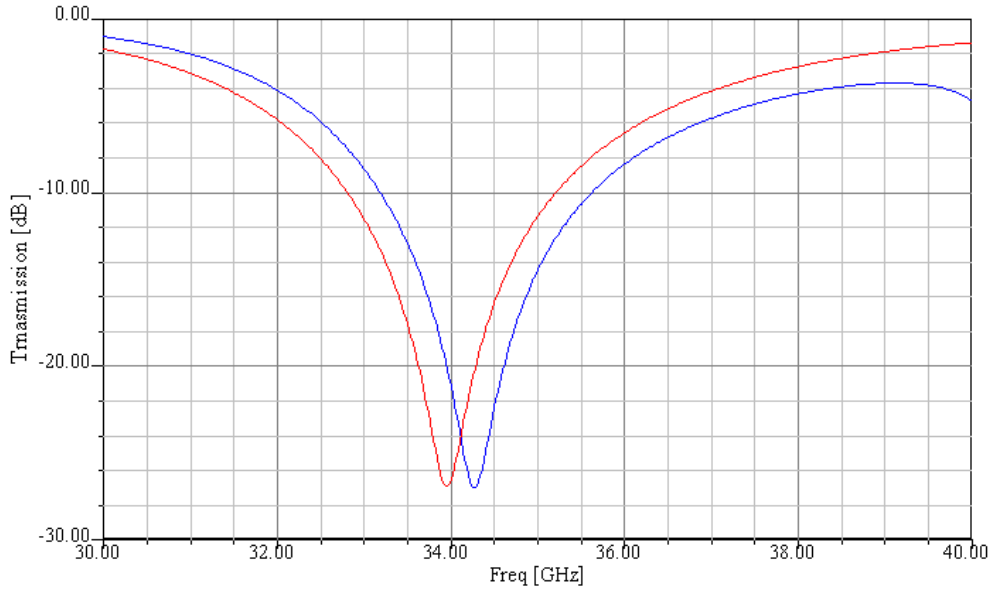


Figure 2-4: Effect of vacuum length in H field direction on resonance frequency (red curve $D_H=1.75$ mm, blue curve $D_H=3.5$ mm).

2.2.2 Simulation Problem 2

In this simulation problem, variation of the resonance frequency of the SRR array in response to changing the periodicity distance along the \overline{E} -field direction will be investigated by changing length (D_E) of the dielectric region from the metal strip to the PEC boundary. The same square shaped SRR unit cell of the first simulation problem is also used in this simulation. The SRR array is simulated for three different values of the parameter $D_E = 0.6, 0.9$ and 1.2 mm corresponding to the periodicity distance of $D_y = 4, 4.6$ and 5.2 mm along the y -axis. Resulting transmission spectra are plotted in Figure 2-5 below.

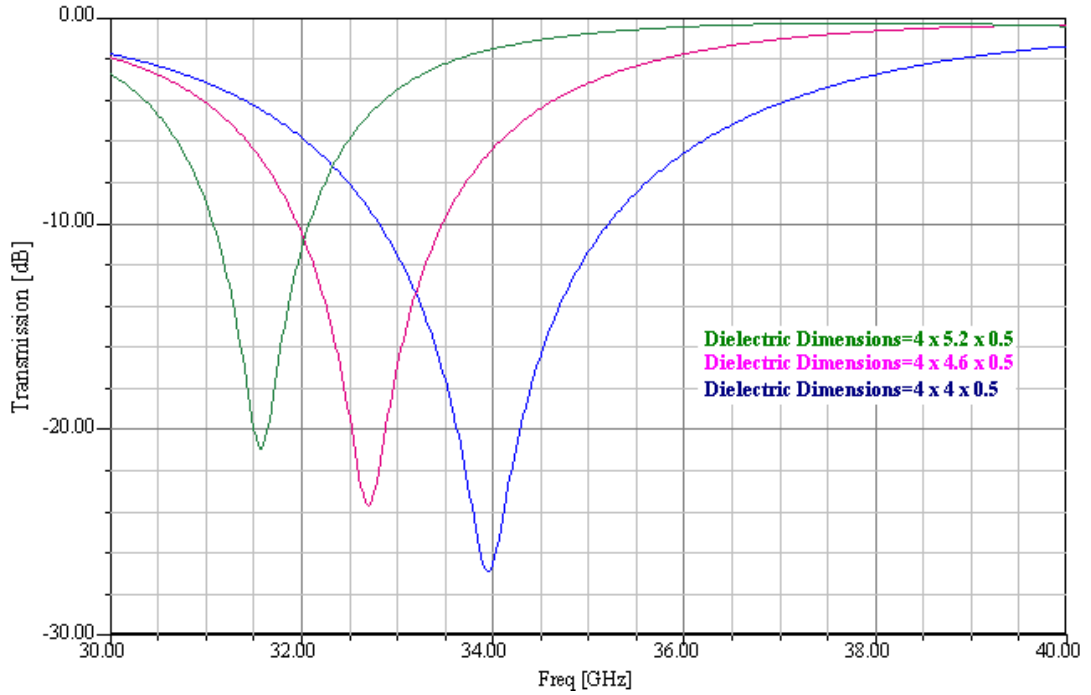


Figure 2-5: Variation of transmission minimum with substrate length in electric field direction.

As observed in this figure, resonance frequency of the SRR array decreases from 33.96 to 31.58 GHz as the periodicity distance along the electric field direction increases from 4 mm to 5.2 mm, which is an expected result. Because, due to the perfect electric conductor (PEC) boundary shown in Figure 2-3 (a), the original SRR cell and its mirror images carry induced currents in the same direction. Therefore, a subtractive mutual inductance is created between the adjacent SRR loops. As the parameter D_E gets larger, mutual inductance (M) obviously gets smaller, leading to increased equivalent inductance (L_{eq}) values. In the mean time, capacitive coupling between neighboring SRR cells also diminishes with increased separation distance. Decreasing coupling capacitance C_{mutual} will cause a smaller equivalent capacitance (C_{eq}) as the equivalent gap capacitance of each SRR cell and the coupling capacitance between adjacent cells are in series. However, based on the formulas given in [20], the coplanar component of the coupling capacitance, which is dominant as compared to the parallel plate component, decreases by the natural logarithm of the increasing separation distance between the adjacent SRR

elements while the mutual inductance term decreases almost linearly under the same effect. Therefore, the increase in L_{eq} is found to be faster than the decrease in C_{eq} and the product $L_{eq} C_{eq}$ increases causing the resonance frequency $\omega_0 = (L_{eq} C_{eq})^{-1/2}$ to decrease as D_E gets larger. To demonstrate this discussion graphically, a MATLAB code is written to compute the mutual inductance (M) and coupling capacitance (C_{mutual}) for various values of the separation distance $d=2D_E$ between the SRR cells in y -direction changing from 1.2 mm to 2.4 mm with 0.2 mm steps. Resulting curves are plotted in Figure 2-6 and Figure 2-7.

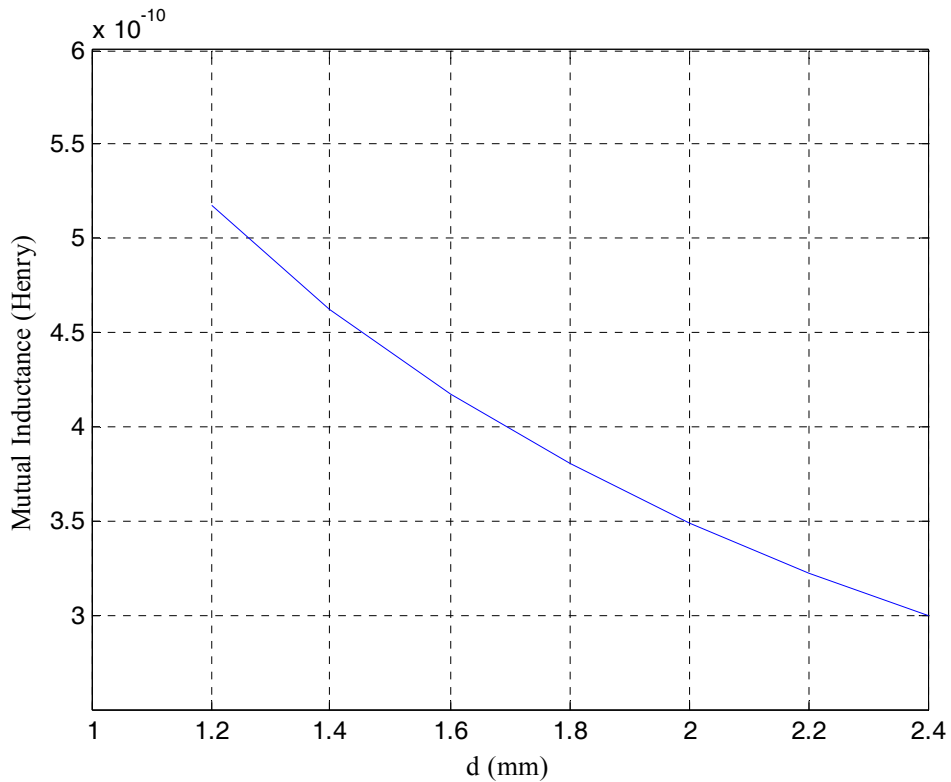


Figure 2-6: Variation of mutual inductance with cell to cell separation distance along the electric field direction.

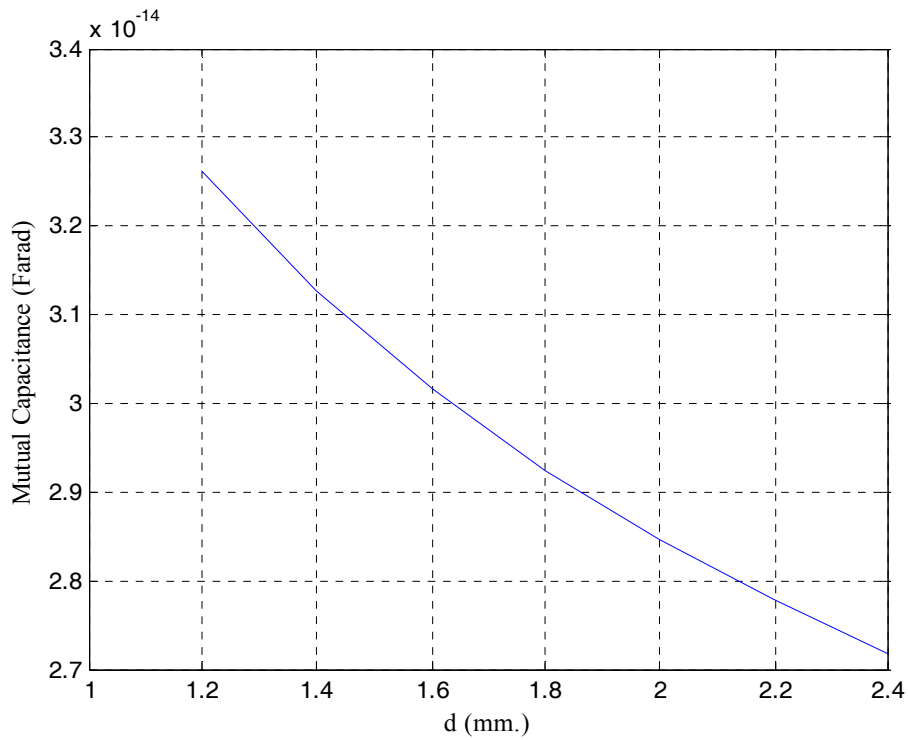


Figure 2-7: Variation of mutual capacitance with cell to cell separation distance along the electric field direction.

Rate of decreases of the mutual inductance and mutual capacitance curves (i.e. their local slopes at the sampling points) are also computed and plotted against $d=2D_E$ in Figure 2-8 and Figure 2-9. It is indeed seen that mutual inductance decreases more sharply than the mutual capacitance. Finally, the resonance frequency f_0 of the array is plotted versus $d=2D_E$ in Figure 2-10 showing the expected decrease in f_0 with increasing separation distance d based on the calculated circuit parameters.

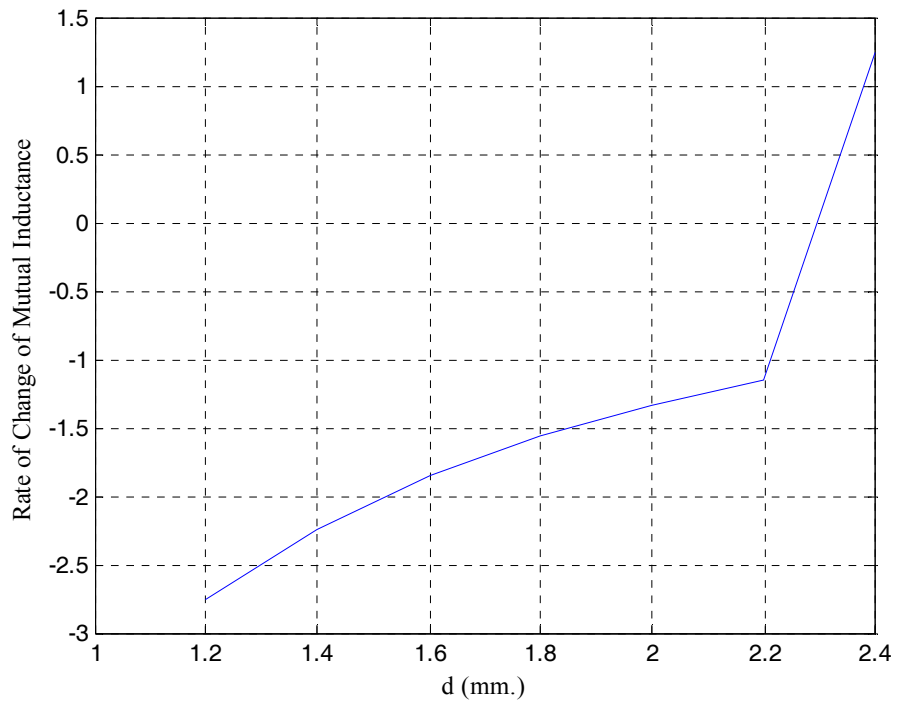


Figure 2-8: Rate of change of mutual inductance with d .

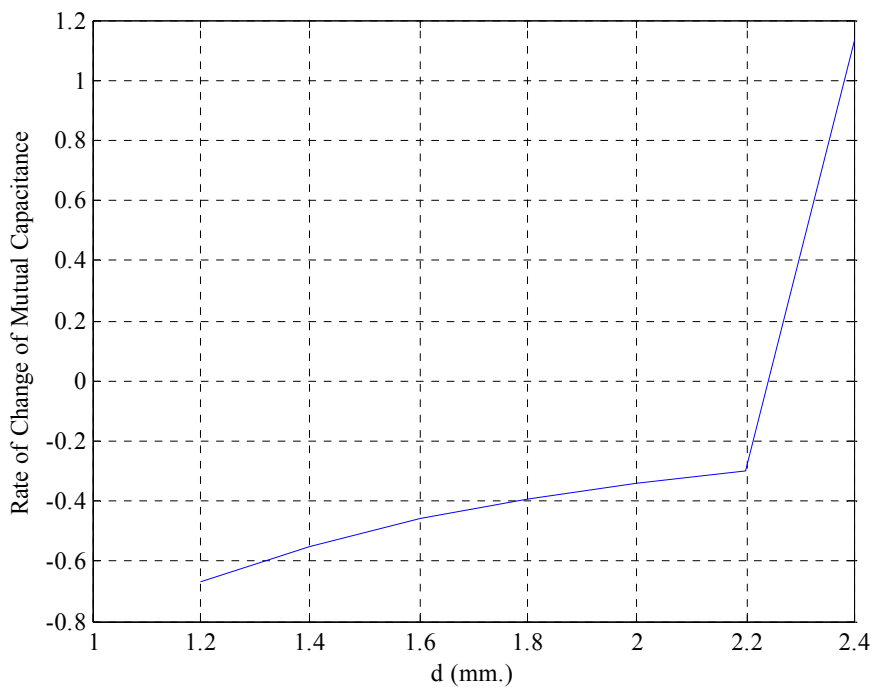


Figure 2-9: Rate of change of mutual capacitance with d .

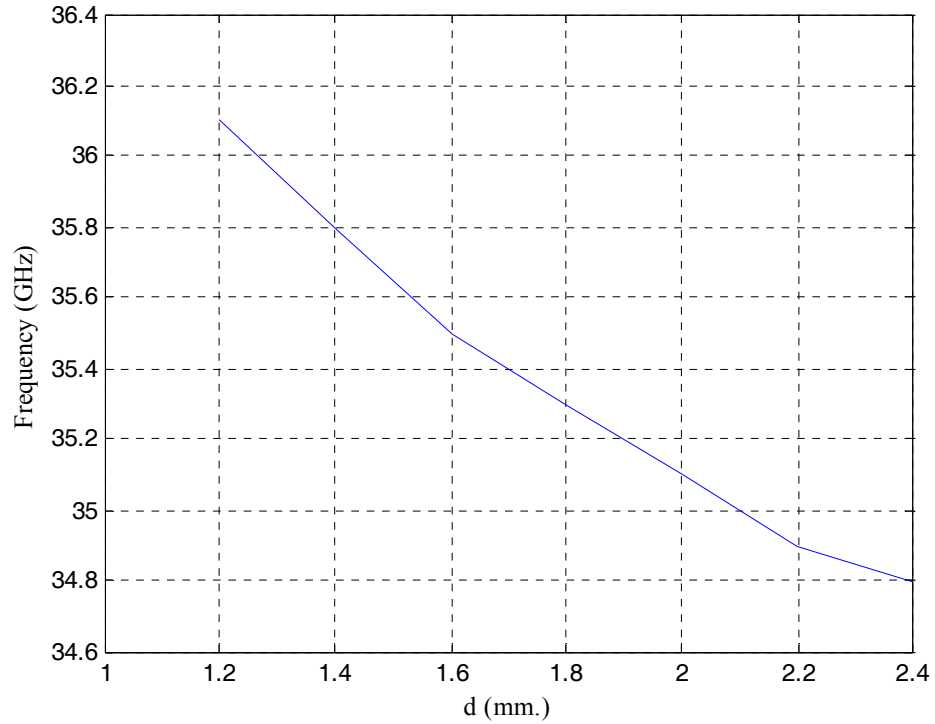


Figure 2-10: Variation of resonance frequency with d based on calculated circuit parameters.

2.2.3 Simulation Problem 3

As discussed at the beginning of section 2.2, type of boundary conditions (whether PEC/PMC or PML) changes the nature of the SRR simulation problem drastically and produces different transmission spectrum curves. To observe the effect of mutual interactions between neighboring SRR cells within an array topology, we have simulated four different array structures of dimensions 1x2x1, 1x3x1, 1x4x1 and 1x5x1 (i.e. one dimensional arrays of SRR cells in E-field direction) in addition to a single SRR unit cell by using HFSS software with PML boundary conditions. The metallic strips of the SRR unit cell are made of copper with 0.035 mm thickness and the 0.762 mm thick substrate is made of the AD350 dielectric material with the relative permittivity of $\epsilon_r=3.5$. Side length of the square shaped SRR loop (L) is 8 mm, gap width (g) is 0.3 mm and metal strip width (w) is 0.6

mm. The dielectric substrate has dimensions of $D_x=D_y=10$ mm both in x and y directions within one period of the array (see Figure 2-11). Transmission spectra of the infinite SRR array (implemented by PEC boundary conditions) and that of the isolated SRR cell (simulated by using the PML boundary conditions) were quite different from each other, as shown in Figure 2-12. However, transmission spectrum curves of the isolated “1x2x1 array” and isolated “1x3x1 array” looked more and more similar to that of the infinite SRR array, as expected, due to the included mutual interaction effects. Note that “isolation” condition is satisfied by using PML boundary conditions in HFSS simulations. Obviously, the isolated “1xnx1 array” should behave more and more similarly to the infinite array as n (number of array elements in E-field direction) gets larger. To see further convergence to the transmission spectra of the infinite array, the isolated “1x4x1 array” and “1x5x1 array” were also simulated. However, for these last two HFSS simulations the expected “converging” transmission spectrum curves could not be obtained (and the HFSS simulations needed extremely long run-times) due to insufficient mesh numbers (see Figure 2-12 and Table 2-1) used in FEM computations.

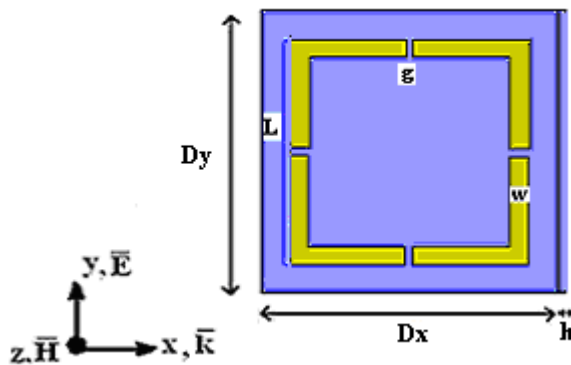


Figure 2-11: Unit cell geometry used for comparison of boundary conditions.

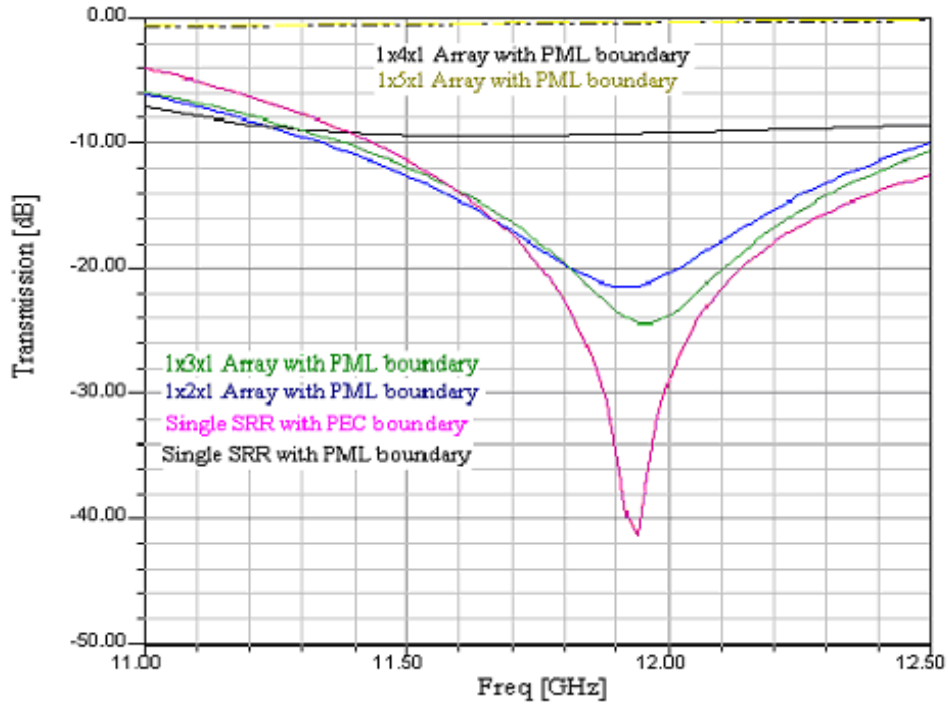


Figure 2-12: Comparison of transmission spectrum of different SRR configurations with PEC and PML boundaries using $D_E=1$ mm and $D_H=11.049$ mm.

Table 2-1: Comparison of mesh numbers used in HFSS simulations with PML boundary conditions for different number of array elements in electric field direction

Number of SRR elements	Single SRR	1x2x1 Array	1x3x1 Array	1x4x1 Array	1x5x1 Array
Mesh Number	13711	19675	23425	24621	30522

As seen in Table 2-1, number of elements of the 1x4x1 array and hence its computational volume is doubled as compared to those for the 1x2x1 array, for instance, but the mesh number is increased by only 25 percent. If these simulations were run using a more powerful computer, much better numerical resolution would be obtained as a result of using sufficiently large mesh numbers. Therefore the transmission curves to be obtained for the 1x4x1 and 1x5x1 arrays would look much more similar to 1x ∞ x1 array result shown in Figure 2-12 which is obtained

when the transmission spectra of an SRR unit cell is simulated by HFSS with PEC boundary conditions.

So far, issues relevant to HFSS simulations of SRR structures have been discussed. In the following section, basics of equivalent circuit modeling for SRR unit cells and arrays will be presented.

2.3 Basics of SRR Modeling by Equivalent Lumped Circuit Models

The need for developing equivalent circuit models for SRR structures has already been discussed in the Introduction chapter. Most of the studies reported in literature [5, 6, 10-12,16] have attempted to represent the conventional SRR or BC-SRR unit cell structures by a simple LC resonant circuit so that the resonance frequency can be obtained from the well-known formula $f_0 = (2\pi\sqrt{LC})^{-1}$ where C is the equivalent lumped capacitance and L is the equivalent lumped inductance of this basic model. A few of these papers included the loss effects into the SRR cell model by suggesting equivalent resistance expressions as well [5, 6, 11]. Expressions of L, C and R are functions of the SRR unit cell geometry, dimensions and electrical parameters of the metal and dielectric substrate materials. The mutual capacitance and mutual inductance values pertinent to the conventional two ring SRR and multiple-ring SRR [6] unit cells are implicitly included in the equivalent capacitance and inductance expressions used in the above mentioned references. Johnson *et al* [12] provided the expressions for the mutual inductance and coupling capacitance effects between two neighboring (single ring with single split type) SRR unit cells resonating at infrared frequencies. The main purpose of equivalent circuit modeling was the estimation of resonance frequency in all the studies mentioned above except for the work in [11] where the estimation of the S-parameter spectra was demonstrated by Wu *et al*.

In this thesis, not only the resonance frequency values but also the transmission spectrum of SRR unit cells (single square ring with multiple split type) and SRR arrays are estimated by using two-port equivalent circuits to model individual SRR behaviors and coupling effects resulting from array topologies. Ohmic loss effects (taking place in conductors and dielectric parts) are also taken into account to improve the accuracy of the equivalent circuit models. Then, transmission spectra of the investigated SRR structures are computed with simple and fast Matlab codes by using Z-parameter, Y-parameter and chain parameter matrices, whenever needed. The results are converted finally to S-parameter forms since the transmission spectrum is the magnitude of the complex S_{21} spectrum of the overall SRR array. Accuracy of the resulting equivalent circuit models is tested by comparing the modeling results with the results obtained from HFSS simulations.

2.3.1 Modeling an SRR Unit Cell by a Proper RLC Circuit

There have been attempts in literature to model individual SRR unit cells by LC circuits and compute the resonance frequency from $f_0 = (2\pi\sqrt{LC})^{-1}$ formula. Since our purpose is to compute the whole transmission spectrum (or the complex S-parameters S_{21} , S_{11} , etc. in general), we should do more than that and suggest a properly described two-port circuit representation for the SRR unit cell considered. At this point, four possibilities have emerged: (i) Series RLC resonant circuit in the shunt branch, (ii) Parallel RLC resonant circuit in the shunt branch, (iii) Series RLC resonant circuit in the series branch or (iv) Parallel RLC resonant circuit in the series branch of the two-port representation of the SRR. The feasible or most suitable resonant two-port configuration is determined as outlined below. For simplicity, but without any loss of generality, the loss effects are neglected in the following investigation.

Case 1: If the SRR unit cell is represented by a resonant LC circuit as in the cases (i) or (ii) mentioned above, the corresponding equivalent two-port circuit

representations will look like the one shown in Figure 2-13 where Z is the equivalent impedance of the lumped elements in the shunt branch.

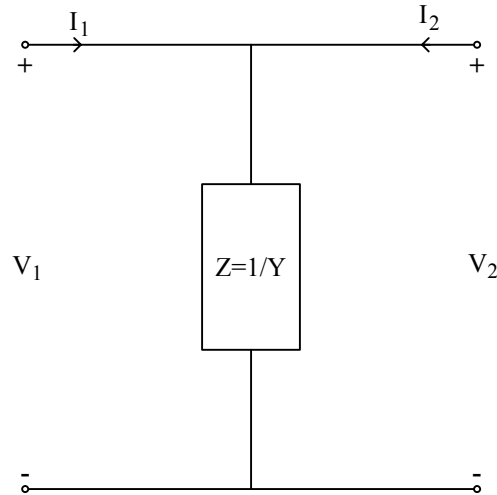


Figure 2-13: Two-port equivalent circuit representation of a single loop SRR cell with either series or parallel LC resonant circuit in the shunt branch.

The Z -matrix representation of this two-port circuit is given as:

$$\begin{bmatrix} V_1 \\ V_2 \end{bmatrix} = \begin{bmatrix} Z_{11} & Z_{12} \\ Z_{21} & Z_{22} \end{bmatrix} \begin{bmatrix} I_1 \\ I_2 \end{bmatrix} \quad (1)$$

$$Z_{11} = \left. \frac{V_1}{I_1} \right|_{I_2=0} = Z \quad (2)$$

$$Z_{21} = \left. \frac{V_2}{I_1} \right|_{I_2=0} = Z \quad (3)$$

$$Z_{12} = \left. \frac{V_1}{I_2} \right|_{I_1=0} = Z \quad (4)$$

$$Z_{22} = \left. \frac{V_2}{I_2} \right|_{I_1=0} = Z \quad (5)$$

Hence the $[Z]$ matrix is obtained as:

$$[Z] = \begin{bmatrix} Z & Z \\ Z & Z \end{bmatrix} \quad (6)$$

The Y-matrix representation of the same two-port is given by:

$$\begin{bmatrix} I_1 \\ I_2 \end{bmatrix} = \begin{bmatrix} Y_{11} & Y_{12} \\ Y_{21} & Y_{22} \end{bmatrix} \begin{bmatrix} V_1 \\ V_2 \end{bmatrix} \quad (7)$$

However, the $[Y]$ matrix is not defined for this particular two-port circuit as $[Y] = [Z]^{-1}$ and $\det(Z) = |Z| = 0$

As another alternative, chain $[ABCD]$ matrix representation of this two-port circuit can be obtained from:

$$\begin{bmatrix} V_1 \\ I_1 \end{bmatrix} = \begin{bmatrix} A & B \\ C & D \end{bmatrix} \begin{bmatrix} V_2 \\ -I_2 \end{bmatrix} \quad (8)$$

$$A = \left. \frac{V_1}{V_2} \right|_{I_2=0} = 1 \quad (9)$$

$$B = \left. \frac{V_1}{-I_2} \right|_{V_2=0} = 0 \quad (10)$$

$$C = \left. \frac{I_1}{V_2} \right|_{I_2=0} = Y \quad (11)$$

$$D = \left. \frac{I_1}{-I_2} \right|_{V_2=0} = 1 \quad (12)$$

$$\begin{bmatrix} A & B \\ C & D \end{bmatrix} = \begin{bmatrix} 1 & 0 \\ Y & 1 \end{bmatrix} \quad (13)$$

This representation will be used later in Chapters 3 and 4 for model computations. It should be noted that the conversion between impedance parameters and chain parameters is given by the rule [21]:

$$\begin{bmatrix} A & B \\ C & D \end{bmatrix} = \begin{bmatrix} \frac{Z_{11}}{Z_{21}} & \frac{\Delta Z}{Z_{21}} \\ 1 & \frac{Z_{22}}{Z_{21}} \end{bmatrix} = \begin{bmatrix} 1 & 0 \\ Y_z & 1 \end{bmatrix} \quad (14)$$

where

$$\Delta Z = \det(Z) \quad (15)$$

It is also possible to obtain the scattering parameters of a given two-port network from its Z -parameters as summarized below [21]:

$$S_{11} = \frac{(Z_{11} - Z_0)(Z_{22} + Z_0) - Z_{12}Z_{21}}{(Z_{11} + Z_0)(Z_{22} + Z_0) - Z_{12}Z_{21}} = \frac{(Z - Z_0)(Z + Z_0) - Z^2}{(Z + Z_0)(Z + Z_0) - Z^2}$$

$$S_{11} = \frac{-Z_0}{2Z + Z_0} \quad (16)$$

$$S_{21} = \frac{2Z_{21}Z_0}{(Z_{11} + Z_0)(Z_{22} + Z_0) - Z_{12}Z_{21}} = \frac{2ZZ_0}{(Z + Z_0)(Z + Z_0) - Z^2}$$

$$S_{21} = \frac{2Z}{2Z + Z_0} \quad (17)$$

$$S_{12} = \frac{2Z_{12}Z_0}{(Z_{11} + Z_0)(Z_{22} + Z_0) - Z_{12}Z_{21}} = \frac{2ZZ_0}{(Z + Z_0)(Z + Z_0) - Z^2}$$

$$S_{12} = \frac{2Z}{2Z + Z_0} = S_{21} \quad (18)$$

$$S_{22} = \frac{(Z_{11} - Z_0)(Z_{22} + Z_0) - Z_{12}Z_{21}}{(Z_{11} + Z_0)(Z_{22} + Z_0) - Z_{12}Z_{21}} = \frac{(Z - Z_0)(Z + Z_0) - Z^2}{(Z + Z_0)(Z + Z_0) - Z^2}$$

$$S_{22} = \frac{-Z_0}{2Z + Z_0} = S_{11} \quad (19)$$

The parameter Z_0 used in equations (16)-(19) is the terminal impedance at the input and output ports, by definition. Data for this normalization factor is provided by the HFSS simulation of the analyzed SRR structure while comparing the HFSS simulation results and the equivalent circuit modeling results. As mentioned earlier, we have two possibilities for the topology of the shunt branch in Figure 2-13, a series LC resonant circuit as shown in Figure 2-14 (a) or a parallel LC resonant circuit as shown in Figure 2-14 (b). In both cases, the structure resonates at

$$2\pi f_0 = \omega_0 = \frac{1}{\sqrt{LC}}.$$

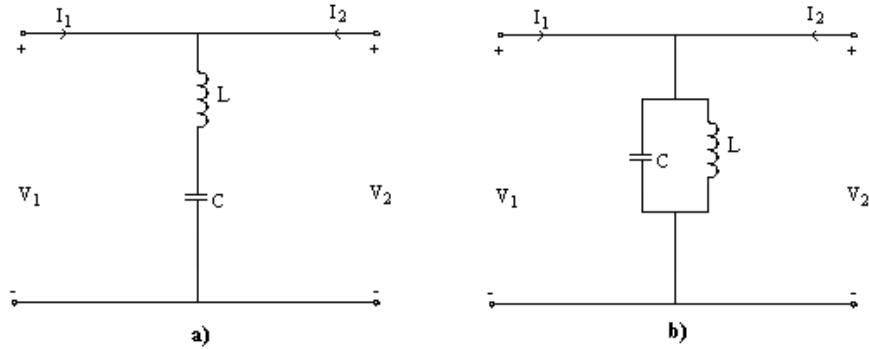


Figure 2-14: Two different representations for the impedance Z a) Series LC circuit, b) Parallel LC circuit.

For the first case in Figure 2-14 (a), Z becomes:

$$Z = j\omega L + \frac{1}{j\omega C} = \frac{1 - \omega^2 LC}{j\omega C} \quad (20)$$

Obviously, we have $Z=0$ at the resonance frequency $f_0 = \frac{1}{2\pi\sqrt{LC}}$. Also, from equation (17), it can be seen that the transmission spectrum becomes also zero as $S_{21}=0$ at $f=f_0$. It can be also concluded from equations (17) and (20) that S_{21} approaches to unity as frequency f approaches to both zero and infinity. In other words, the two-port circuit topology shown in Figure 2-14 (a) has the expected “band-stop” or “notch” type transmission spectrum with a minimum (at the zero level in this lossless case) at the resonance frequency f_0 .

For the second case shown in Figure 2-14 (b), on the other hand, the impedance Z becomes:

$$Z = \frac{1}{j\omega C + \frac{1}{j\omega L}} = \frac{j\omega L}{1 - \omega^2 LC} \quad (21)$$

Obviously, Z approaches to infinity at the resonance frequency $f=f_0$. Therefore, S_{21} approaches to unity at resonance based on the equation (17) which is not an expected behavior for the transmission spectrum of the SRR unit cell. In conclusion, parallel LC resonant circuit in the shunt branch of Figure 2-14 (b) is not an acceptable circuit representation for the SRR while the series LC resonant circuit in the shunt branch is a perfectly acceptable choice. Figure 2-15 shows an improved version of this acceptable equivalent circuit model where the total conductor losses are represented by the resistance, R_c , which is connected in series with the total self inductance L , and dielectric losses around the gaps are represented by the resistance, R_d , which is connected in parallel to the equivalent gap capacitance, C .

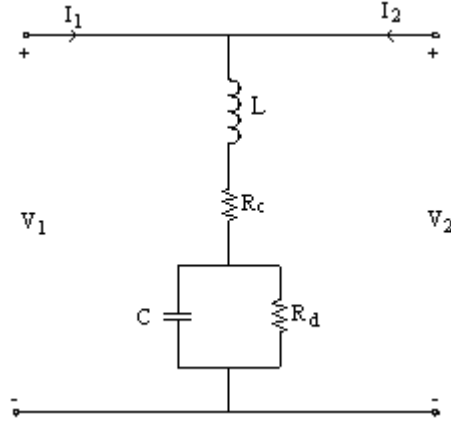


Figure 2-15: A feasible two-port equivalent circuit representation for SRR unit cell including ohmic loss effects.

The impedance Z for this improved branch model is given as:

$$Z = R_c + j\omega L + \left(\frac{\frac{1}{j\omega C} R_d}{\frac{1}{j\omega C} + R_d} \right) \quad (22)$$

Inserting Z into the equations (16) and (17), S-parameters S_{11} and S_{21} can be obtained as:

$$S_{11} = \frac{-(1 + j\omega C R_d) Z_0}{2R_c + 2R_d - 2\omega^2 L C R_d + j\omega(2C R_c R_d + 2L + Z_0 C R_d) + Z_0} \quad (23)$$

$$S_{21} = \frac{2R_c + 2R_d - 2\omega^2 L C R_d + 2j\omega(C R_c R_d + L)}{2R_c + 2R_d - 2\omega^2 L C R_d + j\omega(2C R_c R_d + 2L + Z_0 C R_d) + Z_0} \quad (24)$$

$$R_c = \frac{4l}{\sigma \delta 2(w+t)} \quad (25)$$

$$R_d = \frac{g}{(\tan \alpha)(\omega \epsilon)wh} \quad (26)$$

The parameters used in equation (25) are defined as follows: l is the side length of SRR, σ is the conductivity of metal, δ is skin depth in metal, w is width of the metal stripes and t is the thickness of metal layer. While modeling the conductor losses by R_c , good conductor assumption has been made. The perimeter of the cross section of square SRR is given by $2(w+t)$ and multiplying this expression by skin depth gives the effective current carrying surface over the cross section of metallic strip. For good conductors, skin depth δ is given as

$$\delta = \frac{1}{\sqrt{\pi f \mu \sigma}} \quad (27)$$

In the expression of R_d , on the other hand, conductivity σ_d of the low-loss (good dielectric) substrate is replaced by $\sigma_d = \omega \varepsilon \tan \alpha$ where $\omega = 2\pi f$ is the angular frequency, $\varepsilon = \varepsilon_0 \varepsilon_r$ is the permittivity of the substrate and $\tan \alpha$ is the loss tangent of the substrate. As defined earlier, w is the width of metal strip and h is the thickness of substrate. As the substrate thickness is small enough (only 0.5 mm) for the present SRR geometry, electromagnetic waves in the gap (split) region are assumed to penetrate into the substrate through its whole depth along the z direction.

A Matlab code is written to compute the transmission spectrum of SRR unit cell using Equations (24) through (27) for the SRR parameters used in section 2.2.3. The resulting $|S_{21}|$ versus frequency curve is plotted in Figure 2-16 together with the transmission spectrum of this SRR obtained from the HFSS simulation with PML boundary conditions. In this simulation, separation distance D_H is taken to be 5 mm between the SRR surface and the PML layer. These two curves are found in good agreement.

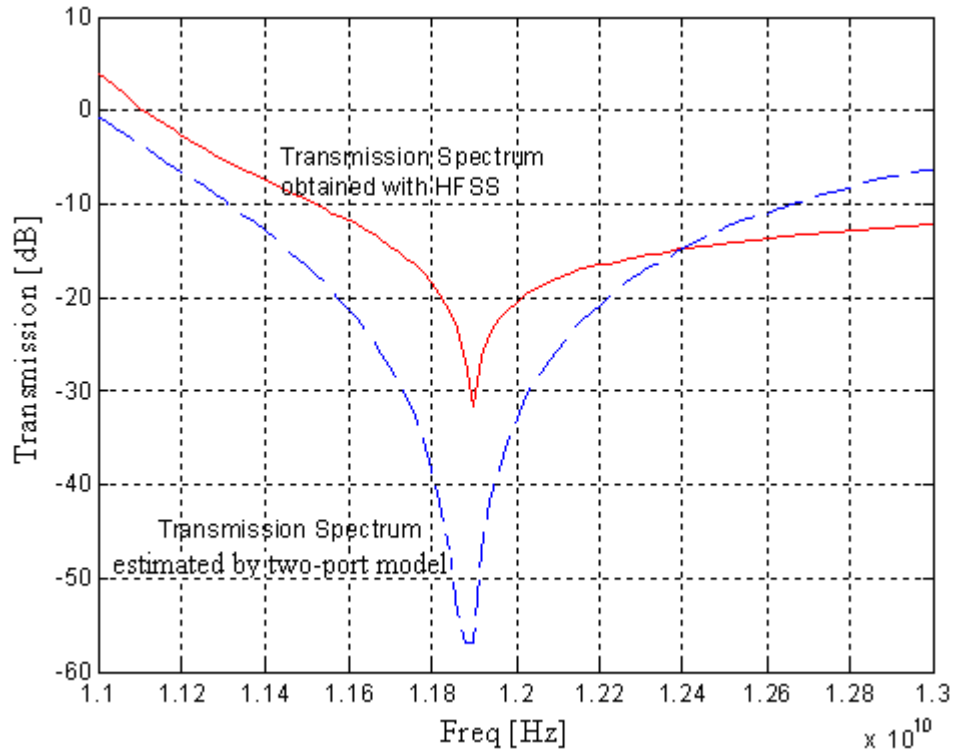


Figure 2-16: Transmission spectrum curves of the isolated SRR cell, which are obtained by HFSS simulation with PML boundary conditions (with $D_E=1$ mm and $D_H=5$ mm) and by equivalent circuit modeling approach. Geometry and dimensions for the SRR cell are described in Section 2.2.3. Equivalent circuit model is given in Figure 2-15.

As seen in Figure 2-16, the resonance frequency obtained from the equivalent circuit model is 11.89 GHz while the HFSS simulation result gives 11.90 GHz. Also, the overall shapes of these two waveforms of transmission spectrum are reasonably close to each other over the whole computational frequency bandwidth.

Case 2: To model a single loop SRR with a two port equivalent circuit model, there are two other possibilities; a series LC resonant circuit or a parallel LC resonant circuit placed in the series branch of the two-port. Possibility of both cases can be investigated using the two-port circuit shown in Figure 2-17.

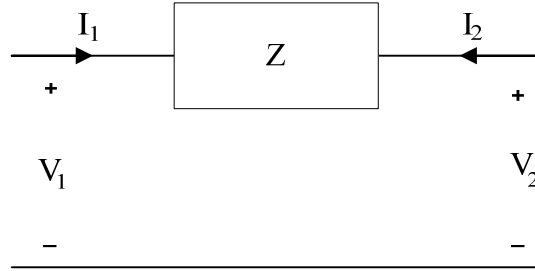


Figure 2-17: Alternative two-port equivalent circuit representation of a single loop SRR with either series or parallel LC resonant circuit in the series branch.

The Y-matrix representation of this two-port is given as:

$$\begin{bmatrix} I_1 \\ I_2 \end{bmatrix} = \begin{bmatrix} Y_{11} & Y_{12} \\ Y_{21} & Y_{22} \end{bmatrix} \begin{bmatrix} V_1 \\ V_2 \end{bmatrix} \quad (28)$$

where

$$Y_{11} = \left. \frac{I_1}{V_1} \right|_{V_2=0} = Y \quad (29)$$

$$Y_{21} = \left. \frac{I_2}{V_1} \right|_{V_2=0} = -Y \quad (30)$$

$$Y_{12} = \left. \frac{I_1}{V_2} \right|_{V_1=0} = -Y \quad (31)$$

$$Y_{22} = \left. \frac{I_2}{V_2} \right|_{V_1=0} = Y \quad (32)$$

$$[Y] = \begin{bmatrix} Y & -Y \\ -Y & Y \end{bmatrix} \quad (33)$$

The Z-matrix representation of this two-port is not defined as $[Z] = [Y]^{-1}$ where determinant of the $[Y]$ matrix is zero.

Also, the chain parameter representation of this two-port can be obtained as

$$\begin{bmatrix} V_1 \\ I_1 \end{bmatrix} = \begin{bmatrix} A & B \\ C & D \end{bmatrix} \begin{bmatrix} V_2 \\ -I_2 \end{bmatrix} \quad (34)$$

$$A = \left. \frac{V_1}{V_2} \right|_{I_2=0} = 1 \quad (35)$$

$$B = \left. \frac{V_1}{-I_2} \right|_{V_2=0} = Z \quad (36)$$

$$C = \left. \frac{I_1}{V_2} \right|_{I_2=0} = 0 \quad (37)$$

$$D = \left. \frac{I_1}{-I_2} \right|_{V_2=0} = 1 \quad (38)$$

$$\begin{bmatrix} A & B \\ C & D \end{bmatrix} = \begin{bmatrix} 1 & Z \\ 0 & 1 \end{bmatrix} \quad (39)$$

Conversion between the Y-parameters and the chain [ABCD] parameters is possible according to the following rules [21]:

$$\begin{bmatrix} A & B \\ C & D \end{bmatrix} = \begin{bmatrix} -\frac{Y_{22}}{Y_{21}} & -\frac{1}{Y_{21}} \\ -\frac{\Delta Y}{Y_{21}} & -\frac{Y_{11}}{Y_{21}} \end{bmatrix} = \begin{bmatrix} 1 & \frac{1}{Y} \\ 0 & 1 \end{bmatrix} \quad (40)$$

$$\Delta Y = |[Y]| = \det([Y]) \quad (41)$$

Finally, the S-Parameters can be obtained from the Y-Parameters [21] as described below:

$$S_{11} = \frac{(Y_0 - Y_{11})(Y_0 + Y_{22}) + Y_{12}Y_{21}}{(Y_{11} + Y_0)(Y_{22} + Y_0) - Y_{12}Y_{21}} = \frac{(Y_0 - Y)(Y_0 + Y) + Y^2}{(Y_0 + Y)(Y_0 + Y) - Y^2}$$

$$S_{11} = \frac{Y_0}{2Y + Y_0} = S_{22} \quad (42)$$

$$S_{21} = \frac{-2Y_{21}Y_0}{(Y_{11} + Y_0)(Y_{22} + Y_0) - Y_{12}Y_{21}} = \frac{2YY_0}{(Y + Y_0)((Y + Y_0) - Y^2)}$$

$$S_{21} = \frac{2Y}{2Y + Y_0} = S_{12} \quad (43)$$

where the normalization term $Y_0 = \frac{1}{Z_0}$ is the terminal admittance seen at the input/output ports, by definition. The magnitude of the S_{21} spectrum must result in a transmission curve which is expected to be zero (in the lossless case) at the resonance frequency $f_0 = \frac{1}{2\pi\sqrt{LC}}$ for the SRR unit cell under consideration. Also, as seen from equation (43), $Y=0$ condition must hold at resonance to satisfy this expectation. This point should be taken into account while evaluating the possibilities of alternative two-port equivalent circuit topologies shown in Figure 2-18.

For the equivalent circuit shown in Figure 2-18 (a), the admittance Y is obtained as given in equation (44) and it is seen that Y approaches to infinity at $f_0 = \frac{1}{2\pi\sqrt{LC}}$ causing S_{21} to approach to unity (see equation (43)). As zero transmittance is expected at resonance, this equivalent circuit can not be a feasible choice to represent the SRR unit cell.

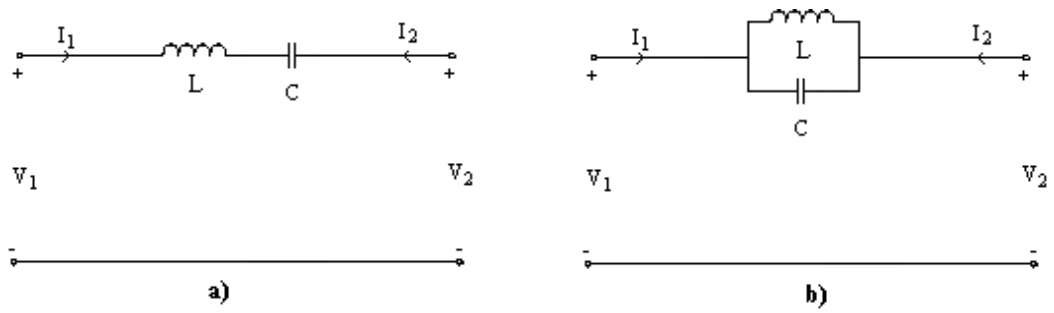


Figure 2-18: Alternative representations of two-port network consisting of series impedance
a) Series LC circuit, b) Parallel LC circuit.

$$Y = \frac{1}{Z} = \frac{j\omega C}{1 - \omega^2 LC} \quad (44)$$

For the two-port equivalent circuit model shown Figure 2-18 (b), on the other hand, expression for the admittance Y is given in equation (45) and it becomes zero at the resonance frequency making the transmittance also zero, as expected.

$$Y = \frac{1}{Z} = \frac{1 - \omega^2 LC}{j\omega L} \quad (45)$$

Therefore, this potentially useful equivalent circuit is investigated in more detail by including the loss effects into the model as shown in Figure 2-19 where the resistance R_c represents the conductor losses and the other resistance R_d represents the dielectric losses occurring around the gap locations. The admittance expression for this improved topology is given in equation (46).

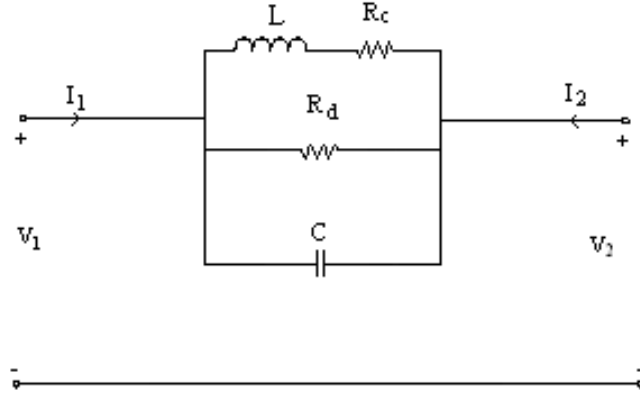


Figure 2-19: Improved version of the two-port circuit representation shown in Figure 2-18 (b) with the inclusion of equivalent loss resistances.

$$Y = \frac{1}{Z} = \frac{(j\omega L + R_c)(1 + j\omega C R_d) + R_d}{(j\omega L + R_c)R_d} \quad (46)$$

Next, expressions for the scattering parameters S_{21} and S_{11} can be computed using equations (42), (43) and (46) to get:

$$S_{11} = \frac{Y_0(j\omega L R_d + R_c R_d)}{2j\omega L - 2\omega^2 L C R_d + 2j\omega C R_c R_d + 2R_c + 2R_d + Y_0(j\omega L R_d + R_c R_d)} \quad (47)$$

$$S_{21} = \frac{-2(j\omega L - \omega^2 L C R_d + j\omega C R_c R_d + R_c + R_d)}{2j\omega L - 2\omega^2 L C R_d + 2j\omega C R_c R_d + 2R_c + 2R_d + Y_0(j\omega L R_d + R_c R_d)} \quad (48)$$

Where the loss resistances R_c and R_d are computed from equations (25) and (26). Again a Matlab code is developed to compute the S_{11} and S_{21} parameters. The magnitude of S_{21} spectrum is plotted against frequency in Figure 2-20. The $|S_{21}|$ spectrum obtained by an HFSS simulation is also plotted on the same figure for comparison. Although these two curves are found similar, the agreement between the results obtained by HFSS and equivalent circuit models are not found good enough as compared to the case demonstrated earlier in Figure 2-16.

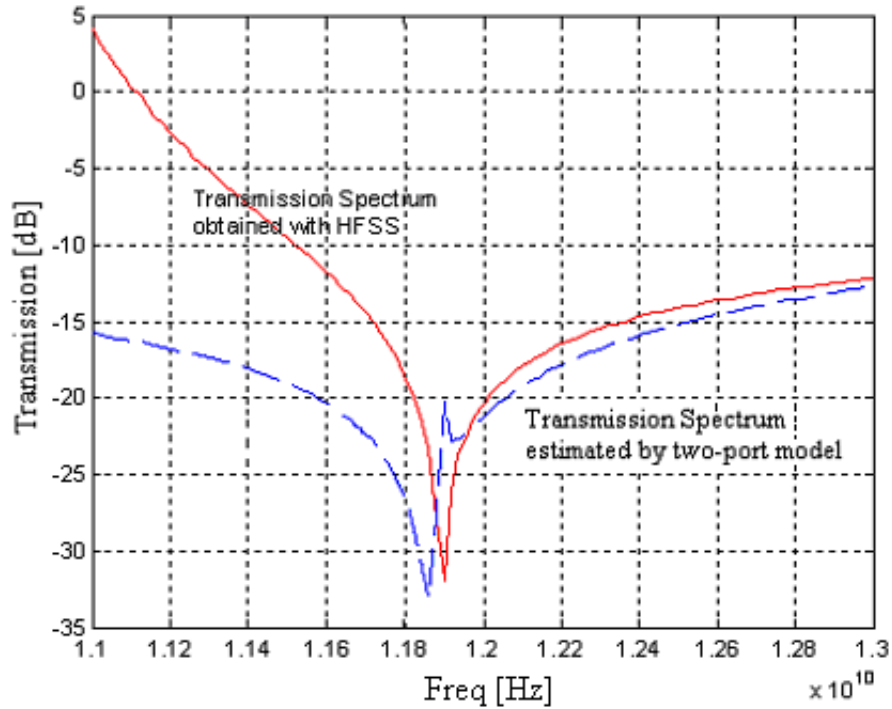


Figure 2-20: Transmission spectrum curves of the isolated SRR cell, which are obtained by HFSS simulation with PML boundary conditions (with $D_E=1$ mm and $D_H=5$ mm) and by equivalent circuit modeling approach. Geometry and dimensions for the SRR cell is described in Section 2.2.3. Equivalent circuit model is given in Figure 2-19.

Based on the conclusions derived from the results of section 2.3, the two-port equivalent circuit model shown in Figure 2-15, i.e the series resonant RLC circuit in the shunt branch of the two-port circuit, is found to be the best lumped circuit model to represent the single loop SRR unit cell structure. Only this equivalent circuit topology will be used in the remaining chapters of this thesis to develop equivalent circuit models of SRR arrays.

CHAPTER 3

NUMERICAL SIMULATIONS AND TWO PORT EQUIVALENT CIRCUIT MODELING OF SQUARE SHAPED SINGLE LOOP SRR STRUCTURES

3.1 Introduction

In this chapter, unit cell and array topologies with square-shaped single loop four-split SRR structures will be modeled using the novel two-port equivalent circuit modeling approach presented in section 2.3 of the previous chapter. Individual SRR unit cells of the arrays will be represented by the series RLC resonant circuit model shown in Figure 2-15. Interaction effects (i.e. the inductive and capacitive coupling effects between the array elements) and additional ohmic losses stemming from the non-zero conductivity of the dielectric substrate will also be modeled using proper two-port circuits.

Transmission spectrum of a given array structure will be computed to be the magnitude of the S_{21} spectrum of the two-port circuit representation of the overall SRR array. Z-parameter, Y-parameter and chain (ABCD) parameter representations will be used whenever needed to obtain the S-parameter matrix of the given topology. Results of equivalent circuit models will be compared to HFSS simulation results for validation. Isolated SRR structures will be simulated using PML type boundary conditions as shown in Figure 3-1 (a). Infinite SRR arrays, on the other hand, will be simulated by using PEC/PMC type boundary conditions as seen in Figure 3-1 (b).

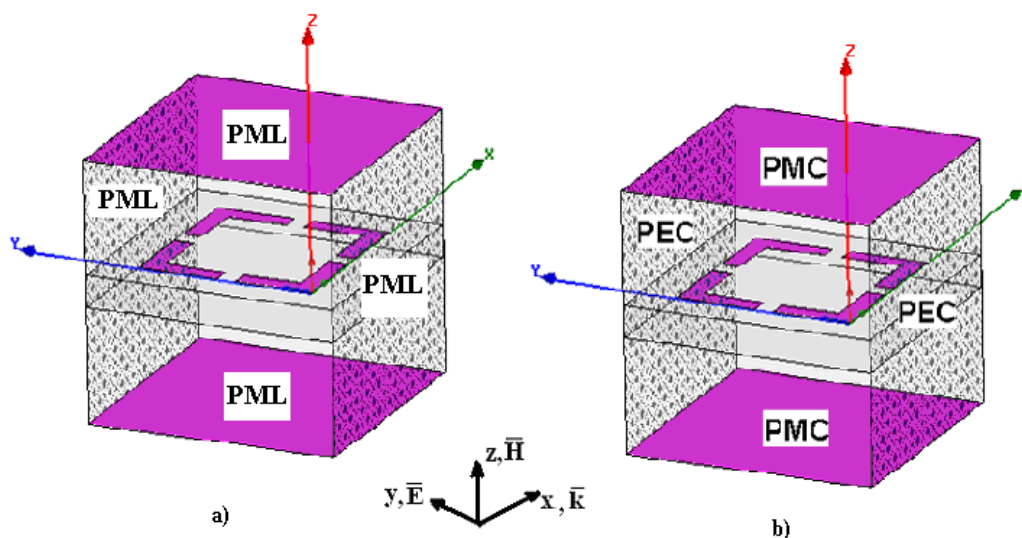


Figure 3-1: Boundary conditions for HFSS simulations: a) PML boundary conditions to examine an isolated SRR unit cell, b) PEC/PMC boundary conditions to examine a two dimensional infinite SRR array.

In this chapter, in addition to the SRR unit cell, arrays of SRR cells with sizes $1 \times 2 \times 1$, $2 \times 1 \times 1$ and $2 \times 2 \times 1$ will be analyzed. The notation used to identify SRR array sizes is previously given in Figure 2-1.

3.2 Single-Loop Square-Shaped SRR Unit Cell

In the first subsection to follow, transmission spectrum of a single-loop square shaped SRR unit cell with four identical gaps will be estimated by using both equivalent circuit modeling approach and HFSS simulation approach. Then, in the next subsection, an infinite SRR array structure will be examined.

3.2.1 Numerical Simulation and Equivalent Circuit Modeling of the Isolated SRR Unit Cell

The isolated SRR unit cell investigated in this subsection has four gaps (splits) of equal width (g) placed at the middle of each side of its square loop as shown in

Figure 3-2 (a) and (b). The copper strips forming this fully-symmetrical multi-split ring are printed on a low-loss dielectric substrate with $\epsilon_r = 4.6$ and $\tan \alpha = 0.01$. Dimensions of this SRR unit cell are given in Table 3-1. Figure 3-2 (b) shows the instantaneous charge polarities induced across the gap locations, due to the magnetic induction phenomena caused by a time-varying incident magnetic field as discussed previously. Geometrical parameters of SRR cells are also indicated in Figure 3-2 (b). The equivalent lumped circuit used to model an individual SRR cell is given in Figure 3-2 (c) where the equivalent capacitance (C_{eq}) is equal to one fourth of individual gap capacitance (C_{gap}) as all four of these equal gap capacitances are connected in series. Computation of circuit parameters L_{self} (total self inductance of the metal ring), C_{gap} , R_c (equivalent resistance representing conductor losses) and R_d (equivalent resistance representing dielectric losses) will be discussed later in this subsection.

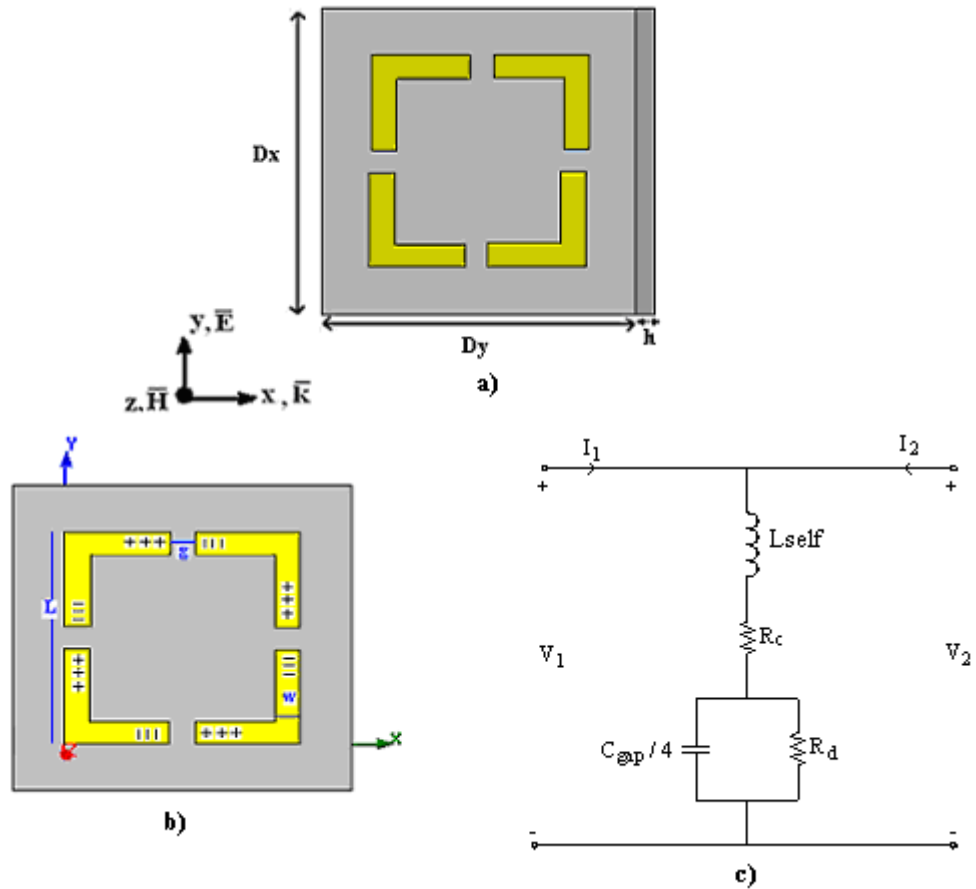


Figure 3-2: a) Unit cell geometry of a single square loop SRR, b) Parameters of the isolated SRR cell, c) Equivalent two-port circuit model of the SRR cell.

Table 3-1: Geometrical parameters of the SRR unit cell shown in Figure 3-2

Substrate Dimensions	L (Side length of the SRR)	g (Gap Width)	w (Width of Metal Strip)	t(Thickness of Metal Strip)
$D_x=D_y=4\text{mm}$ $h=0.5\text{ mm}$	2.8 mm	0.3 mm	0.3 mm	1 μm .

To calculate the gap capacitance, both coplanar (C_{cp}) and parallel-plate (C_{pp}) capacitance contributions should be taken into account [12, 20]. These capacitance

contributions are calculated in this thesis by using equations (49) through (51). Also, the total self inductance of the metal loop is calculated using equation (52) as discussed in reference [22].

$$C_{cp} = \frac{(\varepsilon_r + 1)\varepsilon_0}{2\pi} \ln \left[2 \frac{1 + \sqrt{k'}}{1 - \sqrt{k'}} \right] \text{ F/m} \quad (49)$$

$$k' = \sqrt{1 - \left(\frac{p}{p + 2q} \right)^2} \quad (50)$$

$$C_{pp} = \varepsilon \frac{wt}{g} \quad (51)$$

$$L_{\text{self}} \approx \frac{2\mu_0 L}{\pi} \left[\sinh^{-1} \left(\frac{L}{w/2} \right) - 1 \right] \quad (52)$$

Table 3-2: Calculated values of circuit parameters for the SRR unit cell

C_{cp} (49)	$17.01 * 10^{-15}$ F
C_{pp} (51)	$0.0407 * 10^{-15}$ F
$C_{\text{gap}} = C_{pp} + C_{cp}$	$17.0507 * 10^{-15}$ F
$C_{\text{total}} = C_{\text{gap}}/4$	$4.263 * 10^{-15}$ F
L_{self} (52)	$58.71 * 10^{-10}$ H

While calculating coplanar gap capacitance using equation (49) p is taken as the gap width (g) and q is taken to be equal to (L-g)/2. Values of C_{total} and L_{self} are independent of frequency and computed values for these circuit parameters are listed in Table 3-2. Values of equivalent loss resistances R_c and R_d , however, are functions of frequency. For that reason, they are not listed in Table 3-2. Typical values of R_c and R_d are in the order of 1 Ω and 92 k Ω around the resonance frequency.

Using all these circuit parameters, the transmission spectrum (i.e. $|S_{21}|$ versus frequency curve) of this unit cell is computed by equations (24) through (27) as described in section 2.3. A simple Matlab code with a very short run time is developed for this purpose. The resulting transmission curve is plotted in Figure 3-3 over the frequency range 15-40 GHz. Transmission spectrum of the isolated SRR cell is also computed by HFSS using PML boundary conditions as described in Figure 3-1 (a). The PML boundaries are placed $D_H=2$ mm above the SRR plane in this HFSS simulation. In general, HFSS simulation results are found to be very sensitive to the distance between the SRR plane and the PML boundary along the \overline{H} filed direction. The transmission spectrum computed by HFSS for $D_H=1$ mm separation distance between the SRR plane and PML boundary is also plotted in Figure 3-4. Resonance frequency of the infinite SRR array is known to be around 34 GHz and the resonance frequency of the SRR unit cell is expected to be close to this value. Therefore, the transmission spectrum simulated for the isolated SRR cell for $D_H=1$ mm case looks more reasonable as it has a resonance frequency around $f_0=34$ GHz. The normalization impedance Z_0 is calculated as an output of the HFSS simulations. As experience has shown, Z_0 values change only slightly with frequency when PEC/PMC boundary conditions are used to simulate SRR array structures. On the other hand, Z_0 becomes strongly dependent on frequency when PML boundary conditions are implemented to simulate the isolated SRR unit cell behavior. In order to compare the transmission spectrum results obtained by HFSS and equivalent circuit modeling approaches, we need to convert Z -parameters of the two-port model to S -parameters as described in Chapter 2. At this step, the normalization impedance (Z_0) values must be used in equation (17) at each sample frequency. The Z_0 output array provided by HFSS simulation is used for this parameter conversion. Values of Z_0 arrays provided in $D_H=2$ mm and $D_H=1$ mm cases are appreciably different from each other. Therefore, the transmission spectrum curve estimated by the two-port model is also affected by the use of this normalization impedance data as shown in Figure 3-3 and Figure 3-4. Variations in

the transmission curves below 30 GHz, in particular, are thought to be spurious effects caused by the use of PML boundary conditions.

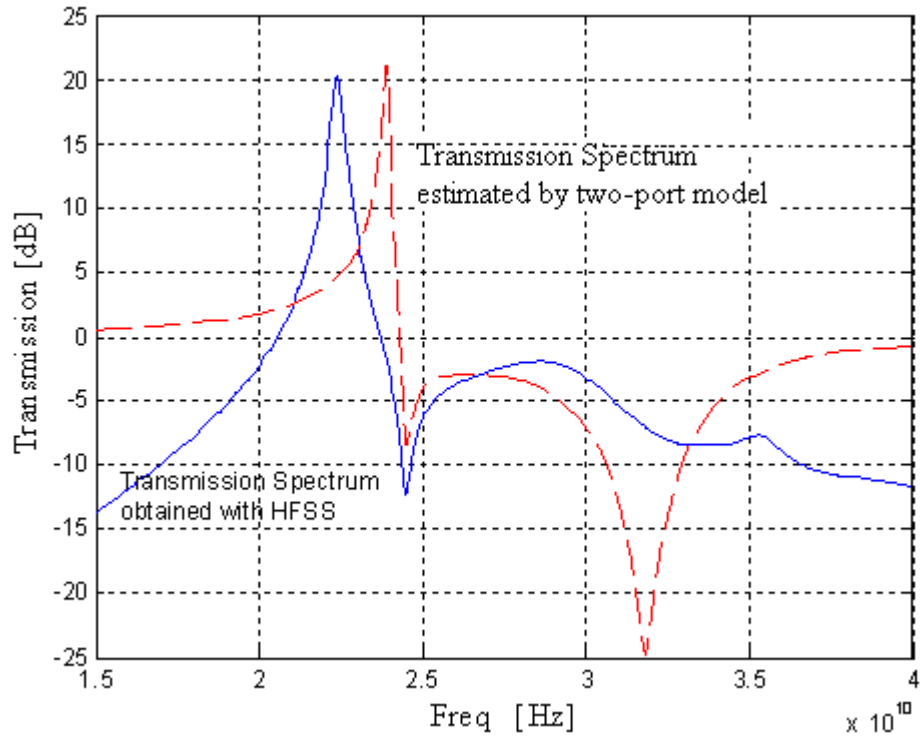


Figure 3-3: Estimated transmission spectra of the SRR unit cell using HFSS simulations with PML boundary conditions and $D_H=2$ mm and using the equivalent two-port circuit given in Figure 3-2 (c).

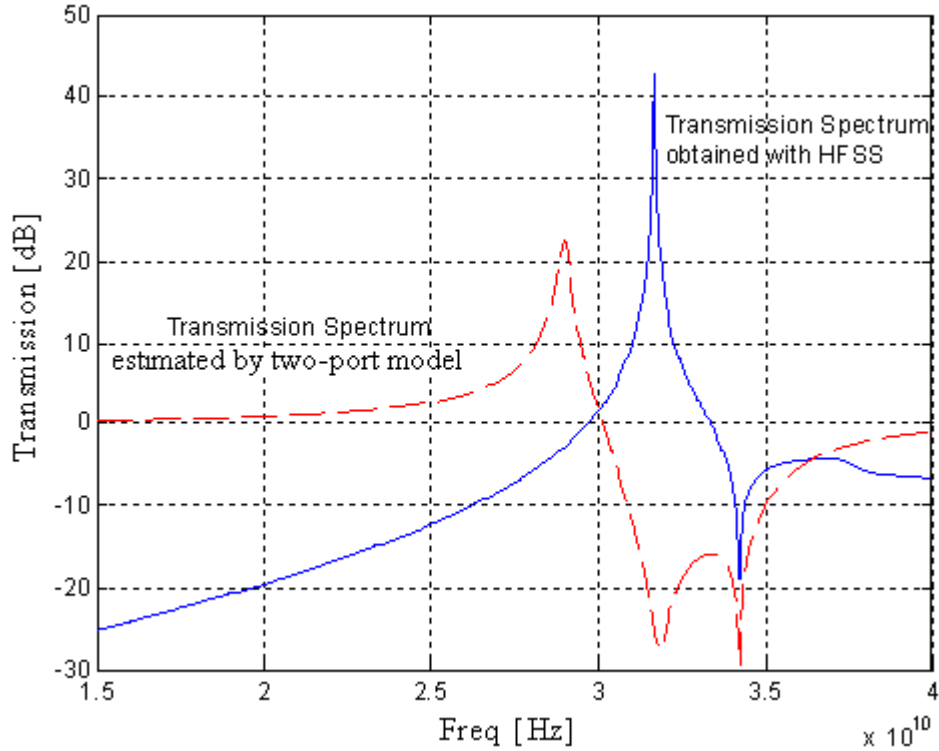


Figure 3-4: Estimated transmission spectra of the SRR unit cell using HFSS simulations with PML boundary conditions and $D_H=1$ mm and using the equivalent two-port circuit given in Figure 3-2 (c).

3.2.2 Numerical Simulation and Equivalent Circuit Modeling of the Infinite SRR Array along the Electric Field Direction

As discussed in Chapter 2 earlier, PEC/PMC type boundary conditions are useful when infinite SRR arrays are simulated by HFSS, especially for these symmetrical SRR unit cells. In this sub-section, we will estimate the resonance frequency of infinite single square SRR array extending along the electric field direction by using the equivalent circuit modeling approach. As discussed in section 2.2, the array effect in magnetic field direction will be ignored as D_H is 1.75 mm, so the array in that direction is sparse. Therefore, the SRR array to be investigated can be considered approximately as a one dimensional infinite array of single-loop four-gap SRR elements extending along the \vec{E} field direction (along the y-axis) as

shown Figure 3-5. In this figure, each block with impedance Z represents an SRR unit cell and each block with impedance Z_m serves to model the coupling capacitance between neighboring SRR elements and the ohmic losses occurring due to leakage currents which flow through the dielectric substrate in the region between neighboring SRR unit cells [23]. It must be emphasized that the two-port SRR model shown in Figure 3-2 (c) with equivalent impedance Z (specified in general by equation (22)) is modified before being used in Figure 3-5 such that the inductance term L_{self} is replaced by $L_{\text{self}}-2M$ to account for the effects of subtractive mutual inductance (M) caused by the neighboring SRR cells on both sides of a given array member. Couplings from more distant members of the array are neglected in this model. The mutual inductance effects act in the subtractive manner as induced currents in all SRR loops of this array are in the same direction as explained by the magnetic induction phenomena. This situation is simulated by the mirror imaging effect of the PEC boundary conditions in HFSS computations used to analyze such infinite SRR arrays. Impedances Z and Z_m can be calculated using equations (53) and (54), respectively. The infinite array can be considered as the limiting case of a finite length array with n SRR elements as n approaches to infinity. Then, this finite length array can be represented by a two-port circuit as the one shown in Figure 2-13, having an equivalent impedance Z_{total} in the shunt branch. As the blocks with impedances Z and Z_m can be considered as individual two-port circuits connected in series, the equivalent impedance of the finite array can be obtained as in equation (55), where $n-1 \approx n$ as n approaches to infinity. Then, the real and imaginary parts of Z_{total} can be obtained as in equations (56) and (57).

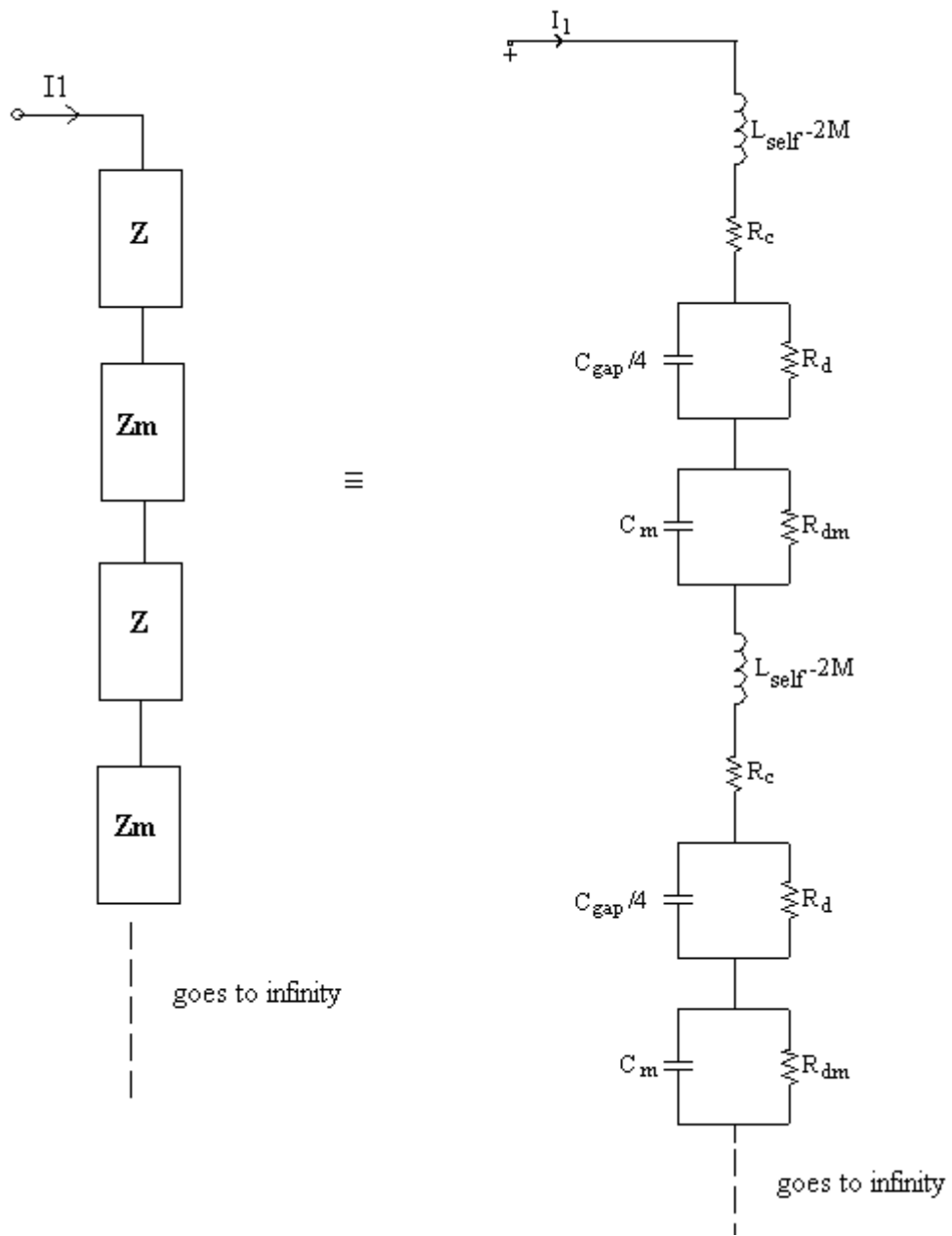


Figure 3-5: Equivalent circuit model for the SRR array which effectively extends to infinity in the electric field direction.

$$Z = \left(R_c + \frac{R_d}{1 + \omega^2 C^2 R_d^2} \right) + j \left(\omega(L_{self} - 2M) - \frac{\omega R_d^2 C}{1 + \omega^2 C^2 R_d^2} \right) \quad (53)$$

$$Z_m = \left(\frac{R_{dm}(1 - j\omega R_{dm} C_m)}{1 + \omega^2 C_m^2 R_{dm}^2} \right) \quad (54)$$

$$Z_{total} = n Z + (n-1) Z_m \quad (55)$$

$$\text{Re}\{Z_{total}\} = n \left(R_c + \frac{R_d}{1 + \omega^2 C^2 R_d^2} + \frac{R_{dm}}{1 + \omega^2 C_m^2 R_{dm}^2} \right) \quad (56)$$

$$\text{Im}\{Z_{total}\} = j\omega n \left((L_{self} - 2M) - \frac{R_d^2 C}{1 + \omega^2 C^2 R_d^2} - \frac{R_{dm}^2 C_m}{1 + \omega^2 C_m^2 R_{dm}^2} \right) \quad (57)$$

At the resonance frequency, Z_{total} becomes real. Then the resonance frequency can be solved by equating the right hand side of equation (57) to zero. In these expressions, C is equivalent gap capacitance of an isolated SRR, L_{self} is the total self inductance of the metal loop, M is the mutual inductance between adjacent SRR elements and C_m is the coupling capacitance. L_{self} and C values are given in Table 3-2 for the SRR cell used in this chapter. M is calculated using equation (60) where L is the side length of SRR and $d_0 = 2D_E + w$ is the centre to centre separation between the adjacent edges of SRR elements. R_{dm} is calculated using equation (61) which is similar to the equation (26) used for calculation of R_d . As discussed earlier R_d and R_{dm} are frequency dependent parameters. While solving for the resonance frequency, $\text{Im}\{Z_{total}\} = 0$ equation can be written as [23]

$$a\omega^4 + b\omega^2 + d = 0 \quad (58)$$

$$a = (L_{self} - 2M) R_d^2 R_{dm}^2 C_m^2 C^2$$

$$b = (L_{self} - 2M) (R_d^2 C^2 + R_{dm}^2 C_m^2) - R_d^2 C R_{dm}^2 C_m^2 - R_d^2 C^2 R_{dm}^2 C_m \quad (59)$$

$$d = (L_{self} - 2M) - R_d^2 C - R_{dm}^2 C_m$$

where

$$M = 0.2L \left(\ln \left(\frac{L}{d_0} + \sqrt{1 + \frac{L^2}{d_0^2}} \right) - \sqrt{1 + \frac{d_0^2}{L^2} + \frac{d_0}{L}} \right) \mu\text{H} \quad (60)$$

and

$$R_{\text{dm}} = \frac{2D_E}{(\tan \alpha)(\omega \epsilon)Lh} \quad (61)$$

Table 3-3: Calculated circuit model parameters of the infinite SRR array extending in the electric field direction

C_{cp} (49)	$17.01 * 10^{-15}$ F
C_{pp} (51)	$0.0407 * 10^{-15}$ F
$C_{\text{gap}} = C_{\text{pp}} + C_{\text{cp}}$	$17.0507 * 10^{-15}$ F
$C_{\text{total}} = C_{\text{gap}}/4$	$4.263 * 10^{-15}$ F
L_{self} (52)	$58.71 * 10^{-10}$ H
C_{mutualep} (49)	$32.625 * 10^{-15}$ F
C_{mutualpp} (51)	$0.0424 * 10^{-15}$ F
C_{mutual}	$32.67 * 10^{-15}$ F
$C_{\text{m}} = 2 * C_{\text{mutual}}$	$65.34 * 10^{-15}$ F
M (60)	$4.39 * 10^{-10}$ H
f_0	35.6 GHz

Parameter values needed in equations (57)-(59) are computed and listed in Table 3-3. Using these values, equation (58) is solved to compute the resonance frequency to be $f_0 = 35.6$ GHz. As a matter of fact, three more roots are solved from equation (58), but two of which are turned out to be imaginary and the third one is found to be negative. Only the fourth root is found meaningful to give $f_0 = 35.6$ GHz. This

result is compared to the resonance frequency value found by HFSS simulation of the infinite SRR array (by using PEC/PMC boundary conditions). As shown in Figure 3-6, the resonance frequency obtained by the numerical simulation approach is $f_0=34$ GHz. The approximation error is found to be about 4.7 %.

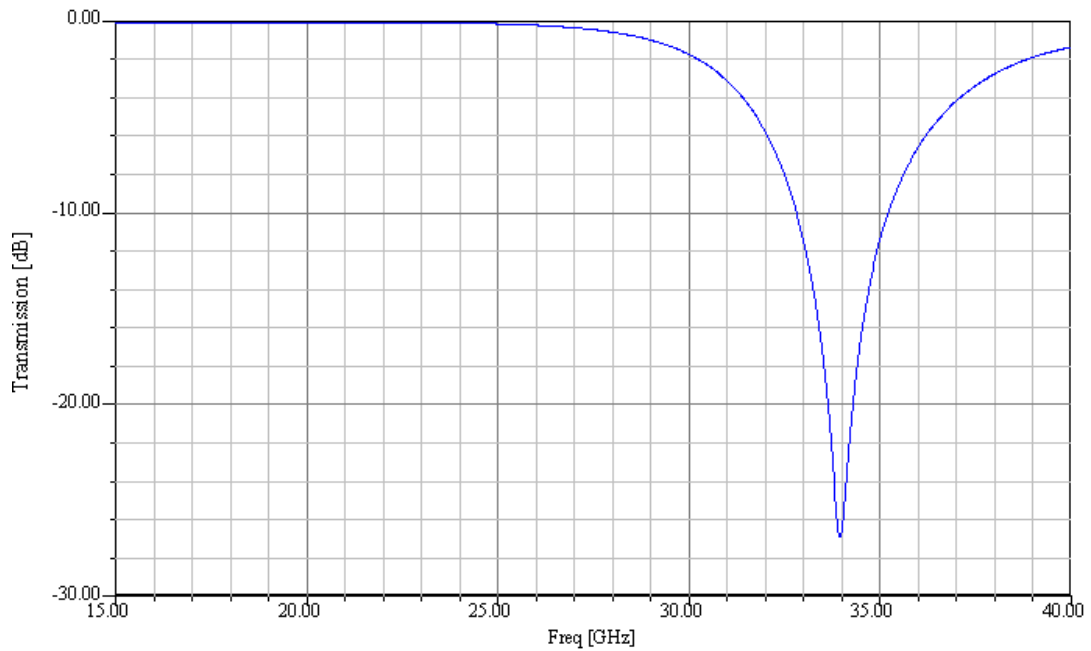


Figure 3-6: Transmission spectrum of the infinite SRR array as estimated by an HFSS simulation using the PEC/PMC boundary conditions.

3.3 An SRR Array Extending Along the Propagation Direction

In this section an SRR array of size $2 \times 1 \times 1$ will be analyzed by both equivalent circuit modeling approach and HFSS simulations. In the next subsection, the structure will be investigated as an isolated 2-element array by using PML boundary conditions in HFSS simulation.

3.3.1 Analysis of the Isolated Two-Element Array of Size 2x1x1

In this section, HFSS simulations of the two-element SRR arrays of size 2x1x1 are performed using PML boundary conditions. Resulting transmission curves are compared with the results obtained from equivalent circuit modeling approach. In Figure 3-7, the array structure, its schematic view and the corresponding equivalent two-port circuit model are shown with substrate dimensions $D_x=8$ mm, $D_y=4$ mm, $h=0.5$ mm.

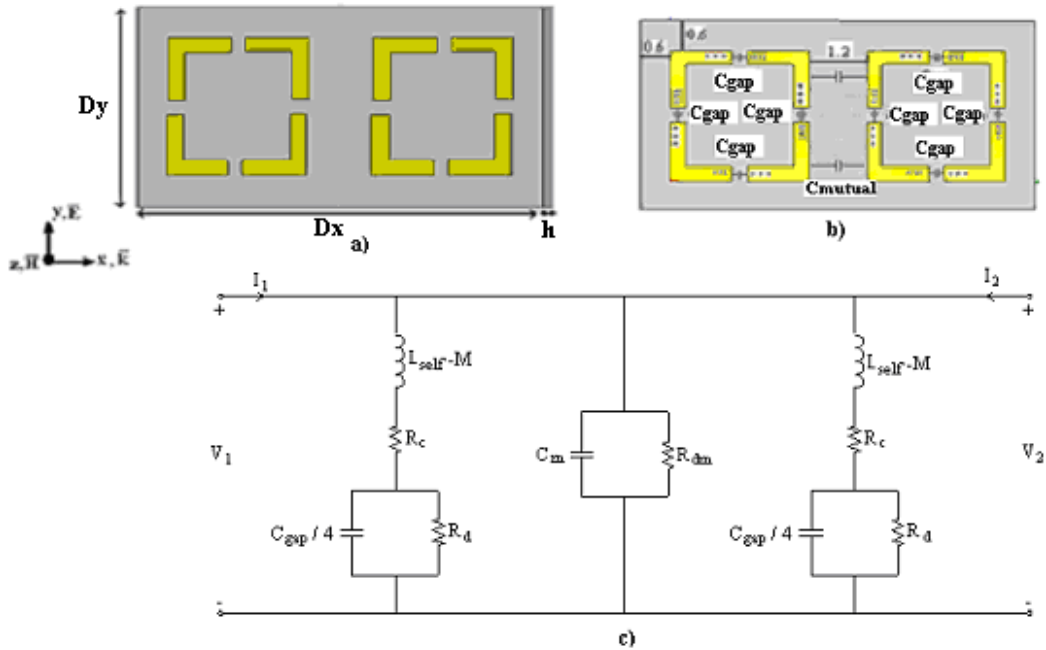


Figure 3-7: a) Geometry of 2x1x1 SRR array, b) Elements of 2x1x1 array, c) Two-port representation of 2x1x1 array (First alternative for the coupling two-port connection).

In this array topology, mutual inductance between the SRR unit cells is subtractive due to the direction of the flux linkages. Therefore, the parameter L_{self} of Figure 3-2 (c) needs to be modified as $L_{self}-M$. The capacitive coupling effect and dielectric ohmic loss effects occurring in the region between the SRR unit cells can be modeled as a parallel two-port RC circuit with parameters C_m and R_{dm} . Two

possible configurations can be considered as shown in Figure 3-7 (c) and Figure 3-9 for this coupling two-port circuit. For the first coupling configuration shown in Figure 3-7 (c), following the similar steps as in section 2.3, we obtain chain (ABCD) parameters of the circuit.

As this two-element SRR array extends in the direction of propagation, the equivalent circuit of the overall 2x1x1 array can be considered as the cascade connection of three equivalent two-port circuits: The SRR two-ports and the coupling two-port between them. Therefore, the chain parameters of the overall two-port representation can be computed by making use of equation (13) and equations (62) through (66) as shown below:

$$\begin{bmatrix} A & B \\ C & D \end{bmatrix}_{cascade} = \begin{bmatrix} 1 & 0 \\ Y_{firstSRR} & 1 \end{bmatrix} \begin{bmatrix} 1 & 0 \\ Y_{mutual} & 1 \end{bmatrix} \begin{bmatrix} 1 & 0 \\ Y_{secondSRR} & 1 \end{bmatrix} \quad (62)$$

defining

$$Y_{total} = Y_{firstSRR} + Y_{mutual} + Y_{secondSRR} \quad (63)$$

equation (62) becomes

$$\begin{bmatrix} A & B \\ C & D \end{bmatrix}_{cascade} = \begin{bmatrix} 1 & 0 \\ Y_{total} & 1 \end{bmatrix} \quad (64)$$

where

$$Y_{firstSRR} = Y_{secondSRR} = \frac{1}{Rc + j\omega(L_{self} - M) + \frac{Rd}{1 + j\omega Rd \frac{C_{gap}}{4}}} \quad (65)$$

and

$$Y_{mutual} = \frac{1}{\frac{R_{dm}}{1 + j\omega R_{dm} C_m}} \quad (66)$$

Finally, using the conversion rules between chain and S- parameters [21], the S_{21} parameter can be computed from equation (67) given below

$$S_{21} = \frac{2}{A + \frac{B}{Z_0} + CZ_0 + D} \quad (67)$$

As stated previously in section 2.3, frequency dependent Z_0 array data are taken from the HFSS simulation output which is executed with PML boundary conditions. The values of $C_{\text{gap}}/4$, L_{self} , M and C_m are taken from Table 3-3. The parameters R_{dm} , R_d and R_c are all frequency dependent and their values are calculated by using equations (61), (26) and (25), respectively. In Figure 3-8, the HFSS result along with the result of equivalent circuit model approach (computed by MATLAB codes written in this thesis) are used to plot transmission spectra of the $2 \times 1 \times 1$ SRR array. The transmission spectrum is given by the $|S_{21}|$ curve and the value of transmission can not exceed unity (corresponding to the zero decibel level). Positive logarithmic transmission values seen in Figure 3-8 are not physically meaningful but they are spurious effects due to the use of PML boundary conditions. Also, the transmission spectrum obtained by HFSS simulation indicates much higher losses which is an expected result as PMLs are highly lossy structures. Two transmission curves shown in Figure 3-8 are similar around the resonance frequency which is very close to 34 GHz.

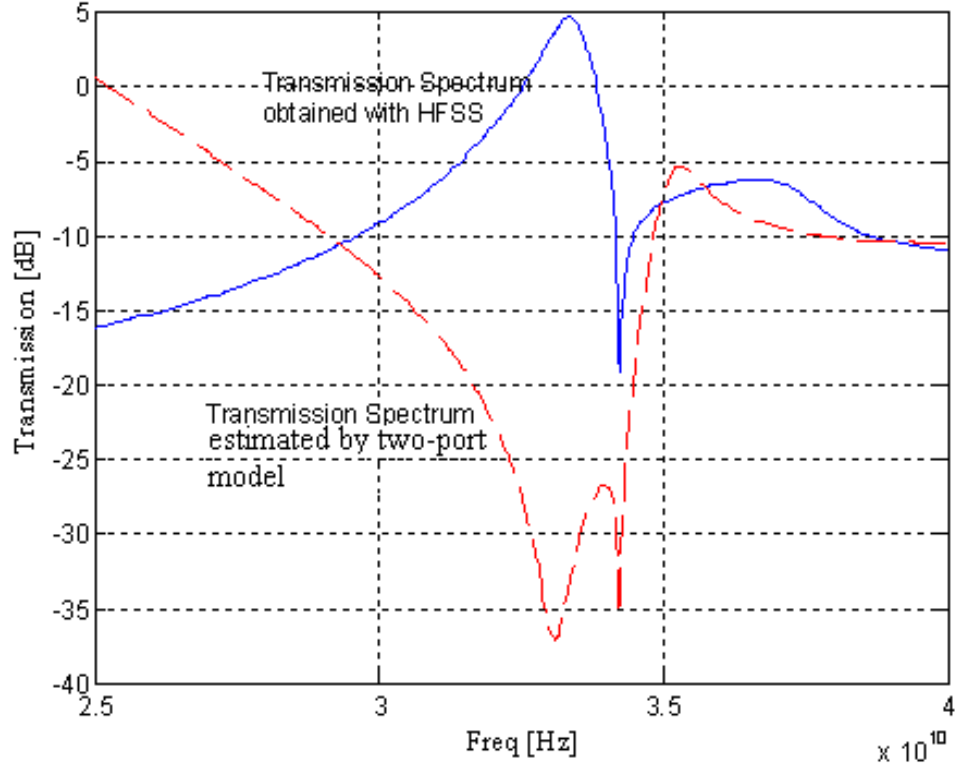


Figure 3-8: Estimated transmission spectrum of 2x1x1 SRR array using HFSS simulations with PML boundary conditions and $D_H=1$ mm and using the equivalent two-port circuit given in Figure 3-7(c).

The second possible coupling configuration is shown in Figure 3-9 where the coupling two-port circuit has a parallel $C_m R_{dm}$ combination in its series branch. Now, the ABCD parameters of the overall two-port network can be obtained as given in equations (68) and (69) below:

$$\begin{bmatrix} A & B \\ C & D \end{bmatrix}_{cascade} = \begin{bmatrix} 1 & 0 \\ Y_{firstSRR} & 1 \end{bmatrix} \begin{bmatrix} 1 & 1/Y_{mutual} \\ 0 & 1 \end{bmatrix} \begin{bmatrix} 1 & 0 \\ Y_{sec ondSRR} & 1 \end{bmatrix} \quad (68)$$

$$\begin{bmatrix} A & B \\ C & D \end{bmatrix}_{cascade} = \begin{bmatrix} 1 + \frac{Y_{sec ondSRR}}{Y_{mutual}} & \frac{1}{Y_{mutual}} \\ Y_{firstSRR} + \frac{Y_{firstSRR} Y_{sec ondSRR}}{Y_{mutual}} + Y_{sec ondSRR} & 1 + \frac{Y_{firstSRR}}{Y_{mutual}} \end{bmatrix} \quad (69)$$

After converting these chain parameters to S-parameters [21], the estimated transmission spectrum of the $2 \times 1 \times 1$ array is obtained and plotted in Figure 3-10. The transmission spectrum obtained by HFSS with PML boundary conditions is also plotted in the same figure for comparison. The spurious effects caused by PML usage are observed in these results. However, both transmission curves indicate the expected resonance around 34 GHz.

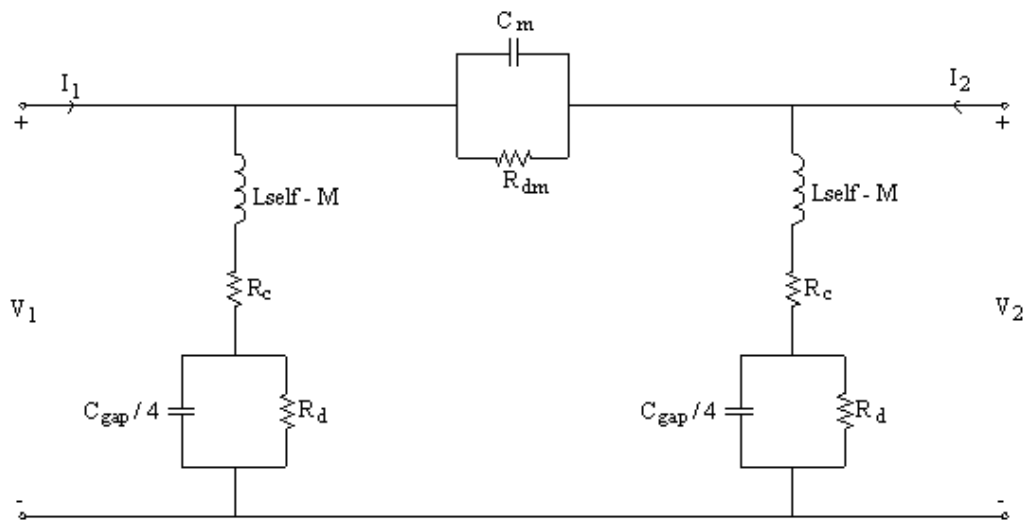


Figure 3-9: Two-port representation of the $2 \times 1 \times 1$ array (Second alternative for the coupling two-port connection).

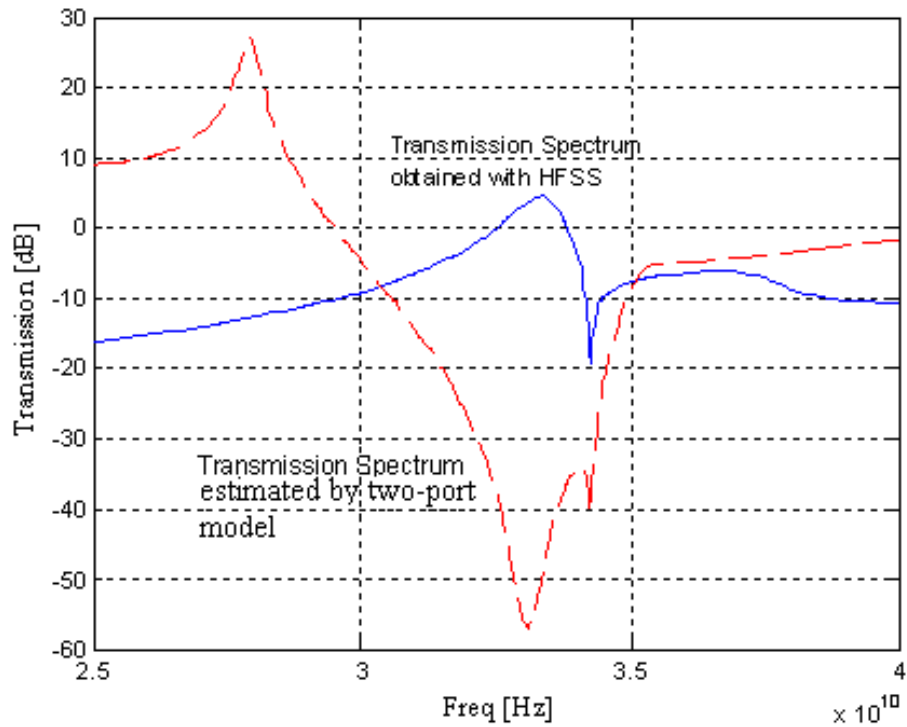


Figure 3-10: Estimated transmission spectrum of the 2x1x1 SRR array using HFSS simulations with PML boundary conditions and $D_H=1$ mm, and using the equivalent two-port circuit given in Figure 3-9.

3.3.2 Numerical Simulation and Equivalent Circuit Modeling of Two Layer Infinite SRR Array

The SRR array to be examined in this subsection is assumed to be infinitely large in the \bar{E} field and \bar{H} field directions. It has only two layers along the propagation direction. The array parameters D_E and D_H are taken as 0.6 mm and 1.75 mm, respectively, to have an array which is sparse along the \bar{H} field direction. Therefore, the array can be considered as an $m \times n \times p$ array, effectively, where $m=2$, $p=1$ (approximately) and n approaches to infinity. Such an array can be simulated by HFSS using PEC/PMC boundary conditions as discussed in section 3.2.2. An approximate equivalent two-port circuit model for this array is shown in Figure 3-11 where the capacitive coupling and dielectric losses in the region between

neighboring SRR cells along the propagation direction are neglected for simplicity. The inductive coupling between such SRR cells, however, is taken into account by the $(L_{\text{self}}-3M-2M_c)$ term. Here M is the mutual inductance between two adjacent SRR cells along the incident electric field and propagation directions. M_c is the mutual inductance between two SRR cells in cross locations. The parameter M_c is computed using equation (60) with $d_0=\sqrt{2}(2D_E + w)$. Mathematical expressions for the impedances Z and Z_m are given in equations (70) and (71), respectively. Following the approach used in section 3.2.2., the real and imaginary parts of the equivalent impedance Z_{total} for the overall two-port array representation are obtained as in equations (72) and (73). The resonance frequency of the array can be obtained by solving equations (74) and (75) after equating the imaginary part of Z_{total} to zero.

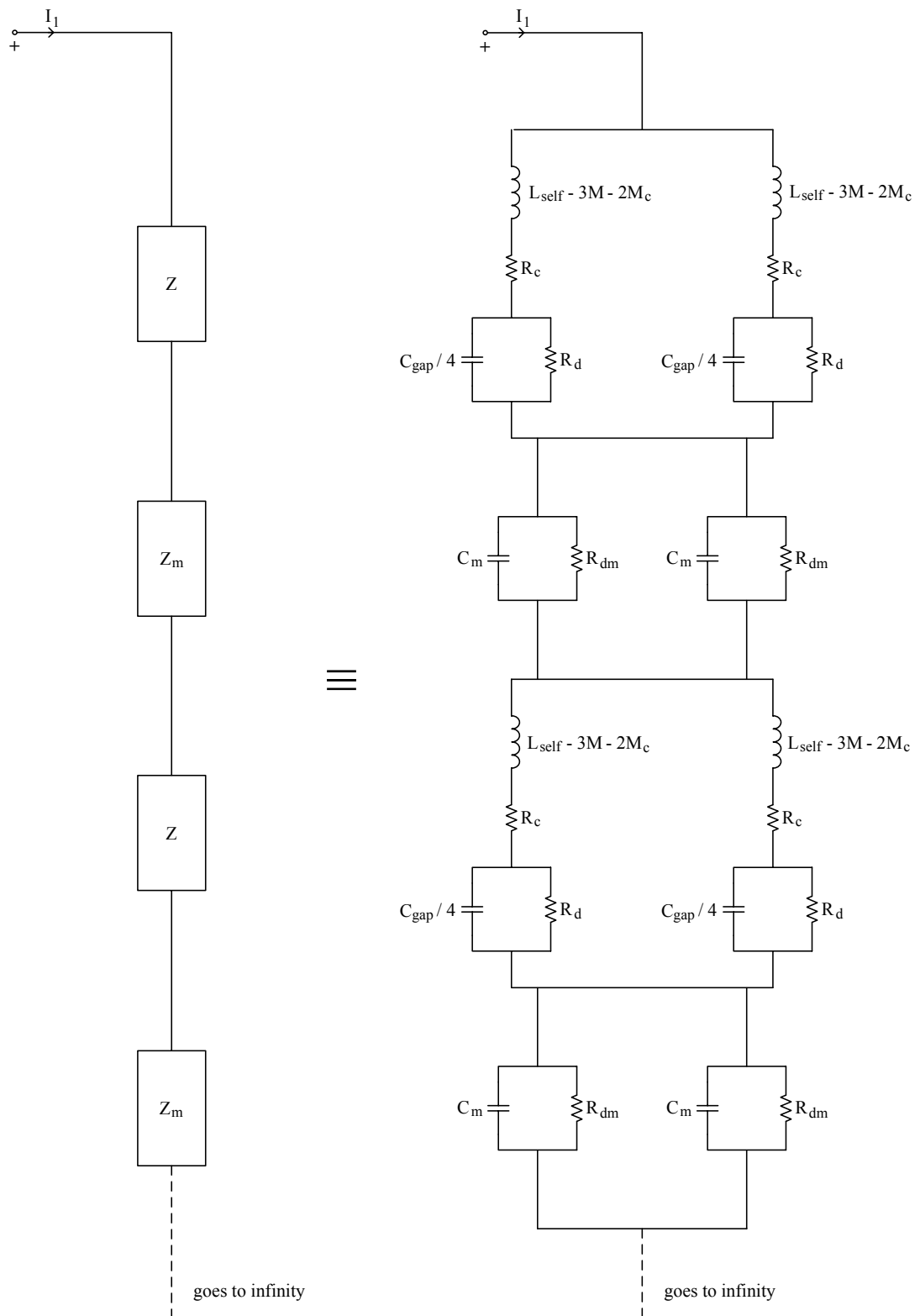


Figure 3-11: An equivalent circuit model for the double layer SRR array ($m \times n \times p$) where $m=2$, $p=1$ (due to sparse array approximation) and n approaches to infinity.

$$Z = \frac{1}{2} \left[\left(R_c + \frac{R_d}{1 + \omega^2 C^2 R_d^2} \right) + j \left(\omega(L_{self} - 3M - 2M_c) - \frac{\omega R_d^2 C}{1 + \omega^2 C^2 R_d^2} \right) \right] \quad (70)$$

$$Z_m = \left(\frac{R_{dm} (1 - j\omega R_{dm} C_m)}{2(1 + \omega^2 C_m^2 R_{dm}^2)} \right) \quad (71)$$

$$Z_{total}(\text{real}) = n \left(\frac{R_c}{2} + \frac{R_d}{2(1 + \omega^2 C^2 R_d^2)} + \frac{R_{dm}}{2(1 + \omega^2 C_m^2 R_{dm}^2)} \right) \quad (72)$$

$$Z_{total}(\text{im}) = j\omega n \left(\frac{L_{self} - 3M - 2M_c}{2} - \frac{R_d^2 C}{2(1 + \omega^2 C^2 R_d^2)} - \frac{R_{dm}^2 C_m}{2(1 + \omega^2 C_m^2 R_{dm}^2)} \right) \quad (73)$$

$$a\omega^4 + b\omega^2 + d = 0 \quad (74)$$

$$a = (L_{self} - 3M - 2M_c) R_d^2 R_{dm}^2 C_m^2 C^2$$

$$b = (L_{self} - 3M - 2M_c) (R_d^2 C^2 + R_{dm}^2 C_m^2) - R_d^2 C R_{dm}^2 C_m^2 - R_d^2 C^2 R_{dm}^2 C_m \quad (75)$$

$$d = (L_{self} - 3M - 2M_c) - R_d^2 C - R_{dm}^2 C_m$$

The values of parameters in equation (75) are already calculated in section 3.2.2 and given in Table 3-3. Only the parameter M_c is used for the first time here and it is calculated using equation (60). All of the resulting values are given in Table 3-4. The only meaningful root of equation (74) is found to be 39.7 GHz with about 12.5 percent error as compared to the resonance frequencies (34 GHz and 35.3 GHz) estimated by the HFSS simulation with PEC/PMC boundary conditions. The error in the equivalent circuit model estimation for the resonance frequency can be explained by the fact that coupling effects along the \bar{H} field direction and more importantly, the capacitive coupling and loss effects along the propagation direction are neglected in the equivalent circuit model. It should be also indicated that the present approximate two-port model can estimate only one resonance frequency, misses the other. The transmission spectrum of the SRR array is shown in Figure 3-12.

Table 3-4: Calculated model parameters for the infinite SRR array in electric field direction

$C_{\text{gap}}/4$	$4.263 * 10^{-15}$ F
$L_{\text{self}}(52)$	$58.71 * 10^{-10}$ H
C_{mutual}	$32.67 * 10^{-15}$ F
$C_m (2 * C_{\text{mutual}})$	$65.34 * 10^{-15}$ F
$M(60)$	$4.39 * 10^{-10}$ H
$M_c(60)$	$3.3 * 10^{-10}$ H
f_0	39.7 GHz

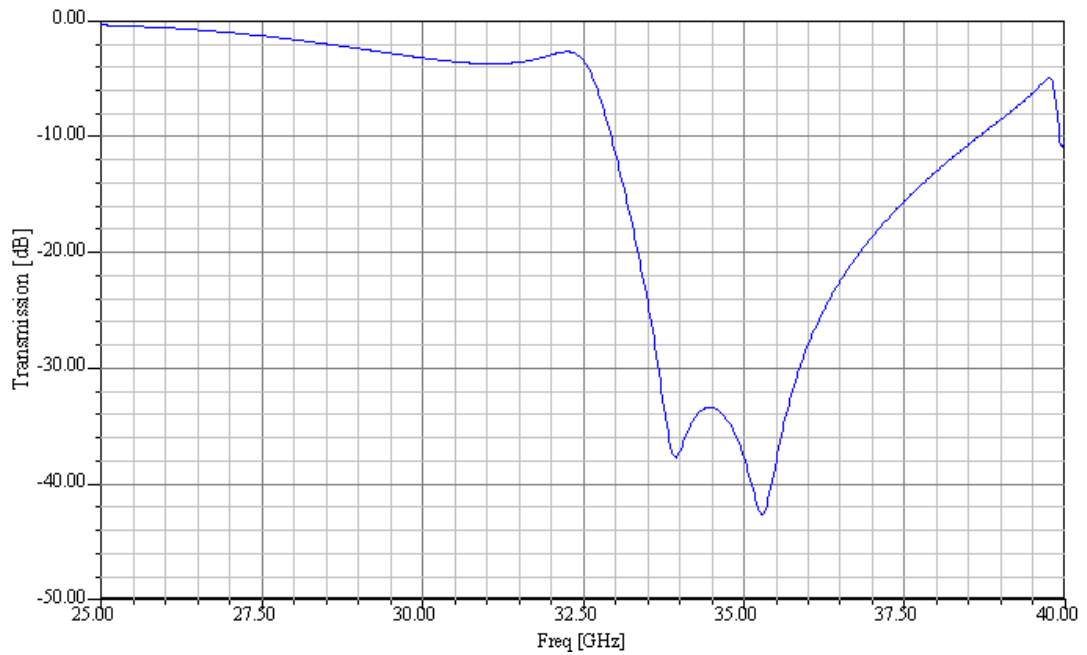


Figure 3-12: Simulation of 2x1x1 array with PEC/PMC boundary.

3.4 An SRR Array Extending Along the Electric Field Direction

In this section, an SRR array of size 1x2x1 will be analyzed over the frequency band from 25 GHz to 40 GHz. First, this small array will be considered in isolation

and its transmission spectrum will be obtained by HFSS using PML boundary conditions. Then, it will be analyzed by using PEC/PMC boundary conditions to simulate an infinite SRR array.

3.4.1 Analysis of the Isolated Two-Element Array of Size 1x2x1

The 1x2x1 SRR array and its equivalent two-port model are shown in Figure 3-13 where the substrate dimensions are $D_x=4$ mm, $D_y=8$ mm, $h=0.5$ mm.

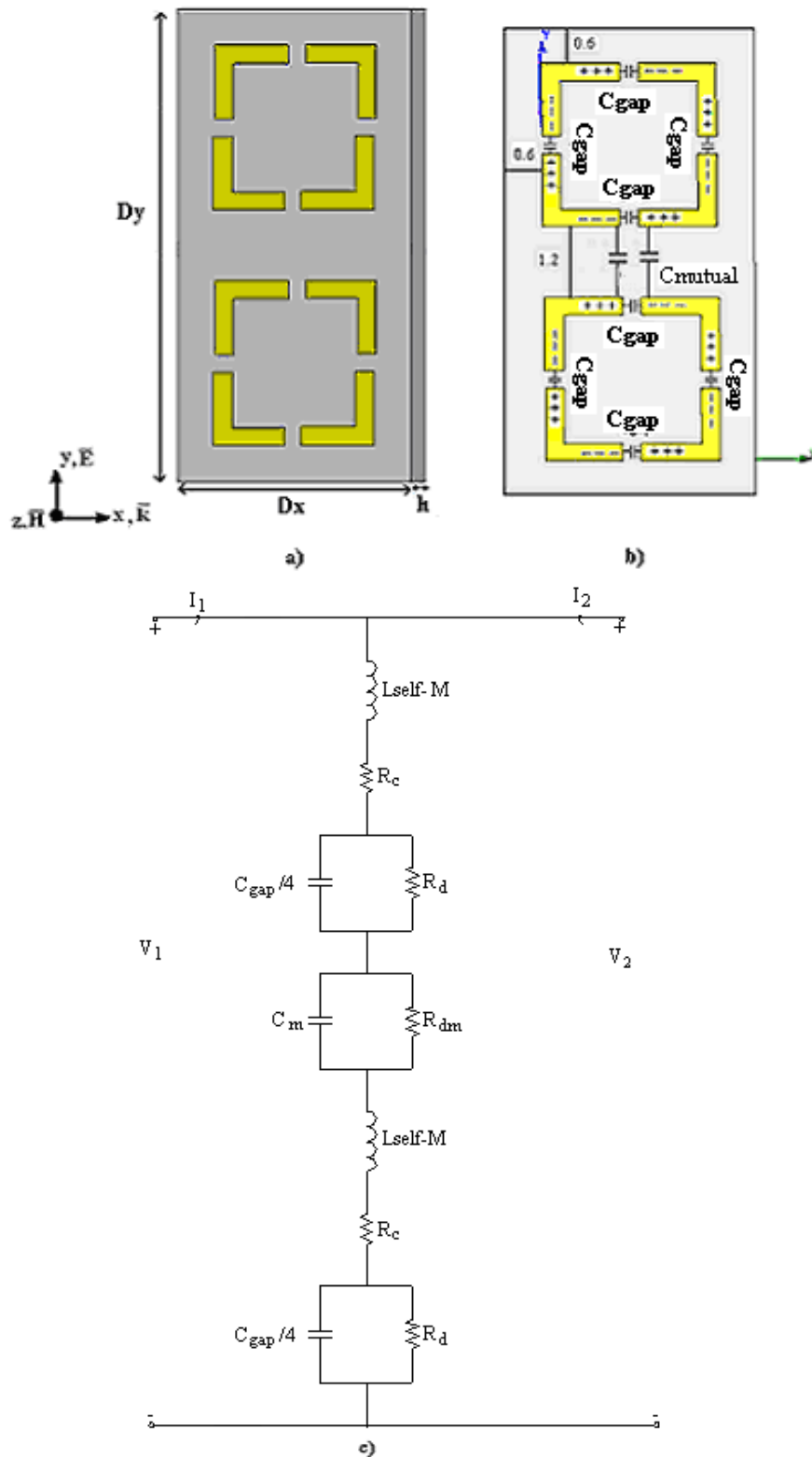


Figure 3-13: a) Geometry of the 1x2x1 array, b) Elements of 1x2x1 array, c) Equivalent two-port circuit model for the 1x2x1 array.

All of the circuit parameters shown in Figure 3-13 (c) are calculated in section 3.2.2 and given in Table 3-3. In addition, expressions of loss parameters R_c , R_d and R_{dm} , are given in equations (25),(26) and (61), respectively. To obtain the transmission spectrum of the 1x2x1 array, ABCD parameters of the equivalent two-port circuit need to be obtained. Since the two-port circuit models representing individual SRRs and mutual effects are connected in series along the electric field direction, their individual Z parameter matrices are added to get the overall Z matrix of the array. Chain matrices of each SRR unit cell are the same and given by equation (76) where the admittance term Y is computed using equation (78). The chain matrix of the coupling circuit is determined by the help of equations (77) and (79). Then, the overall Z-matrix of the 1x2x1 array two-port is obtained using equations (80) through (84).

$$\begin{bmatrix} A & B \\ C & D \end{bmatrix}_{firstSRR} = \begin{bmatrix} A & B \\ C & D \end{bmatrix}_{secondSRR} = \begin{bmatrix} 1 & 0 \\ Y & 1 \end{bmatrix} \quad (76)$$

$$\begin{bmatrix} A & B \\ C & D \end{bmatrix}_{mutual} = \begin{bmatrix} 1 & 0 \\ Y_m & 1 \end{bmatrix} \quad (77)$$

where

$$Y = \frac{1}{R_c + j\omega(L_{self} - M) + \frac{R_d}{1 + j\omega R_d \frac{C_{gap}}{4}}} \quad (78)$$

and

$$Y_m = \frac{1}{\frac{R_{dm}}{1 + j\omega R_{dm} C_m}} \quad (79)$$

Then, using the general conversion rule:

$$\begin{bmatrix} Z_{11} & Z_{12} \\ Z_{21} & Z_{22} \end{bmatrix} = \begin{bmatrix} \frac{A}{C} & \frac{AD-BC}{C} \\ \frac{1}{C} & \frac{D}{C} \end{bmatrix} \quad (80)$$

Z matrices of the SRR cells and the coupling two-port are given as:

$$\begin{bmatrix} Z_{11} & Z_{12} \\ Z_{21} & Z_{22} \end{bmatrix}_{\text{firstSRR}} = \begin{bmatrix} Z_{11} & Z_{12} \\ Z_{21} & Z_{22} \end{bmatrix}_{\text{secondSRR}} = \begin{bmatrix} \frac{1}{Y} & \frac{1}{Y} \\ \frac{1}{Y} & \frac{1}{Y} \end{bmatrix} \quad (81)$$

and

$$\begin{bmatrix} Z_{11} & Z_{12} \\ Z_{21} & Z_{22} \end{bmatrix}_{\text{mutual}} = \begin{bmatrix} \frac{1}{Y_m} & \frac{1}{Y_m} \\ \frac{1}{Y_m} & \frac{1}{Y_m} \end{bmatrix} \quad (82)$$

Then, defining:

$$Z_{\text{total}} = Z_{\text{firstSRR}} + Z_{\text{mutual}} + Z_{\text{secondSRR}} \quad (83)$$

Z matrix of the overall array two-port is found as:

$$[Z_{\text{total}}] = \begin{bmatrix} \frac{2}{Y} + \frac{1}{Y_m} & \frac{2}{Y} + \frac{1}{Y_m} \\ \frac{2}{Y} + \frac{1}{Y_m} & \frac{2}{Y} + \frac{1}{Y_m} \end{bmatrix} \quad (84)$$

Next, the complex S-parameters are obtained using the $[Z_{\text{total}}]$ matrix [21]. The transmission curve ($|S_{21}|$ versus frequency curve) obtained via equivalent circuit modeling is shown in Figure 3-14. This array structure is also analyzed with HFSS using PML boundary conditions with $D_H = 1.75$ mm and the resulting curve is also plotted in Figure 3-14 for comparison. This curve looks like a compressed and lossy version of the transmission curve obtained by equivalent modeling. Resonance

frequencies are found to be 33.6 and 34.6 GHz from the circuit model approach whereas the resonances are observed at 34.6 and 35.1 GHz according to the HFSS simulation results.

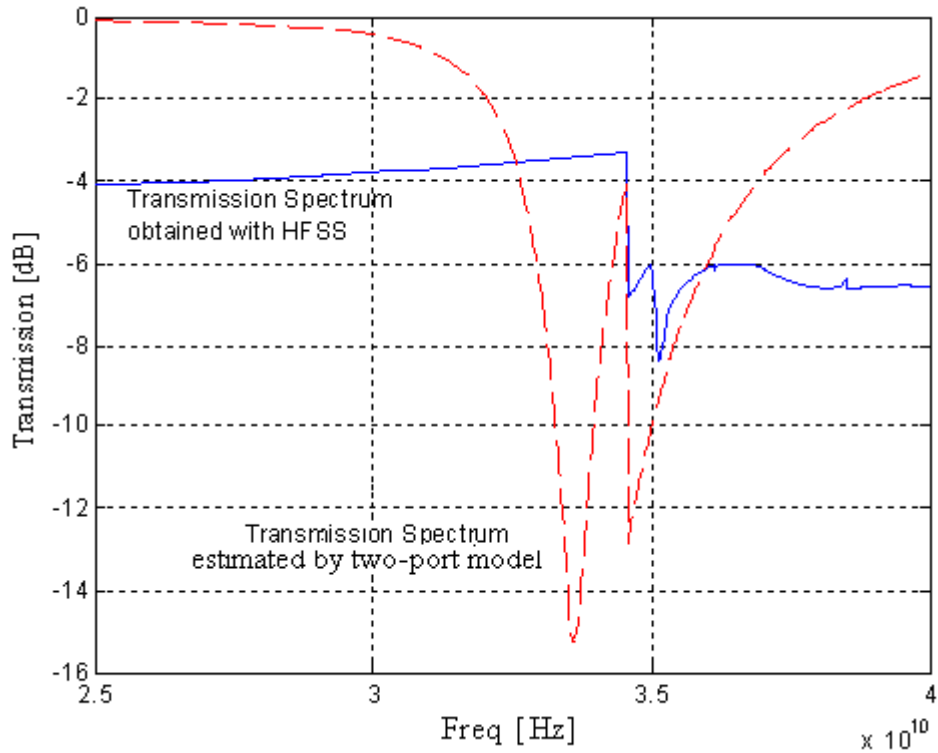


Figure 3-14: Estimated transmission spectra of the 1x2x1 SRR array using HFSS simulations with PML boundary conditions and $D_H=1.75$ mm and using the equivalent two-port circuit given in Figure 3-13 (c).

3.4.2 Numerical Simulation and Equivalent Circuit Modeling of Infinite SRR Array Along the Electric Field Direction

When PEC/PMC boundary conditions are used instead of PML boundary condition, an infinite array is formed in both \overline{E} field and \overline{H} field directions. As D_H is chosen to be a relatively large value, the array is sparse in \overline{H} field direction. Hence, the

resulting array can be considered as an infinitely long, one-dimensional array of size $1 \times \infty \times 1$. In this section, the resonance frequency of this infinite SRR array will be calculated and compared with the resonance frequency obtained from the HFSS simulation results. In section 3.2.2, the resonance frequency of this infinite SRR array has already been calculated to be 35.6 GHz. The transmission spectrum of this array obtained by using HFSS with PEC/PMC boundary conditions is shown in Figure 3-15, which is the exact replica of Figure 3-6. The resonance frequency obtained by HFSS simulations is 34 GHz and very close to the result of 35.6 GHz, which is obtained from the equivalent circuit approach.

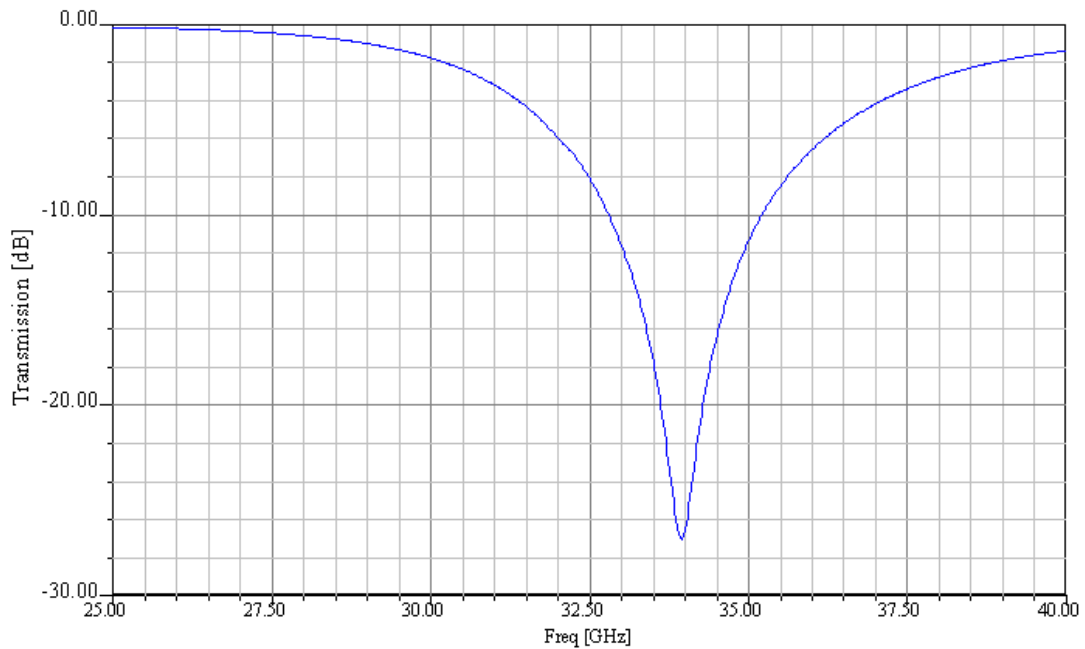


Figure 3-15: Transmission spectrum of the 1x2x1 SRR array obtained by HFSS simulation with PEC/PMC boundary conditions.

3.5 The 2x2x1 SRR Array

Combining two arrays of sizes $2 \times 1 \times 1$ and $1 \times 2 \times 1$, it is possible to form a $2 \times 2 \times 1$ array. The geometry, dimensions and some parameters of this array are shown in Figure 3-16, where the substrate dimensions are $D_x = D_y = 8$ mm and $h = 0.5$ mm.

Geometry, dimensions and material properties of the SRR unit cell used in this array are the same as those used earlier in Chapter 3. In this section, we will first examine this $2 \times 2 \times 1$ array in isolation. Then, we will extend investigation to an infinite array form.

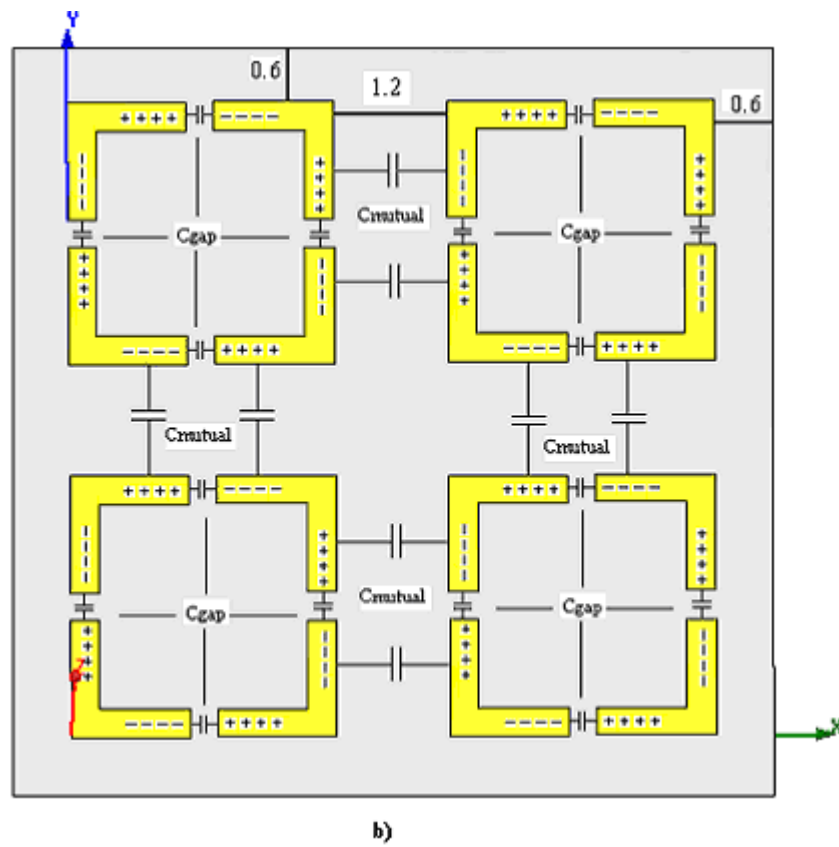
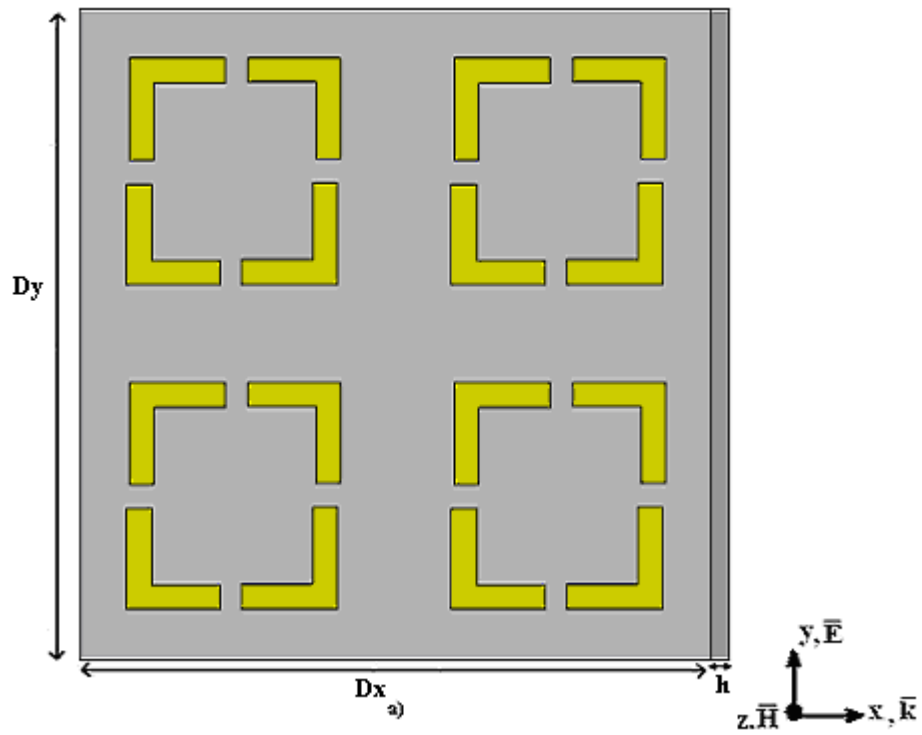


Figure 3-16: a) Unit cell geometry of $2 \times 2 \times 1$ array, b) Parameters of the $2 \times 2 \times 1$ SRR array.

3.5.1 Analysis of the Isolated Four Element Array of Size 2x2x1

Equivalent two-port circuit model of the 2x2x1 array is shown in Figure 3-17. In this model, cross mutual inductance effects are also considered and included in the model via the parameter M_c . The SRR equivalent circuit shown in Figure 3-2 (c), the coupling circuit (along the \bar{E} field direction) shown in Figure 3-5 and the coupling circuit alternative (along the propagation direction) shown in Figure 3-7 (c) are used to form the equivalent two-port circuit model of 2x2x1 array shown in Figure 3-17. The chain parameter matrix and the corresponding Z-parameter matrix of the overall 2x2x1 array structure are computed using equations (85) through (93). Then, the complex S parameter (S_{21}) is computed from the Z-parameters using equation (67). The $|S_{21}|$ versus frequency curve of the array is plotted in Figure 3-18. The transmission spectrum obtained using HFSS with PML boundary conditions ($D_H=1.75$ mm) is also plotted in the same figure for comparison.

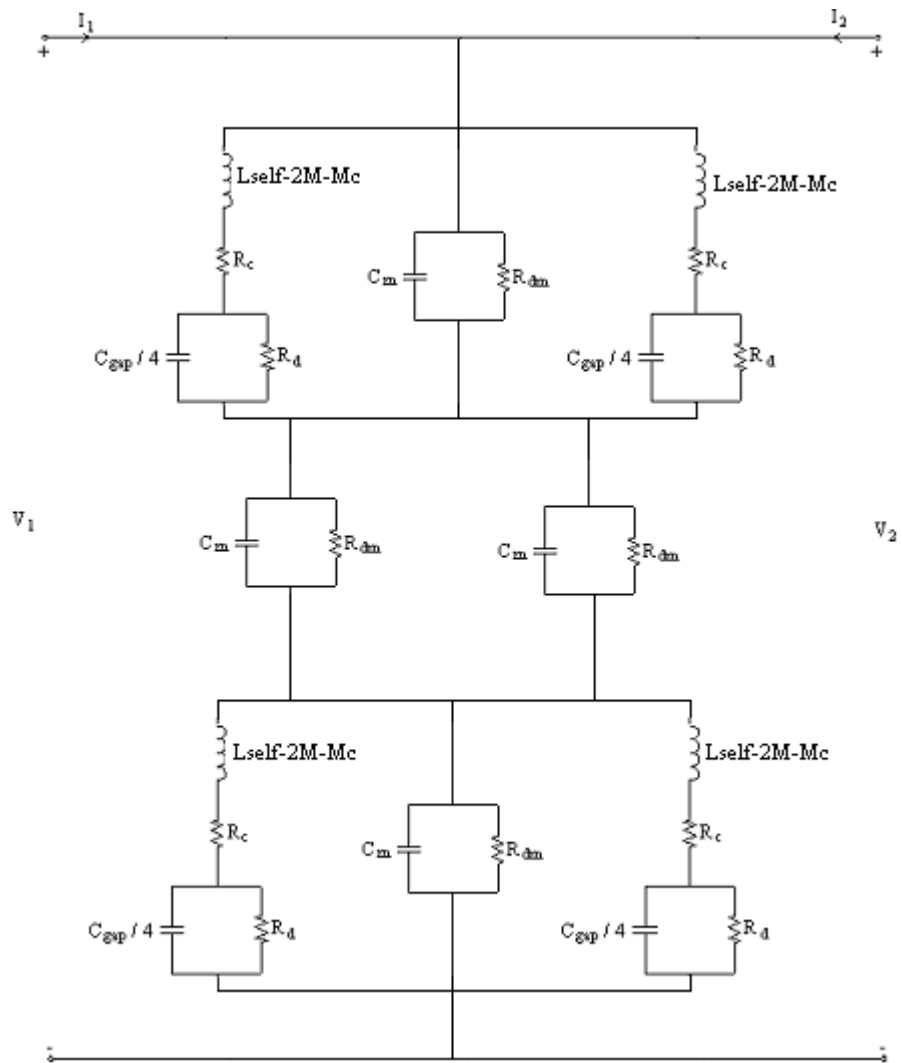


Figure 3-17: Two-port model for 2x2x1 SRR array.

$$\begin{bmatrix} A & B \\ C & D \end{bmatrix}_{upperSRRblock} = \begin{bmatrix} A & B \\ C & D \end{bmatrix}_{lowerSRRblock} = \begin{bmatrix} 1 & 0 \\ 2Y + Y_m & 1 \end{bmatrix} \quad (85)$$

$$\begin{bmatrix} A & B \\ C & D \end{bmatrix}_{mutual} = \begin{bmatrix} 1 & 0 \\ 2Y_m & 1 \end{bmatrix} \quad (86)$$

where

$$Y = \frac{1}{R_c + j\omega(L_{self} - 2M - M_c) + \frac{R_d}{1 + j\omega R_d \frac{C_{gap}}{4}}} \quad (87)$$

and

$$Y_m = \frac{1}{\frac{R_{dm}}{1 + j\omega R_{dm} C_m}} \quad (88)$$

Using

$$\begin{bmatrix} Z_{11} & Z_{12} \\ Z_{21} & Z_{22} \end{bmatrix} = \begin{bmatrix} \frac{A}{C} & \frac{AD - BC}{C} \\ \frac{1}{C} & \frac{D}{C} \end{bmatrix} \quad (89)$$

Z parameter matrices for the SRR unit cell and coupling circuit two-ports can be obtained as:

$$\begin{bmatrix} Z_{11} & Z_{12} \\ Z_{21} & Z_{22} \end{bmatrix}_{firstSRR} = \begin{bmatrix} Z_{11} & Z_{12} \\ Z_{21} & Z_{22} \end{bmatrix}_{secondSRR} = \begin{bmatrix} \frac{1}{2Y + Y_m} & \frac{1}{2Y + Y_m} \\ \frac{1}{2Y + Y_m} & \frac{1}{2Y + Y_m} \end{bmatrix} \quad (90)$$

and

$$\begin{bmatrix} Z_{11} & Z_{12} \\ Z_{21} & Z_{22} \end{bmatrix}_{mutual} = \begin{bmatrix} \frac{1}{2Y_m} & \frac{1}{2Y_m} \\ \frac{1}{2Y_m} & \frac{1}{2Y_m} \end{bmatrix} \quad (91)$$

Defining

$$Z_{total} = Z_{firstblock} + Z_{mutual} + Z_{secondblock} \quad (92)$$

The equivalent Z parameter matrix of the overall array can be obtained as:

$$[Z_{total}] = \begin{bmatrix} \frac{2}{2Y + Y_m} + \frac{1}{2Y_m} & \frac{2}{2Y + Y_m} + \frac{1}{2Y_m} \\ \frac{2}{2Y + Y_m} + \frac{1}{2Y_m} & \frac{2}{2Y + Y_m} + \frac{1}{2Y_m} \end{bmatrix} \quad (93)$$

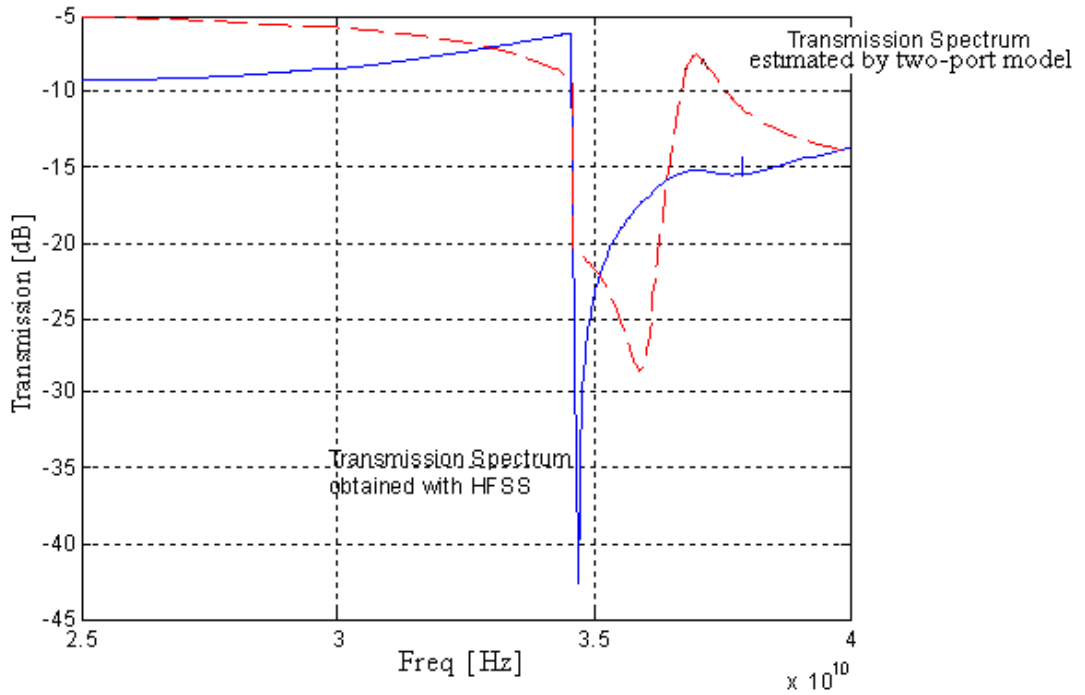


Figure 3-18: Estimated transmission spectra of the 2x2x1 SRR array using HFSS simulations with PML boundary conditions and $D_H = 1.75$ mm and using the equivalent circuit model shown in Figure 3-17.

3.5.2 Numerical Simulation and Equivalent Circuit Modeling of Infinite Two Layer SRR Array

When the 2x2x1 array is simulated by HFSS using PEC/PMC boundary conditions, the resulting infinite array with two layers along the propagation direction turns out to be exactly the same array examined in section 3.3.2. Therefore, exactly the same transmission curve shown in Figure 3-19 and the same resonance frequencies at 34 GHz and 35.3 GHz are obtained with HFSS simulations. Also a resonance frequency of 39.7 GHz is estimated by the equivalent circuit model. As the capacitive coupling between the SRR cells in the propagation direction is neglected, only one resonance frequency is estimated with this approach.

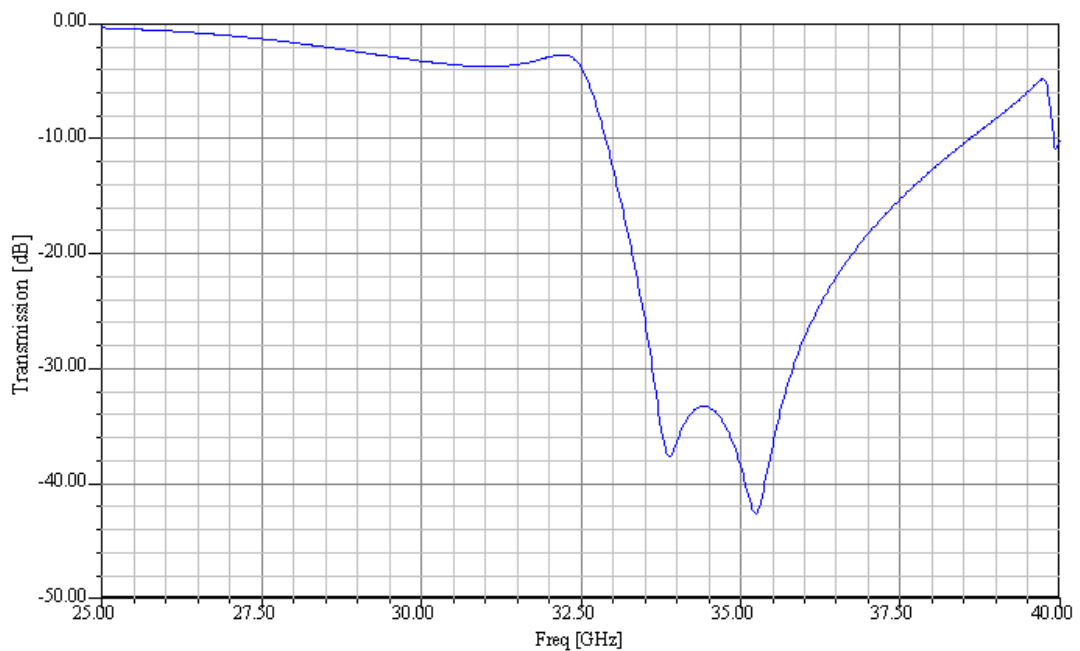


Figure 3-19: Transmission spectrum for the 2x2x1 SRR array estimated by HFSS with PEC/PMC boundary conditions.

CHAPTER 4

NUMERICAL SIMULATIONS, MEASUREMENTS AND TWO PORT EQUIVALENT CIRCUIT MODELING OF SQUARE SHAPED SINGLE LOOP SRR STRUCTURES

4.1 Introduction

In this chapter, a single square loop SRR with four splits and its 4x1x1 array are investigated. In addition to HFSS simulations and equivalent circuit modeling results, these structures are also fabricated and their transmission spectra are measured. Due to the limitations in our measurement setup, the SRR unit cell is designed to resonate around 12 GHz and the measurements are carried on over the [10 GHz -13] GHz frequency band.

Transmission spectrum of the SRR unit cell is obtained by HFSS using both PML and PEC type boundary conditions as shown in Figure 4-1. The isolated unit cell structure is analyzed when PML boundaries are used. Behavior of a single layer (in the propagation direction) infinite SRR array within a metallic waveguide is simulated when PEC boundary conditions are employed. The same approach is also used to investigate the behavior of the 4x1x1 SRR array as to be presented in this chapter. As the transmission spectra of these structures are measured within a metallic waveguide, PEC boundary conditions are used in the associated HFSS simulations for meaningful comparison of the results.

In the fabrication of the SRR unit cell and the 4x1x1 array, copper inclusions are formed over the low-loss dielectric substrate Arlon AD350, which has a thickness of $h=0.762$ mm and relative permittivity of $\epsilon_r = 3.5$. Thickness of copper strips is $t=0.035$ mm.

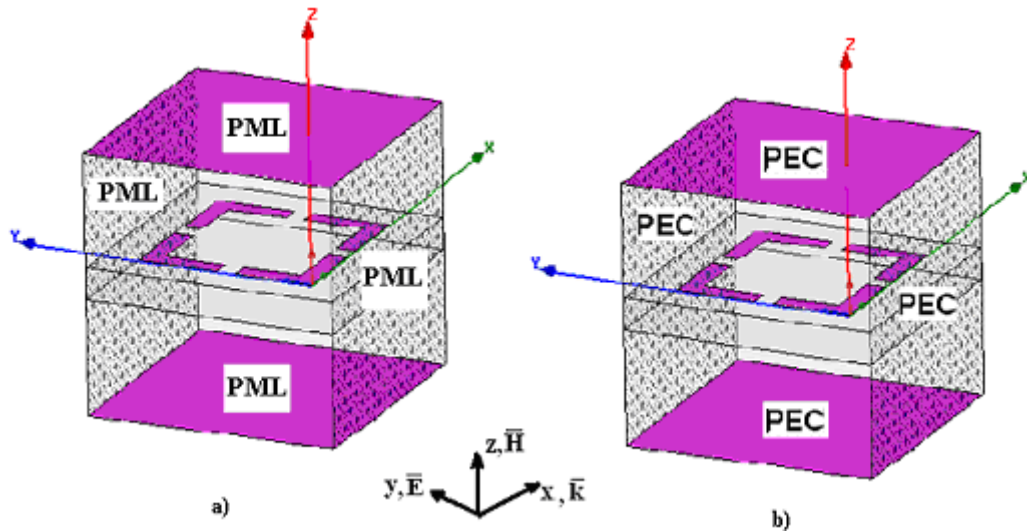


Figure 4-1: Boundary conditions used in HFSS simulations: a) Use of PML conditions to examine the isolated SRR cell, b) Use of PEC boundary conditions to simulate SRR behavior within a metallic waveguide.

4.2 Analysis and Measurements of the SRR Unit Cell

Geometrical parameters of the fabricated SRR unit cell are shown in Figure 4-2. Values of these geometrical parameters are given in Table 4-1.

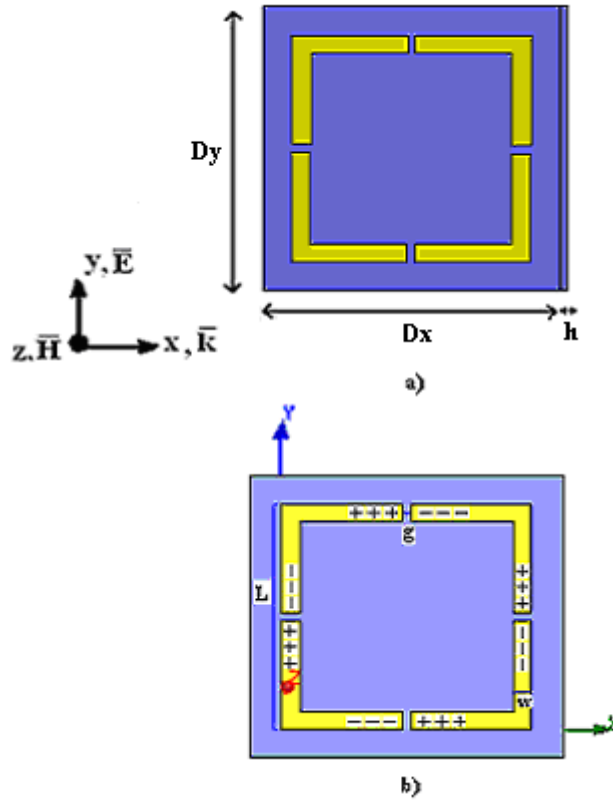


Figure 4-2: SRR unit cell a) Geometry and excitation, b) Design parameters.

Table 4-1: Geometrical parameters of the fabricated SRR unit cell

Substrate Dimensions	L (Side length of the SRR)	g (Gap Width)	w (SRR Width)
$D_x=D_y=10\text{mm}$ $h=0.762\text{ mm}$	8 mm	0.3 mm	0.6 mm

4.2.1 Analysis of the Isolated SRR Unit Cell

Two-port equivalent circuit model for the isolated SRR unit cell is shown in Figure 4-3. The values of calculated circuit elements are given in Table 4-2. The equivalent loss resistance values for R_c and R_d are calculated using equations (25)

and (26) as functions of frequency. The transmission spectrum of the unit cell is computed using equation (24) based on this equivalent circuit model. Also, the transmission spectrum of this SRR unit cell is computed using HFSS with PML boundary conditions. Transmission curves obtained using both approaches are plotted in Figure 4-4. In this figure, it is observed that the resonance frequency values of these two transmission curves are very close to each other, both of which are approximately at 11.90 GHz. The overall shapes of both transmission curves are sufficiently close to each other as well.

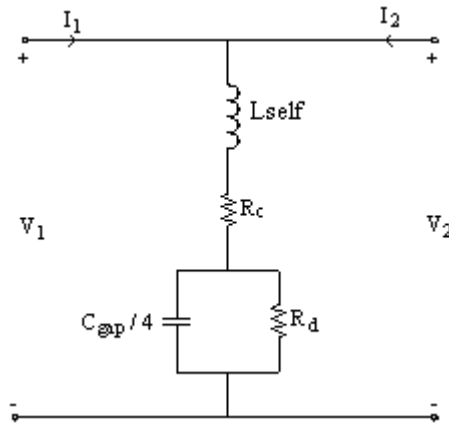


Figure 4-3: Equivalent two-port circuit representation of the SRR unit cell.

Table 4-2: Model parameters of the fabricated SRR unit cell

C_{cp} (49)	$35.483 \cdot 10^{-15}$ F
C_{pp} (51)	$2.17 \cdot 10^{-15}$ F
C_{gap} ($C_{pp} + C_{cp}$)	$37.652 \cdot 10^{-15}$ F
C_{total} ($C_{gap}/4$)	$9.413 \cdot 10^{-15}$ F
L_{self} (52)	$191 \cdot 10^{-10}$ H

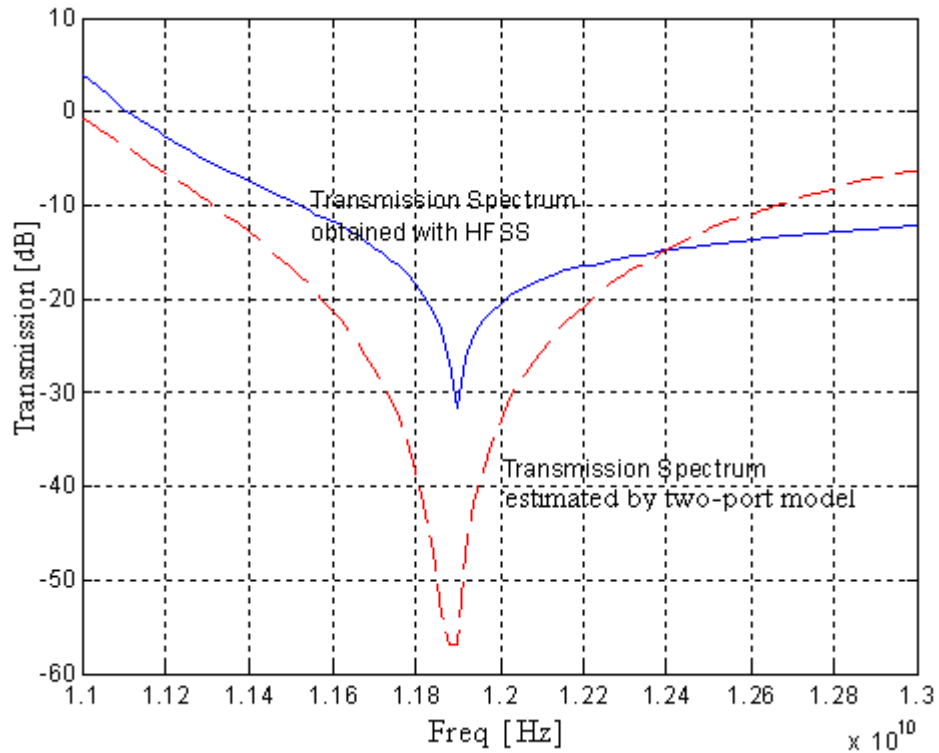


Figure 4-4: Estimated transmission spectra of the SRR unit cell using HFSS simulations with PML boundary conditions and $D_H=5$ mm, and using the equivalent two-port circuit given in Figure 4-3.

4.2.2 Numerical Simulation, Equivalent Circuit Modeling and Measurement of the SRR Unit Cell within Waveguide

As indicated earlier, transmission curve of the fabricated SRR structures are measured within a waveguide. Therefore, to account for the imaging effect of the metallic walls of the waveguide, PEC type boundary conditions are used in HFSS simulations while estimating the transmission spectrum of the measured structures. In other words, a single layer (in propagation direction) infinite SRR array is effectively created by these simulations and measurements when the SRR unit cell is placed within a waveguide. As the separation distance between the SRR surface and PEC walls of the waveguide is large along the \overline{H} field direction, the resulting

array can roughly be considered as a one-dimensional infinite SRR array extending in the \overline{E} field direction. Equivalent circuit model of the resulting array structure is suggested as shown in Figure 4-5 based on this one-dimensional periodical array assumption. The equivalent circuit model in this figure has been previously suggested and studied in section 3.2.2.

For the SRR parameters and materials used in the fabrication of the SRR unit cell, parameters of the two-port equivalent circuit are calculated and listed in Table 4-3. Then using the equations (53) through (61), resonance frequency of the effective SRR array structure is estimated to be 13.3 GHz as shown in Table 4-3. The transmission curve obtained with HFSS using PEC boundary conditions, on the other hand, is given in Figure 4-6 which shows a resonance at 11.95 GHz. Finally, the measured transmission spectrum is plotted in Figure 4-7 indicating a resonance frequency of 12 GHz.

In conclusion, the measurement and HFSS simulation results are found in very good agreement. The error made in the estimation of the resonance frequency by the equivalent circuit model approach is about ten percent and it can be explained by the fact that coupling effects along the \overline{H} field direction are neglected in this model.

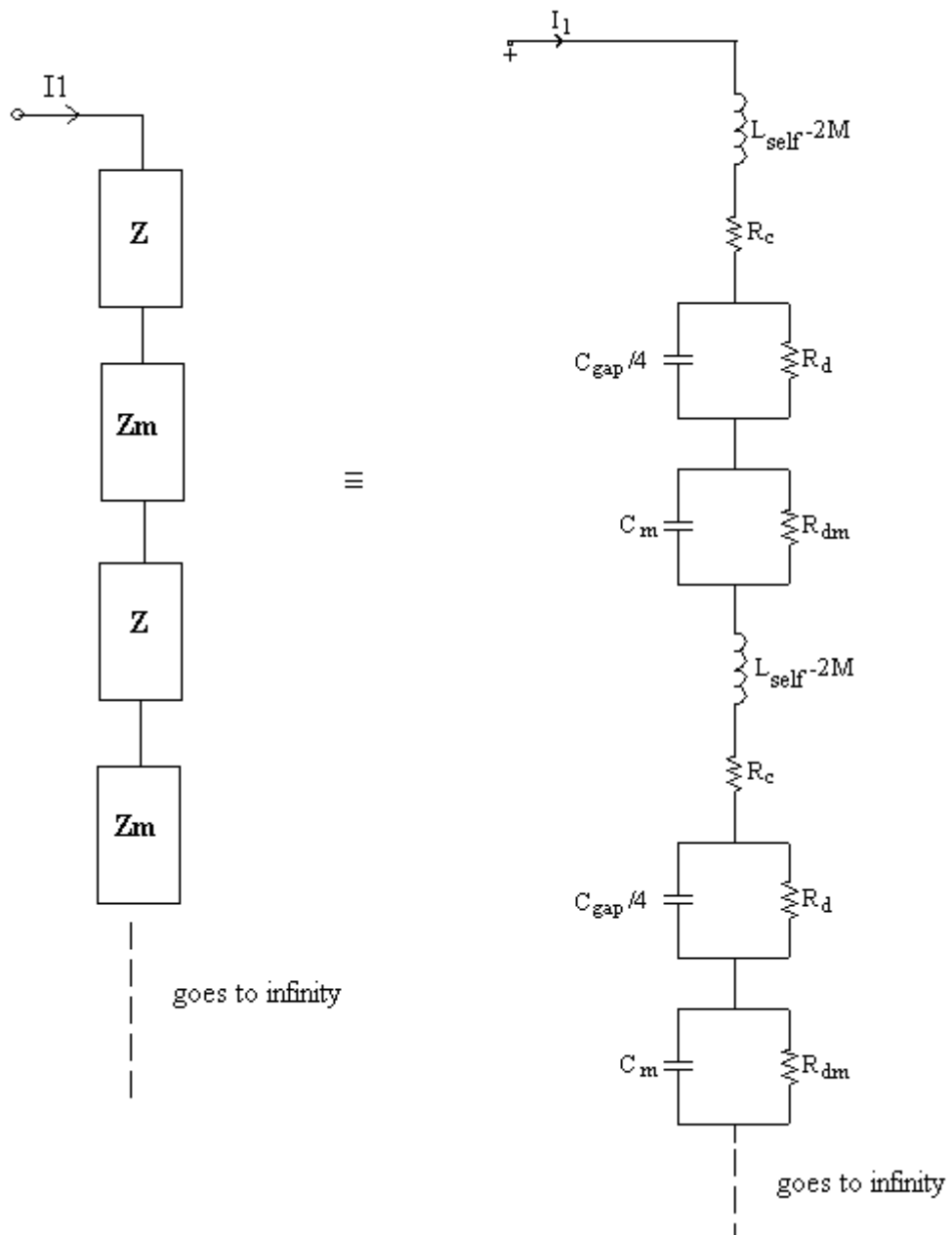


Figure 4-5: Equivalent circuit model of the effective SRR array formed by placing SRR unit cell within the waveguide in measurements.

Table 4-3: Calculated model parameters of the infinite SRR array extending along the incident electric field direction

C_{cp} (49)	$35.483 \cdot 10^{-15}$ F
C_{pp} (51)	$2.17 \cdot 10^{-15}$ F
$C_{gap} (C_{pp} + C_{cp})$	$37.652 \cdot 10^{-15}$ F
$C_{total} (C_{gap}/4)$	$9.413 \cdot 10^{-15}$ F
L_{self} (52)	$191 \cdot 10^{-10}$ H
$C_{mutualcp}$ (49)	$84.76 \cdot 10^{-15}$ F
$C_{mutualpp}$ (51)	$2.085 \cdot 10^{-15}$ F
C_{mutual}	$86.85 \cdot 10^{-15}$ F
$C_m (2 \cdot C_{mutual})$	$173.7 \cdot 10^{-15}$ F
M (60)	$17.9 \cdot 10^{-10}$ H
f_0	13.3 GHz

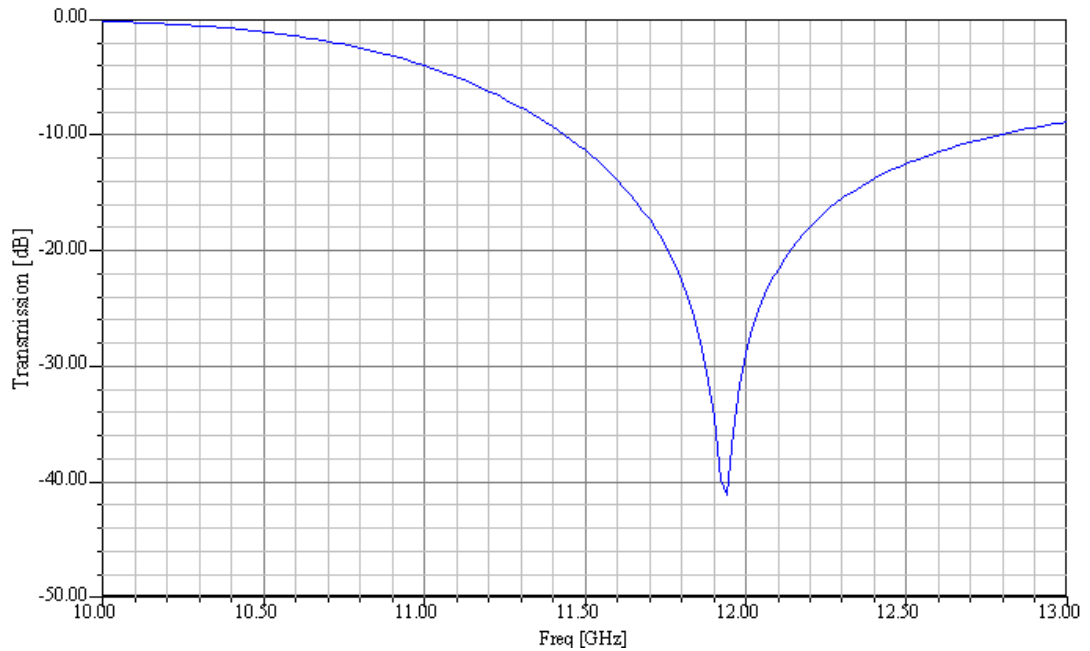


Figure 4-6: Simulated transmission spectrum of the fabricated SRR unit cell using HFSS with PEC boundary conditions.

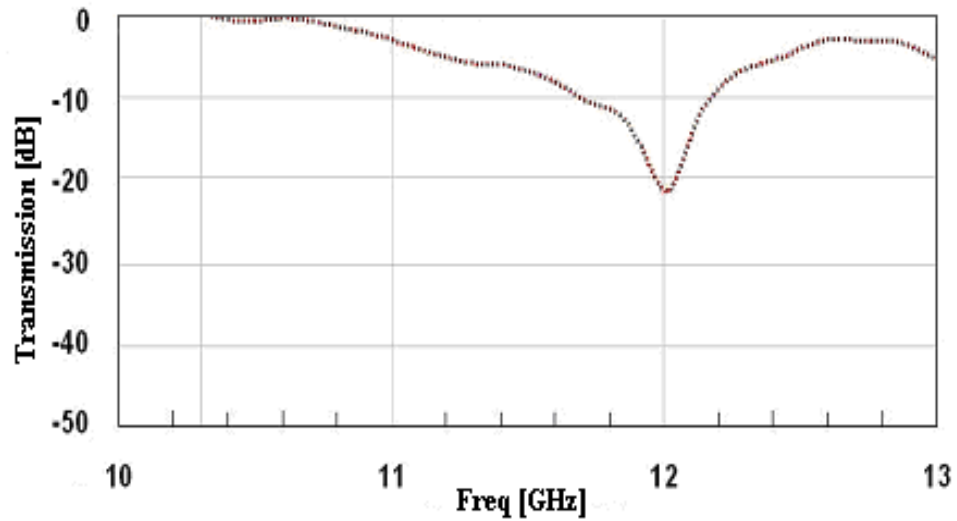


Figure 4-7: Measured transmission spectrum of the fabricated SRR unit cell when it is placed within a measurement waveguide.

4.3 Analysis and Measurements of the 4x1x1 SRR Array

The basic geometry and parameters of the four-element SRR array of size 4x1x1 is shown in Figure 4-8 where the capacitive coupling effects are also schematically indicated in Figure 4-8(b). This small sized SRR array is also investigated with HFSS simulations, equivalent circuit model and measurements both in isolation and within a waveguide in subsections 4.3.1 and 4.3.2, respectively.

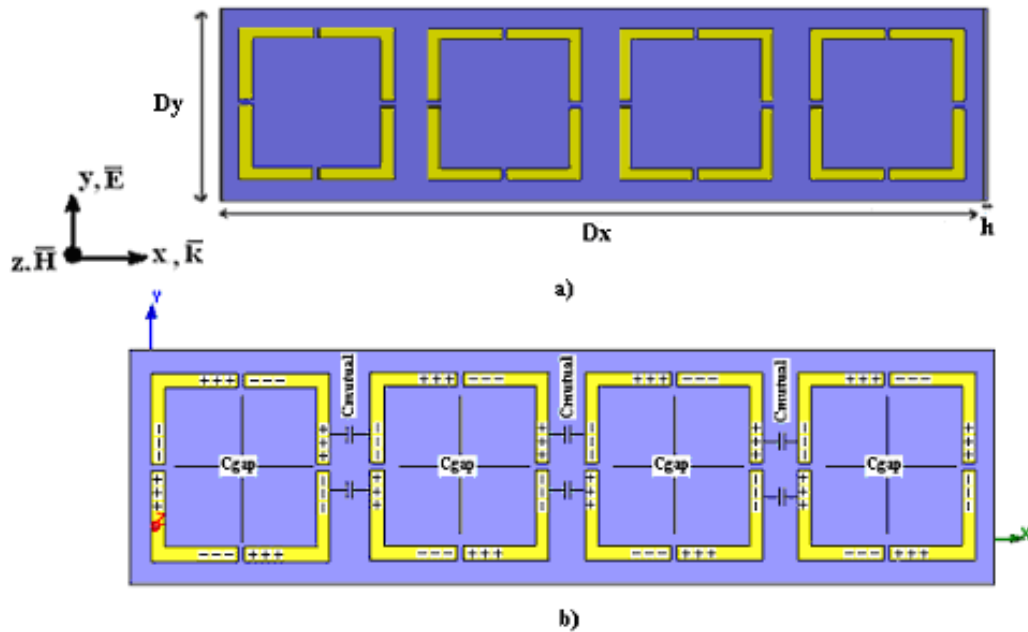


Figure 4-8: Four element SRR array of size 4x1x1 a) Geometry and excitation, b) Capacitive coupling effects along the propagation direction.

4.3.1 Analysis of the Isolated 4x1x1 SRR Array

The equivalent circuit model suggested for the isolated 4x1x1 array is seen in Figure 4-9. In this two-port model, all of the mutual inductance and capacitance effects along with losses are considered using the coupling two-port model suggested earlier in section 3.3.1 and Figure 3-7 (c). The only difference between the equivalent circuit models given in Figure 3-7 (c) and Figure 4-9 is that the inductance term $L-M$ is replaced by $L-2M$ for the SRR unit cells which have neighboring SRR cells on their both sides.

Following the same computational steps as in section 3.3.1 and using equations (94) through (98) (which are the adapted versions of the equations of (62) through (66) in this four-element array case), the transmission spectrum curve is computed (using equation (67) for S_{21} calculation also) and plotted in Figure 4-10. Transmission spectrum curve of the same isolated SRR array is also obtained by HFSS using

PML boundary conditions and plotted in Figure 4-10 for comparison. Ignoring the spurious effects stemming from the use of PML, both curves in this figure resemble each other around the expected resonance frequency of 11.90 GHz.

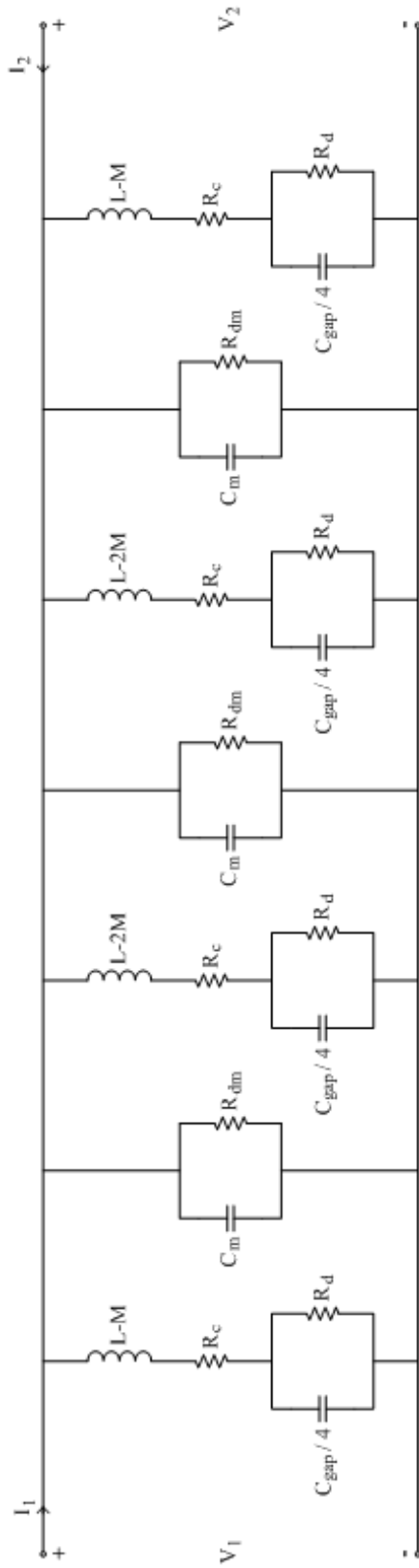


Figure 4-9: Two-port equivalent circuit model suggested for the isolated 4x1x1 SRR array

$$\begin{bmatrix} A & B \\ C & D \end{bmatrix}_{cascade} = \begin{bmatrix} 1 & 0 \\ Y_1 & 1 \end{bmatrix} \begin{bmatrix} 1 & 0 \\ Y_m & 1 \end{bmatrix} \begin{bmatrix} 1 & 0 \\ Y_2 & 1 \end{bmatrix} \begin{bmatrix} 1 & 0 \\ Y_m & 1 \end{bmatrix} \begin{bmatrix} 1 & 0 \\ Y_3 & 1 \end{bmatrix} \begin{bmatrix} 1 & 0 \\ Y_m & 1 \end{bmatrix} \begin{bmatrix} 1 & 0 \\ Y_4 & 1 \end{bmatrix} \quad (94)$$

$$\begin{bmatrix} A & B \\ C & D \end{bmatrix}_{cascade} = \begin{bmatrix} 1 & 0 \\ Y_1 + Y_2 + Y_3 + Y_4 + 3Y_m & 1 \end{bmatrix} \quad (95)$$

where

$$Y_1=Y_4 = \frac{1}{Rc + j\omega(L_{self} - M) + \frac{Rd}{1 + j\omega Rd \frac{C_{gap}}{4}}} \quad (96)$$

$$Y_2=Y_3 = \frac{1}{Rc + j\omega(L_{self} - 2M) + \frac{Rd}{1 + j\omega Rd \frac{C_{gap}}{4}}} \quad (97)$$

and

$$Y_m = \frac{1}{\frac{R_{dm}}{1 + j\omega R_{dm} C_m}} \quad (98)$$

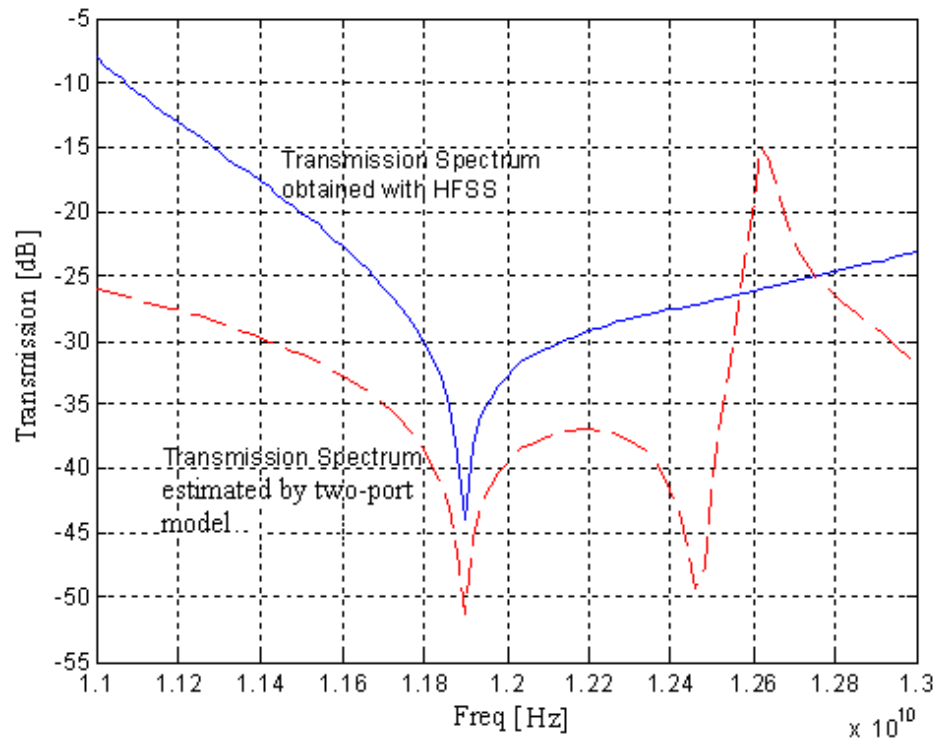


Figure 4-10: Estimated transmission spectrum of the isolated 4x1x1 SRR array using HFSS with PML boundary conditions and using the equivalent two-port model given in Figure 4-9.

4.3.2 Measurements and Numerical Simulations for the 4x1x1 SRR Array Placed Within a Waveguide

In this section, transmission spectrum of the 4x1x1 SRR array is both measured and estimated using HFSS (with PEC boundary conditions) within the measurement waveguide. As discussed in section 4.3.1, the effect of placing this SRR array in a waveguide is to create a four-layer (in the propagation direction) infinite SRR array both in \bar{E} field and \bar{H} field directions. The transmission curves obtained by HFSS simulations and by laboratory measurements are given in Figure 4-11 and Figure 4-12, respectively. Except for a shift in frequency, the overall variations of these two curves are very similar to each other with resonance frequencies observed at 11.72 and 11.96 GHz in HFSS simulation results and 12 and 12.4 GHz in the measurement results.

Pictures of the fabricated SRR unit cell and the 4x1x1 SRR array are shown in Figure 4-13 and Figure 4-14. Picture of a simple open-air measurement set-up using a pair of probes and a network analyzer is shown in Figure 4-15. It should be noted that this is not the actual waveguide-measurement set-up used in our experimental studies. This picture is given just for giving a rough idea about the open air measurement set-up.

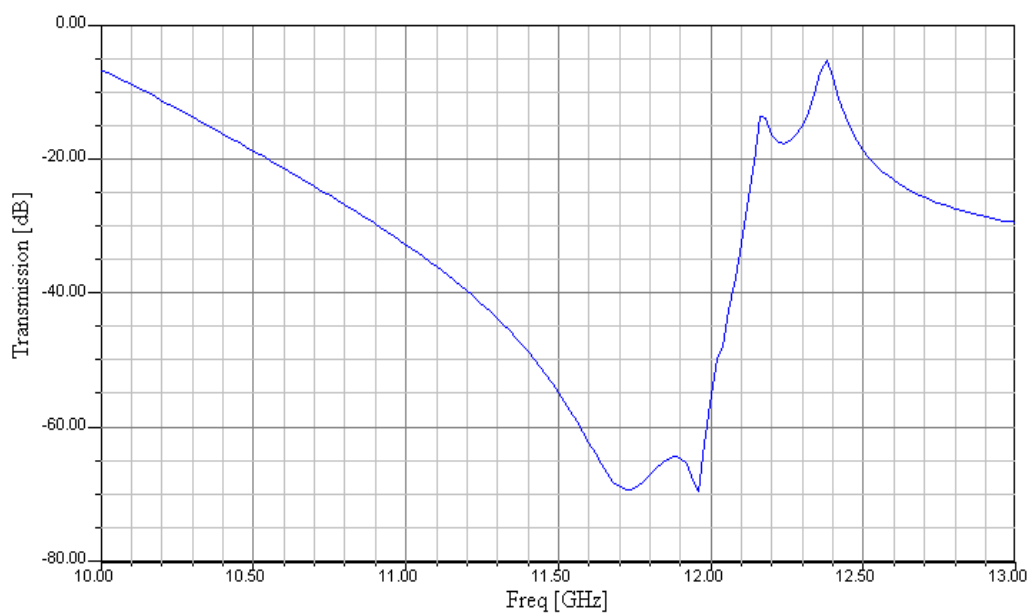


Figure 4-11: Transmission spectrum of the 4x1x1 array simulated by HFSS with PEC boundary conditions.

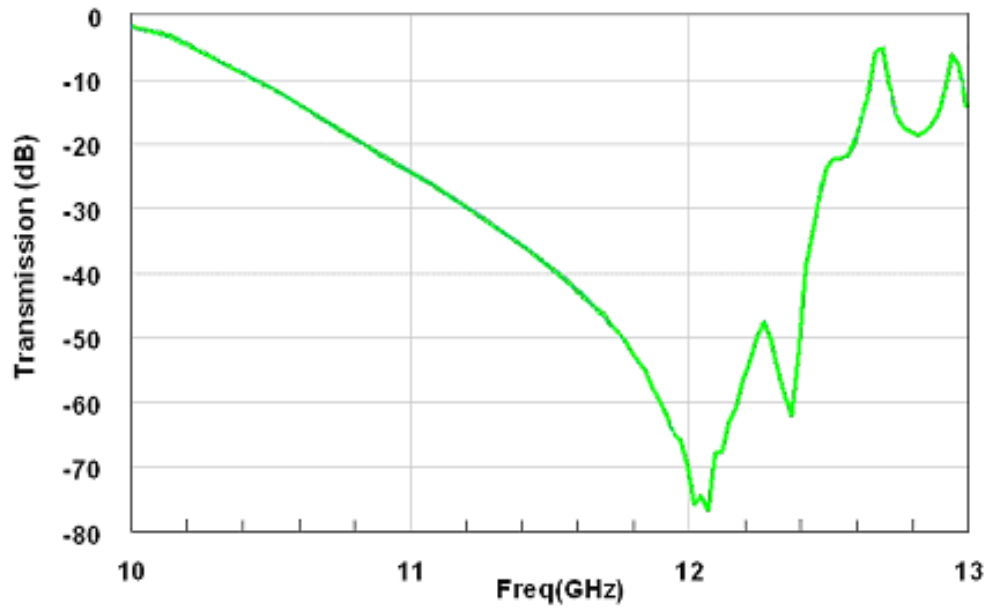


Figure 4-12: Measured (within a waveguide) transmission spectrum of the 4x1x1 SRR array.

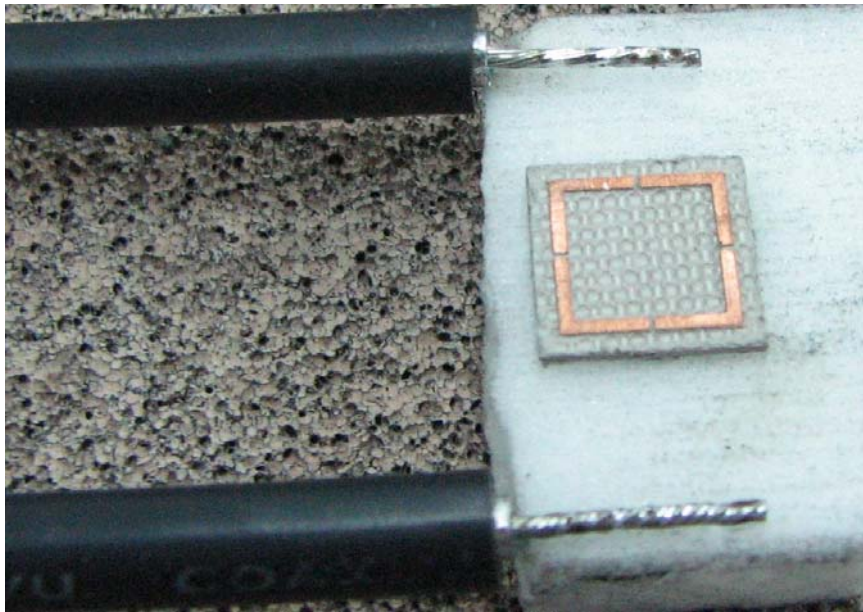


Figure 4-13: Fabricated SRR unit cell and probes used to measure its transmission spectrum.

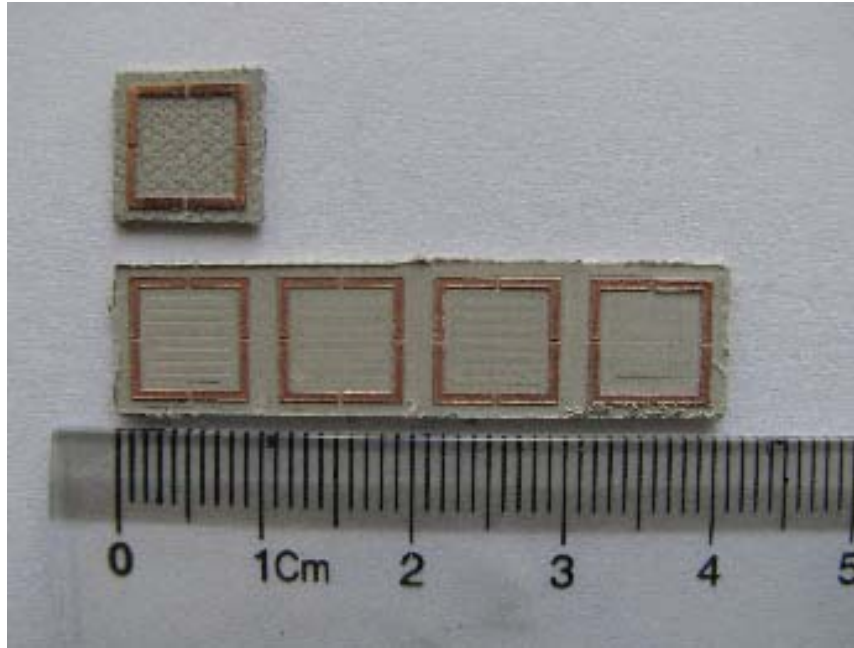


Figure 4-14: Comparison of the fabricated SRR unit cell and 4x1x1 SRR array.

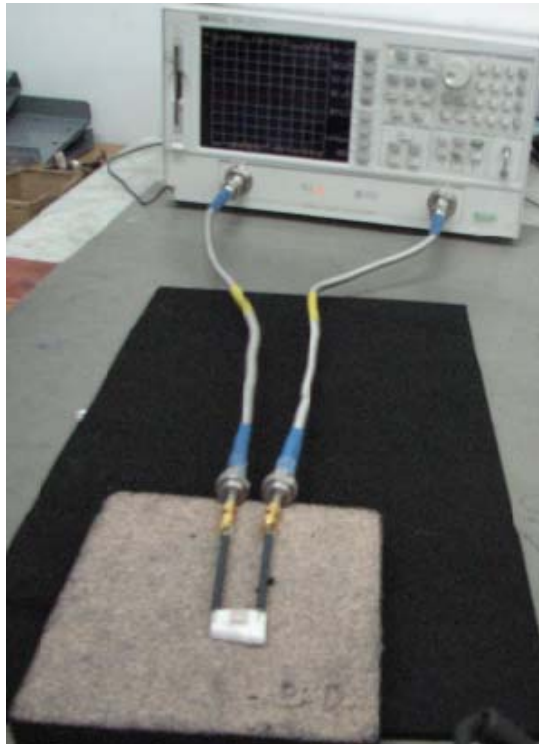


Figure 4-15: A simple experimental set-up used to measure transmission spectrum of SRR structures in air.

CHAPTER 5

CONCLUSIONS AND FUTURE WORK

Split ring resonator (SRR) is one of the main sub-wavelength components used to design left handed metamaterials in microwave or optical frequencies. SRR arrays provide engineered materials with negative values of effective permeability. In this thesis, a simple and fully symmetrical SRR unit cell topology composed of a single square-shaped metallic loop with four splits at the middle of each edge is investigated. Geometrical simplicity is preferred in the design of such sub-wavelength structures especially in millimeter wave, terahertz and upper optical frequency ranges. Therefore, investigations in this thesis are restricted to this simple but practically useful SRR unit cell geometry.

The basic purpose of this thesis research has been to establish equivalent lumped element circuit models to describe the two-port circuit characterization of SRR arrays with special emphasis on cell-to-cell coupling effects. Obviously, such equivalent circuit representations can describe actual array behavior only approximately. On the other hand, full-wave electromagnetic solvers making use of numerical methods such as the FEM (finite elements method) or FDTD (finite difference time domain) method provide much better accuracy in the expense of highly increased computer memory and run time requirements especially for larger array sizes. Availability of sufficiently accurate equivalent circuit models for SRR arrays offer an approximate yet computationally efficient and fast way of analysis for finite but large size arrays. This approach would also make the solution of optimization problems possible for the design of metamaterials with specific design requirements.

In this thesis, the basic SRR unit cell topology is represented by a two-port equivalent circuit model having a series RLC resonant circuit in its shunt branch. Other than the self inductance of the metallic loop and the total capacitance accounting for the equivalent effect of four individual gap capacitances (all connected in series), the model has two equivalent resistances; a resistor serially connected to the inductor to model conductor losses and another resistor connected in parallel to the capacitor to model ohmic losses occurring within the dielectric substrate. Values of the self inductance of the metallic loop, equivalent capacitance and the values of loss resistances are computed using the geometrical and material properties of the SRR unit cell. The electromagnetic coupling effects between two neighboring cells of a given SRR array in the electric field and in the propagation directions are modeled by a proper RC two-port coupling circuit in addition to the mutual inductance parameter which is used to modify the self inductance values of individual cells.

In this thesis, the basic SRR equivalent circuit model and the coupling circuit two-port models are used to estimate the transmission spectra and resonance frequencies of various array forms over two different frequency bandwidths; 10 GHz to 13 GHz band and 25 GHz to 40 GHz band. The finite size small arrays such as 1x2x1, 2x1x1, 2x2x1 and 4x1x1 arrays are simulated in isolation using HFSS with PML boundary conditions. Transmission spectrum results from such simulations are compared to equivalent circuit model results with good agreement especially around the resonance frequency of the simulation bandwidth. Excess losses and unexpected spurious effects are observed due to the use of PML boundary conditions over very wide bandwidths. Results of these HFSS simulations are also found to be very sensitive to the location of PML boundaries. Alternatively, such basic arrays are turned into infinite array structures by using PEC/PMC boundary conditions in HFSS simulations. This situation is also experimentally implemented by measuring an SRR unit cell and its 4x1x1 SRR array within a waveguide due to the mirror imaging effect of metallic walls of the guide. Resulting infinite array effects are taken into account in equivalent circuit models as well. In the

investigation of these array structures, the periodicity along the applied magnetic field direction is taken to be large enough to omit the array effects coming from that dimension. Then, the resulting arrays are simulated to be of infinite size along the applied electric field direction with one or more layers along the propagation direction of the incident excitation.

In a given array problem, the overall SRR array is eventually represented by a single equivalent two-port circuit by considering the series, parallel or cascade connections of smaller two-port units belonging to SRR unit cells or coupling circuits. The complex S-parameter matrix of the overall array two-port is obtained via conversions from Z-matrix or chain matrix representations appropriately. All these computations are carried on by simple and fast MATLAB codes written during this thesis research. The transmission spectrum (i.e. the $|S_{21}(f)|$ versus frequency (f) curve) estimated by this approach is found to be in very good agreement with transmission spectra obtained both by HFSS simulations and measurements.

For the purpose of experimental verification, two of the investigated structures, the SRR unit cell resonating around 12 GHz in the X-band and a 4x1x1 SRR array (formed by four of such cells in the propagation direction) are fabricated by copper stripes printed over a low loss dielectric substrate. Complex scattering parameters of these two structures are measured within a metallic waveguide. Resulting transmission spectra are compared with the transmission curves obtained by HFSS simulations where PEC boundary conditions are applied at the surfaces of the computational volume (surfaces which coincide with the walls of the waveguide used in the measurement setup). Again, simulation results, equivalent circuit estimations and measurement results are found in good agreement.

As future work, the novel equivalent two-port circuit models suggested in this thesis can be further improved especially by including the coupling effects along the magnetic field direction as well. Effect of asymmetry in the SRR unit cell

geometry, concerning the number or locations of gaps for instance, may be investigated in circuit modeling. Equivalent circuit models of SRR structures under different excitation conditions can be studied. Finally, the suggested equivalent circuit modeling approach can be applied to SRR array optimization to realize special design requirements.

REFERENCES

1. V.G. Veselago, "The Electrodynamics of Substances with Simultaneously Negative Values of Permittivity and Permeability," *Sov. Phys. Uspekhi*, Vol.10, 1968.
2. J. B. Pendry, A. J. Holden, D. J. Robbins, and W. J. Stewart, "Magnetism from Conductors and Enhanced Nonlinear Phenomena," *IEEE Trans. Microwave Theory Tech.*, Vol. 47, No. 11, 1999.
3. D. R. Smith, W. J. Padilla, D. C. Vier, S. C. Nemat-Nasser, and S. Schultz, "Composite Medium with Simultaneously Negative Permeability and Permittivity," *Physical Review Letters*, Volume 84, Number 18, 1 May 2000.
4. R. Marqués, F. Medina, and R. Rafii-El-Idrissi, "Role of Bianisotropy in Negative Permeability and Left-Handed Metamaterials," *Phys. Rev. B*, Vol. 65, 144440, 2002.
5. R. Marqués, F. Mesa, J. Martel, and F. Medina, "Comparative Analysis of Edge- and Broadside-Coupled Split Ring Resonators for Metamaterial Design Theory and Experiments," *IEEE Transactions on Antennas and Propagation*, Vol. 51, No. 10, Oct. 2003.
6. F. Bilotti, A. Toscano, L. Vegni, K. Aydin, K. B. Alici, and E. Ozbay, "Equivalent-Circuit Models for the Design of Metamaterials Based on Artificial Magnetic Inclusions," *IEEE Transactions on Microwave Theory and Techniques*, Vol. 55, No. 12, December 2007.
7. I.I. Smolyaninov, Y.J. Hung, C.C. Davis, "Magnifying Superlens in the Visible Frequency Range," *Science*, 315, 1699-1701, 2007.

8. X. Zhang, Z. Liu, "Superlenses to Overcome the Diffraction Limit," *Nature Mater*, 7, 435-441, 2008.
9. J. B. Pendry, D. Schurig D.R. Smith, "Controlling Electromagnetic Fields," *Science* 312, 1780-1782, 2006.
10. J. Baena, J. Bonache, F. Martín, R. M. Sillero, F. Falcone, Tx. Lopetegui, M. A. G. Laso, J. García-García, I. Gil, M. Flores Portillo and M. Sorolla, "Equivalent-Circuit Models for Split-Ring Resonators and Complementary Split-Ring Resonators Coupled to Planar Transmission Lines," *IEEE Transactions on Microwave Theory and Techniques*, Vol. 53, No. 4, April 2005.
11. Q. Wu, M. Wu and F. Meng, "SRRs' Artificial Magnetic Metamaterials Modeling Using Transmission Line Theory," *Electromagnetics Research Symposium 2005*, Hangzhou, China, August 22-26.
12. N.P. Johnson, A.Z. Khokhar, H.M.H. Chong, R.M. De La Rue and S. McMeekin, "Characterisation at Infrared Wavelengths of Metamaterials Formed by Thin-Film Metallic Split-Ring Resonator Arrays On Silicon," *Electronics Letters* 14th September 2006 Vol. 42 No. 19.
13. J. Wang, S. Qu, Z. Xu, H. Ma, Y. Yang, and C. Gu, "A Controllable Magnetic Metamaterial: Split-Ring Resonator With Rotated Inner Ring," *IEEE Transactions on Antennas and Propagation*, Vol. 56, No. 7, July 2008.
14. O. Sydoruk, E. Tatartschuk, E. Shamonina, and L. Solymar, "Analytical Formulation for the Resonant Frequency of Split Rings," *Journal of Applied Physics* 105, 014903 ,2009.
15. B. Sauviac, C. R. Simovski, S. A. Tretyakov, "Double Split-Ring Resonators: Analytical Modeling and Numerical Simulations," *Electromagnetics*, 24:317–338, 2004, Taylor & Francis Inc.ISSN: 0272-6343 print/1532-527X online,DOI: 10.1080/02726340490457890.

16. H. Chen, L. Ran, J. Huangfu, T. M. Grzegorzcyk and J.Kong, "Equivalent Circuit Model for Left-Handed Metamaterials," *Journal of Applied Physics* 100, 024915, 2006.
17. I. Gil, J. Bonache, M. Gil, J. García-García, and F. Martín, R. Marqués, "Accurate Circuit Analysis of Resonant-Type Left Handed Transmission Lines with Inter-Resonator Coupling," *Journal of Applied Physics* 100, 074908, 2006.
18. T. J.Yen, W.J. Padilla , N. Fang, D.C. Vier , D.R.Smith, J. B. Pendry ,D.N. Basov and X. Zhang , "Terahertz Magnetic Response from Artificial Materials," *Science* 303, 1494, 2004.
19. J. Zhou, T. Koschny and C. M. Soukoulis, "Magnetic and Electric Excitations in Split Ring Resonators," *Optics Express* 17881, Vol. 15, No. 26, 24 December 2007.
20. S.G. McMeekin, and A.Z Khokhar, L. Basudev, R.M. De La Rue, and N.P Johnson, (2007) "Analysis of Resonant Responses of Split Ring Resonators Using Conformal Mapping Techniques," In, Kuzmiak, V.and Markos, P. and Szoplik, T., Eds. *Metamaterials II*, 16-18 April 2007 Proceedings of SPIE--the International Society for Optical Engineering Vol 6581, Prague.
21. D. M. Pozar, "Microwave Engineering," Page 187, 2005.
22. M. T. Thompson, "Inductance Calculation Techniques, Part II: Approximations and Handbook," 1999.
23. G. Turhan-Sayan, "Unpublished Notes on the Equivalent Circuit Modeling for SRR Arrays," METU, 2009.